1992

A preliminary investigation of dual mode fracture sustained by graphiteepoxy laminates impacted by high-velocity spherical metallic projectiles

Gregory Joseph Czarnecki
University of Dayton

A PRELIMINARY INVESTIGATION OF DUAL MODE FRACTURE SUSTAINED BY GRAPHITE/EPOXY LAMINATES IMPACTED BY HIGH-VELOCITY SPHERICAL METALLIC PROJECTILES

Thesis

Submitted to

Graduate Engineering & Research
School of Engineering

UNIVERSITY OF DAYTON

In Partial Fulfillment of the Requirements for

The Degree

Master of Science in Materials Engineering

by

Gregory Joseph Czarnecki

UNIVERSITY OF DAYTON

Dayton, Ohio

April 1992

A PRELIMINARY INVESTIGATION OF DUAL MODE FRACTURE SUSTAINED BY GRAPHITE/EPOXY LAMINATES IMPACTED BY HIGH-VELOCITY SPHERICAL METALLIC PROJECTILES

APPROVED BY:

[redacted]

Joseph Gallagher, Ph.D.
Advisory Committee, Chairman

[redacted]

A. M. Rajendran, Ph.D.
Thesis Technical Advisor

[redacted]

Franklin E. Estep, Ph.D.
Interim Associate Dean/Director
Graduate Engineering & Research
School of Engineering

[redacted]

Patrick J. Sweeney, Ph.D.
Interim Dean
School of Engineering

ABSTRACT

A PRELIMINARY INVESTIGATION OF DUAL MODE FRACTURE SUSTAINED BY GRAPHITE/EPOXY LAMINATES IMPACTED BY HIGH-VELOCITY SPHERICAL METALLIC PROJECTILES

Czarnecki, Gregory Joseph
University of Dayton, 1991

Advisors: Dr. A. M. Rajendran and Dr. Joseph Gallagher

This thesis studies the basis for delamination initiation and propagation within an impacted laminate. The work provides an explanation for fracture mode transformation along the projectile's path.

Post-impact observations of graphite/epoxy (AS4/3501-6) laminates penetrated by steel spheres (0.5-inch diameter) reveal a fracture mode, similar to shear plugging, adjacent to the impacted surface. This fracture mode is contrasted with that of delamination adjacent to the rear surface. The sudden transition from shear plugging to delamination occurs when the projectile interacts with the returning impact-generated tensile wave. To demonstrate the transition, results are presented from ballistically impacted laminates containing a series of imbedded carbon stress and constantan strain gages. Results are based on impact velocities of 1825 and 2380 f/s. Transverse stress waves are shown capable of creating

delamination until attenuated by a localized compression front associated with the on-coming projectile. Based on experimental results, the location of the fracture mode transition plane is predicted both graphically and through a simple equation of motion.

ACKNOWLEDGMENTS

The fruition of this research project leaves me indebted to several individuals; Dr Joseph Gallagher (University of Dayton) for substantial assistance in organizing and editing this work; Dr Rajendran (University of Dayton) for technical advice throughout critical stages of the research; Dr Jacques Charest (Dynasen, Inc) for assistance in sensor choice and signal interpretation; Drs Stephen Bless (University of Dayton), Piyush Dutta (US Army Cold Regions Research and Engineering Laboratory), David Hui (University of New Orleans), and Arnold Mayer (US Air Force Wright Laboratory) for consultation assistance; Mark Morgan (Synergy, Inc) for hands-on assistance throughout the effort; and Tim Seymour (US Air Force Wright Laboratory) for technical range assistance.

TABLE OF CONTENTS

LIST OF FIGURES

LIST OF TABLES

LIST OF SYMBOLS AND ABBREVIATIONS

a_o	Contact radius
ANOVA	Analysis of variance
CW	Clockwise
CCW	Counter clockwise
cm	Centimeter
dia	Diameter
E	Elastic modulus
f/s	Feet per second
g	Acceleration due to gravity
g	Gram
G	Shear modulus
G	Gage factor
G_{Ic}	Mode I fracture toughness (composites)
in	Inch
KHz	Kilo-hertz
K_{Ic}	Mode I fracture toughness (metals)
K_{IIc}	Mode II fracture toughness (metals)
km	Kilometer
ksi	Thousand pounds per square inch
L4	Taguchi experiment consisting of 4 tests
L8	Taguchi experiment consisting of 8 tests
lb	Pound
MHz	Mega-hertz
MPa	Mega-pascal
mm	Millimeter
m-sec	Milli-second
msi	Million pounds per square inch
mV	Millivolt
NDI	Nondestructive investigation
no.	Number
psi	Pounds per square inch (gauge)
PVDF	Polyvinylidine fluoride (piezofilm)
q_o	Impact pressure
Q	Reduced stiffness
R	Resistance
sec	Second
t	Laminate thickness
TBD	To be determined
v	Velocity
V	Volts
V_{50}	Impact velocity at which 50% of the projectiles are expected to penetrate the target

$\bar{X}$	Mean (average)
z	Distance from the impacted surface
%	Percent
Δ	Change (difference)
ε	Strain
μ	Poisson's ratio
μ-sec	Micro-second
ρ	Density
σ	Standard deviation
σ_{zz}	Normal stress in the z-direction
τ_{xz}	Shear stress

CHAPTER I

INTRODUCTION

Composite material systems offer specific stiffnesses and strengths unsurpassed by monolithic material systems. Composites have the added advantage of being designed to meet expected service loading conditions. This design feature of the composite material system offers such complete optimization that severe degradation of mechanical properties can occur if the component is subjected to foreign loads. Even relatively minor low velocity impacts can produce sufficient delamination to cause a loss of compression strength or even catastrophic failure. The ability of a component to sustain an impact without significant mechanical property degradation is crucial to the aerospace industry.

1.1 Problem Definition

Composites absorb significant amounts of impact energy through fracture events rather than by elastic or plastic deformations as do metals[1]. The damage state depends on structural geometry, boundary conditions, stacking sequence, material properties, impact energy, and impactor geometry[2]. Poor laminate out-of-plane mechanical properties allow kinetic energy from any source (dropped tools or missile warhead

fragments) to cause a combination of damage in the form of delamination, transverse matrix cracking, fiber fracture, and fiber-matrix interface disbonds. The predominance of each type of damage depends on the lay-up, thickness, and impact energy[1]. During severe impacts, laminates typically sustain all four modes of fracture. Fiber fracture is the primary means by which tensile properties are reduced[3], whereas delamination is the principal mechanism by which compression properties are degraded[2].

Understanding the low velocity impact problem requires a knowledge of contact behavior, elastic wave propagation, and crack nucleation/propagation. Significant fracture (involving through-the-thickness penetration and delamination several times the projectile's diameter) enters into the high velocity impact problem and requires a more in-depth understanding of fracture mechanisms. Damage tolerance cannot be fully achieved without complete understanding of fracture mechanisms and means of attenuation.

Experimentation is an important means of checking one's hypotheses and achieving an understanding of impact induced fracture. However, some test procedures are more appropriate than others. Charpy and Izod tests do not accurately represent end-use applications. Drop-weight and pendulum tests are performed at such low velocities that significant

mass must be added to the impacting head to provide the desired kinetic energy. The resulting relatively large inertia and length effects are not representative of finite sized projectiles.

Impact induced delamination is often described as a phenomenon created by lamina stiffness mismatches resulting from panel flexure[4], whereas other explanations rely on an analysis of stress waves generated during the impact event. When a composite panel is impacted by a low velocity nonpenetrating projectile, a compressive wave is developed within the laminate. This stress wave propagates through the thickness and when reaching the rear face boundary, is reflected back as a tensile wave. For very low energy impacts, the tensile wave is believed to have sufficient amplitude to delaminate one or two of the rear face plies. With higher energy nonpenetrating impacts, several more plies (beginning at the rear face) are delaminated[5].

Graphite/epoxy laminates impacted by penetrating spherical projectiles exhibit two primary fracture modes. Damage sustained on the laminate's front face resembles a cleanly cut shear plug. Damage sustained near the laminate's rear face is extreme delamination several times the projectile's diameter[6,7]. As shown in Figure 1a, laminate penetration at velocities just above the V_{50} (a velocity where

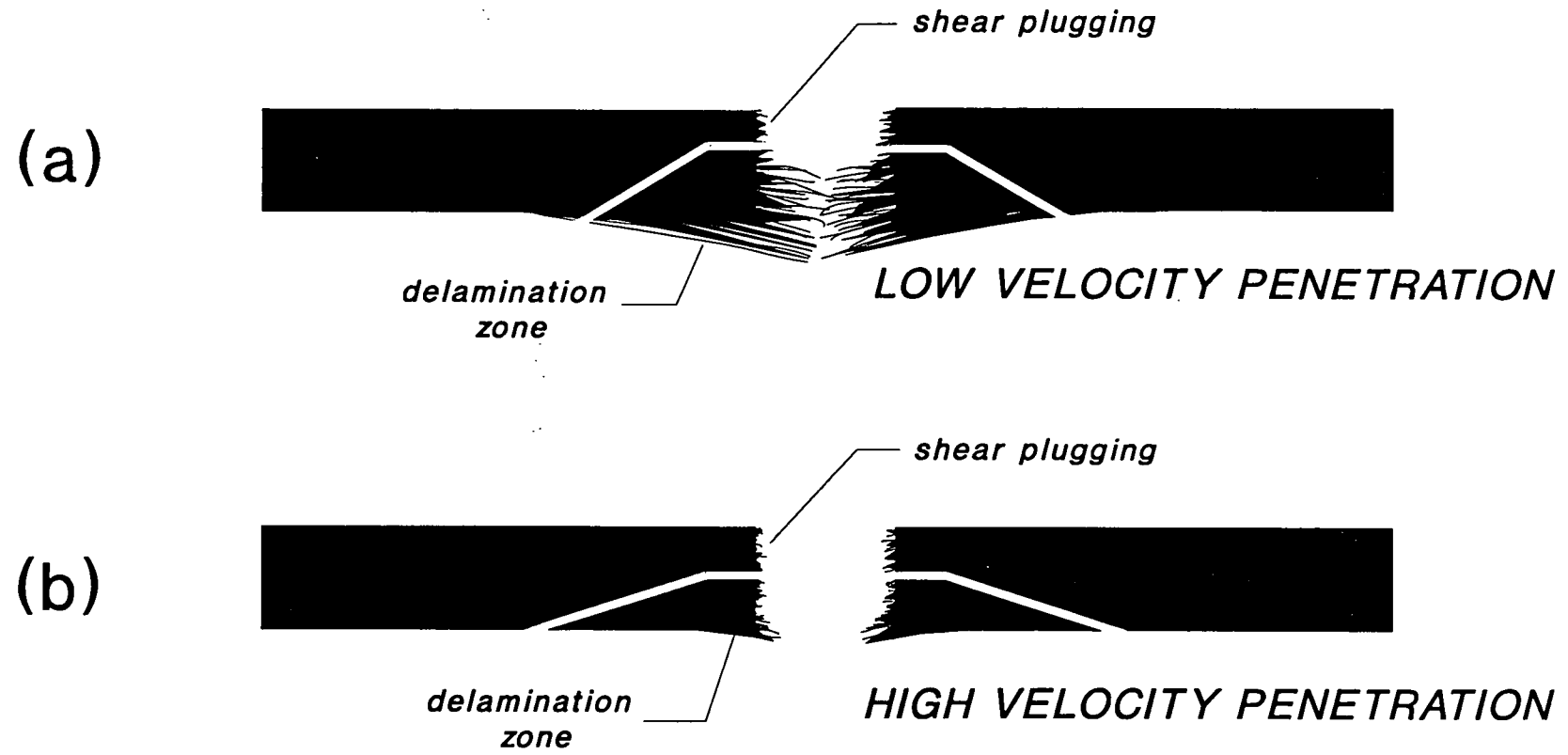

Figure 1. Dual mode fracture damage for low and high velocity impacts.

50% of the projectiles are expected to penetrate the target) often results in rear face delaminated material (having little stiffness) being pushed aside by the projectile, only to rebound forming a closed hole. At higher impact velocities, the fiber's inertia does not allow sufficient flexure, so open holes through the laminate can be obtained as described in Figure 1b.

1.2 Thesis Objective

The objective of this thesis is to determine the basis for delamination initiation and propagation within a laminate impacted at high velocity. The primary goal is to establish and support an explanation for fracture mode transformation along the projectile's path.

1.3 Approach

Post-impact observations of graphite/epoxy (AS4/3501-6) laminates penetrated by steel spheres (0.5-inch diameter) reveal a fracture mode similar to shear plugging adjacent to the impacted surface. This fracture mode is contrasted with that of delamination adjacent to the rear surface. The sudden transition from shear plugging to delamination is hypothesized as occurring when the projectile interacts with the returning impact-generated tensile wave.

To test the hypothesis, ballistic experiments are performed on instrumented laminates containing an alternating series of imbedded carbon stress and constantan strain gages. Using a high projectile velocity (approximately 2380 f/s), the transverse stress wave together with a combination of the wave's dilatational component and Poisson's effects are recorded. Tensile wave attenuation is correlated with the on-coming projectile's localized compression front and used to predict the location of the fracture mode transition from shear plugging to that of delamination.

1.4 Thesis Organization

In Chapter II, previously published research is reviewed. Static and dynamic penetration experiments are examined, as are the mechanics of damage initiation and propagation. In Chapter III, a hypothesis concerning stress wave propagation and attenuation is presented. The test approach (together with several pretests) is presented in Chapter IV. Complexities associated with impact generated stress waves are discussed in Chapter V. Chapter VI reviews the stress wave experiments performed to satisfy thesis goals. Finally, a summary of work associated with this thesis, along with conclusions and recommendations, are presented in Chapter VII.

CHAPTER II

LITERATURE REVIEW

2.1 Static and Dynamic Penetration Experiments

Caprino et al.[8,9] compared energy absorbed during dynamic impact to that from static penetration tests. For the range of impact velocities tested, carbon fiber reinforced epoxy was found to be rate insensitive. Hseih et al.[10] found that graphite fiber reinforced panels react brittlely under all circumstances and similarly exhibit no strain rate sensitivity.

Wardle and Tokarsky[11] obtained initial fracture sequences during quasi-static testing which were similar to those obtained dynamically. Figure 2 shows a 1:1 relationship between static and dynamic tests for all fiber systems except E-glass.

Elber[12] compared load-displacement curves for static penetration to those of impact. Although the impact curve was noisy, it followed the static curve closely as shown in Figure 3. Integrating the impact generated load-displacement curve resulted in a smooth energy-displacement curve which correlated directly with the static curve (Figure 4). Elber

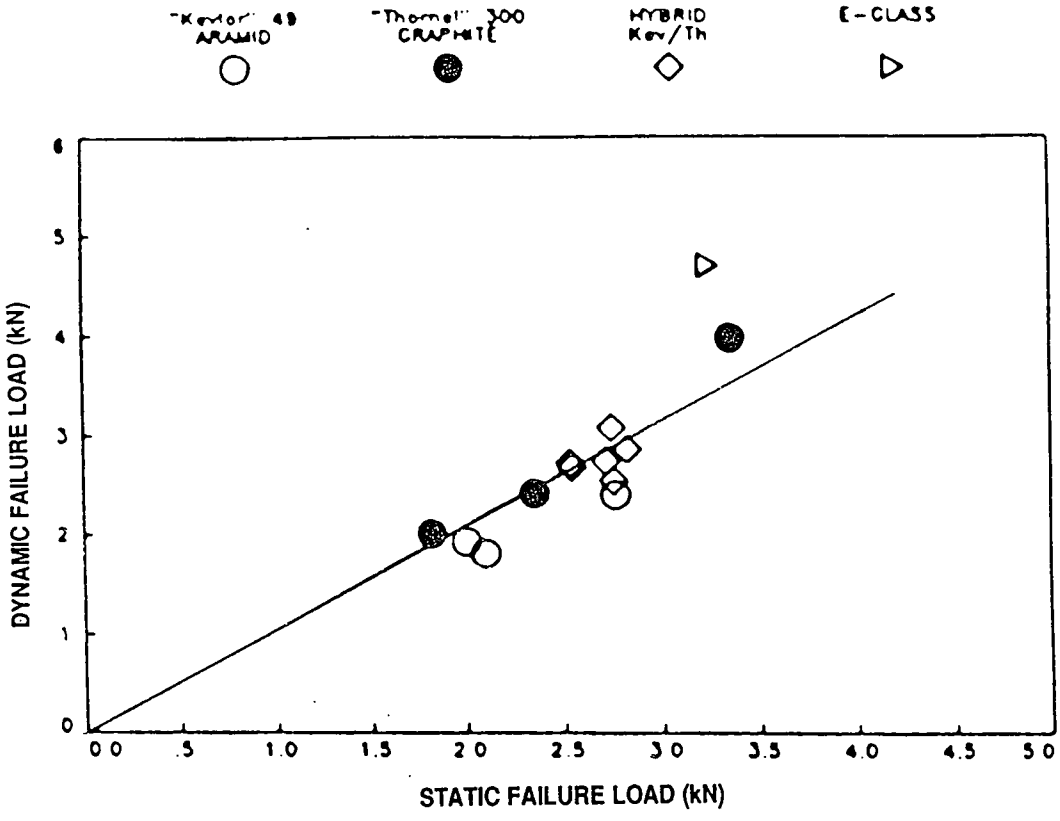

Figure 2. Static vs dynamic failure loads for various composite systems[11].

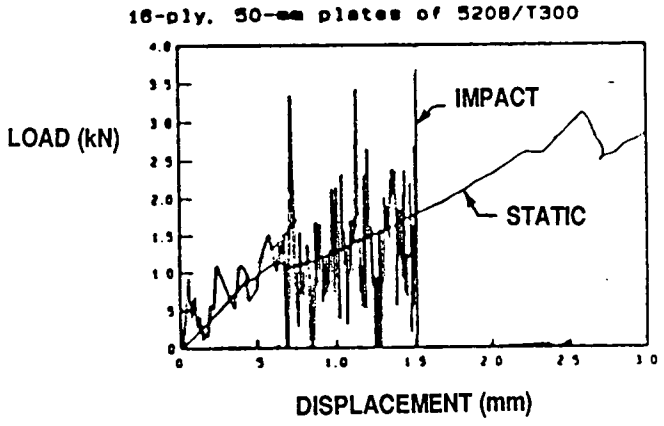

Figure 3. Load vs displacement signals for static and dynamic cases[12].

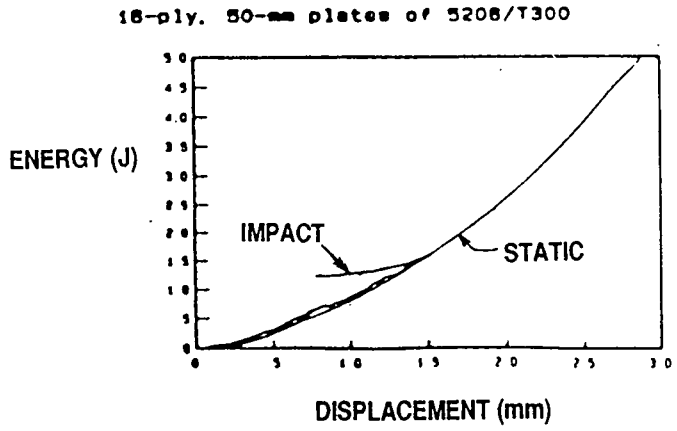

Figure 4. Energy vs displacement for static and dynamic cases[12].

concluded that rate effects were negligible and high spike loads generated during impact do not cause additional damage. Simple plate equations were found capable of predicting deformation in plates up to 32 plies. Static penetration produced roughly the same extent of delamination as impact tests given the same load or energy (Figure 5). The author concluded that static indentation tests can provide quality information about impacted panels.

Sjoblom et al.[13] found that at low velocities (if inertial forces are negated) the impact event is reduced to that of a static case. Cross section photomicrographs show a similar damage pattern between panels tested statically and dynamically. Based on the photomicrographs, the authors state that elastic waves traveling through the panel have a negligible effect on damage sustained. Static penetration of

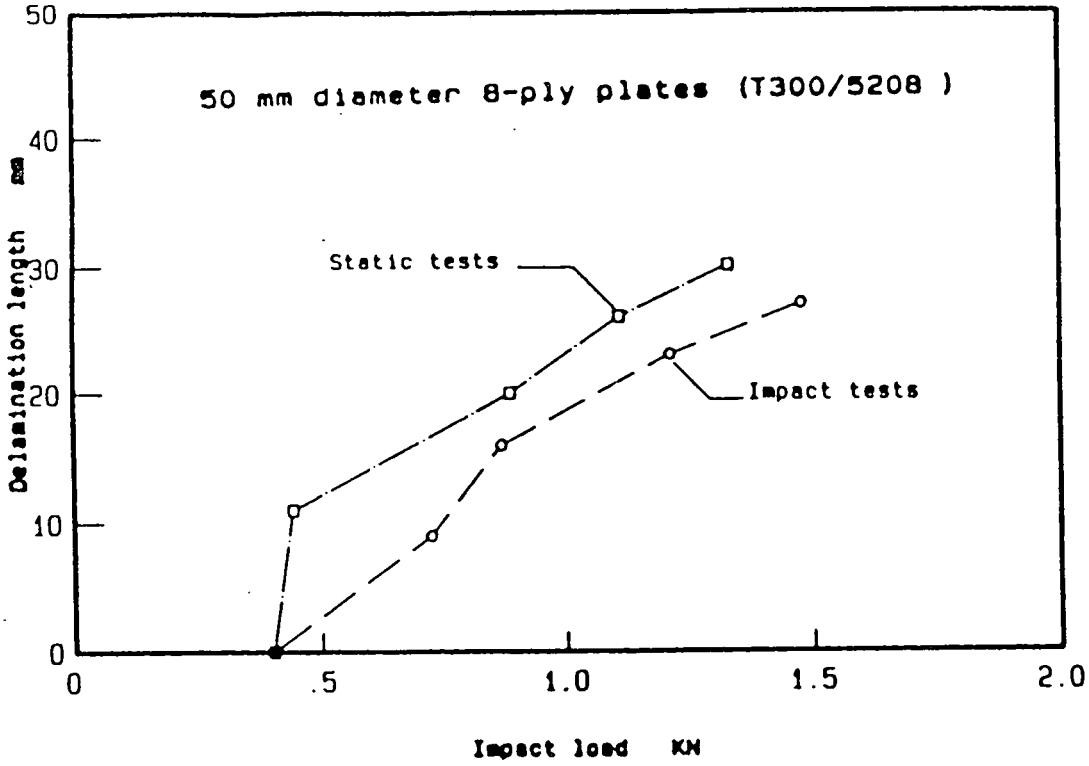

Figure 5. Delamination length vs impact load for static and dynamic cases[12].

carbon/epoxy panels proved elastic until first damage occurred. Further penetration forced a reported increase in damage area and matrix cracking.

Liu and Malvern[14] compared impact generated damage to that obtained during quasi-static penetration tests. In the quasi-static tests, matrix cracking was less significant and did not interact with delamination. In research performed by Pinnell and Sjoblom[15], C-scans and photomicrographs indicated identical damage for both the static and impact tests.

2.2 Damage and Energy Absorption Processes During Impact

Sierakowski and Chaturvedi[16] note that delamination is the dominant fracture mode in graphite systems. Sun and Yang[17] found that factors which affect the extent of damage are the impactor's mass and velocity, the plate's stiffness, and the Hertzian contact behavior. Energy absorbed is believed an indicator of the extent of damage sustained. Fiber breakage, matrix cracking, delamination, and plastic deformations all contribute to the energy absorption.

Hseih et al.[10] found that energy absorption was proportional to panel thickness for the 10, 20, and 30-ply panels. This implies a constant energy loss rate regardless of thickness.

Pinnell and Sjoblom[15] developed relationships between test parameters (i.e., material properties, material thickness, projectile geometry, target dimensions, and impact velocity) and the load required to initiate damage. The damage initiation force (for both thermosets and thermoplastics during static and low velocity impact tests) was found proportional to $t^{1.5}$ (where t is the panel thickness).

Sjoblom et al.[13] performed similar damage initiation studies on graphite/epoxy laminates. The epoxy panels required a 0.74 ft-lb (1 J) impact energy for delamination to

occur as shown in Figure 6. At impact energies above 2.21 ft-lb (3 J), an energy loss occurred which was attributed to rear face fiber fracture. Tests revealed that energy absorbed and damage sustained was not a linear function of impact energy. Using laminates of a different configuration, Avery and Grande[2] found an increase in energy absorption occurred for impact energies between 18.4 and 25.1 ft-lbs. The inflection was similarly attributed to rear face fiber fracture.

Foos[5] determined the average impact energy required to initiate delamination (on a per ply basis) was 0.38 ft-lbs/ply. (See Figure 7). Delamination was also found to be the primary source of energy absorption.

2.3 Effect of Stiffness and Stress Conditions on Damage

Numerous damage theories exist. Several researchers discuss lamina stiffness mismatches as a primary factor leading to delamination. Some researchers believe cracking and delamination are the result of flexure, whereas others suggest shear forces generated during impact lead to matrix cracking and subsequent delamination. One group of researchers believes damage is propagated mechanically (from front to rear) via a generator strip. Conversely, other researchers propose that through-the-thickness tensile forces create delamination beginning at the rear surface and propagating toward the impacted surface. A detailed

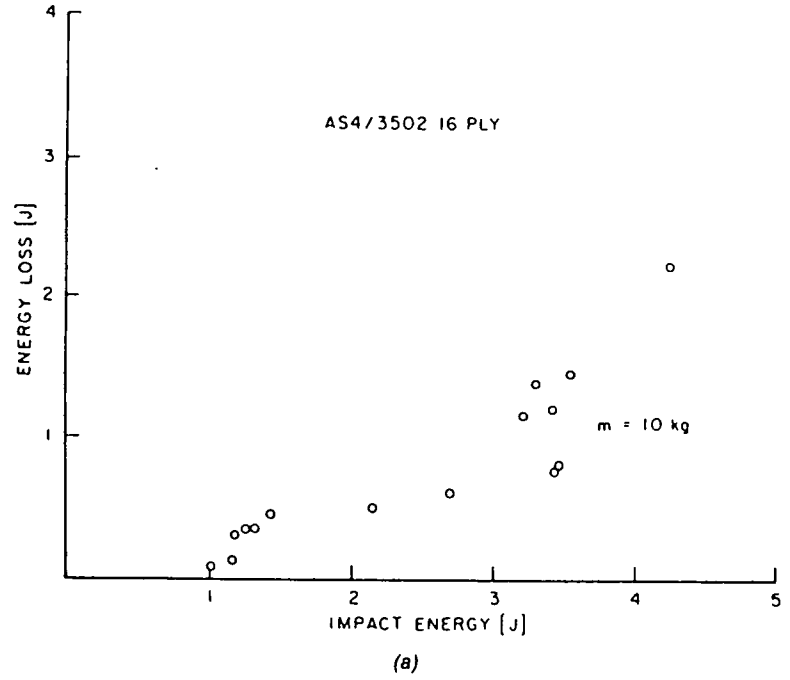

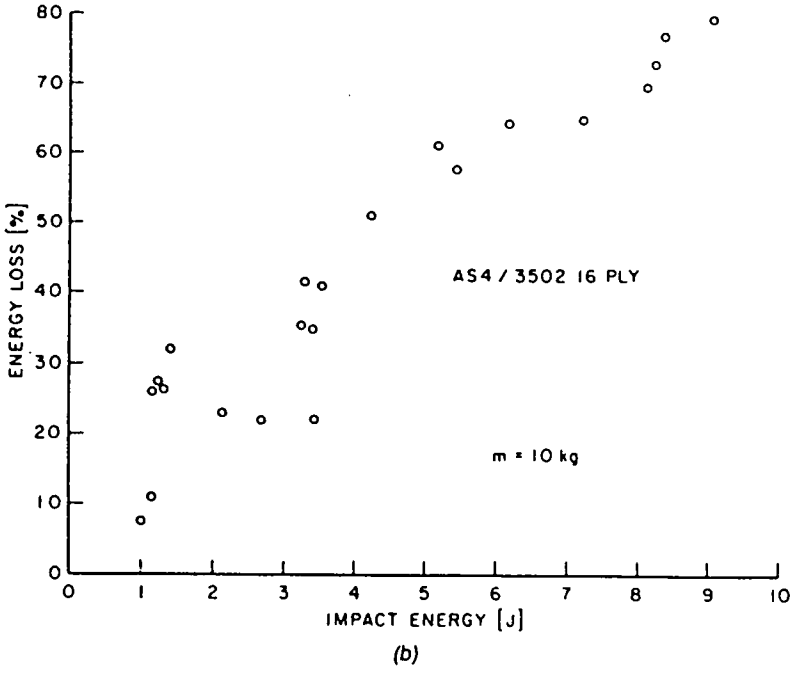

Figure 6. Impact energy vs energy loss behavior for 16-ply graphite/epoxy laminates supported on a 2.8-inch (72mm) diameter ring[13].

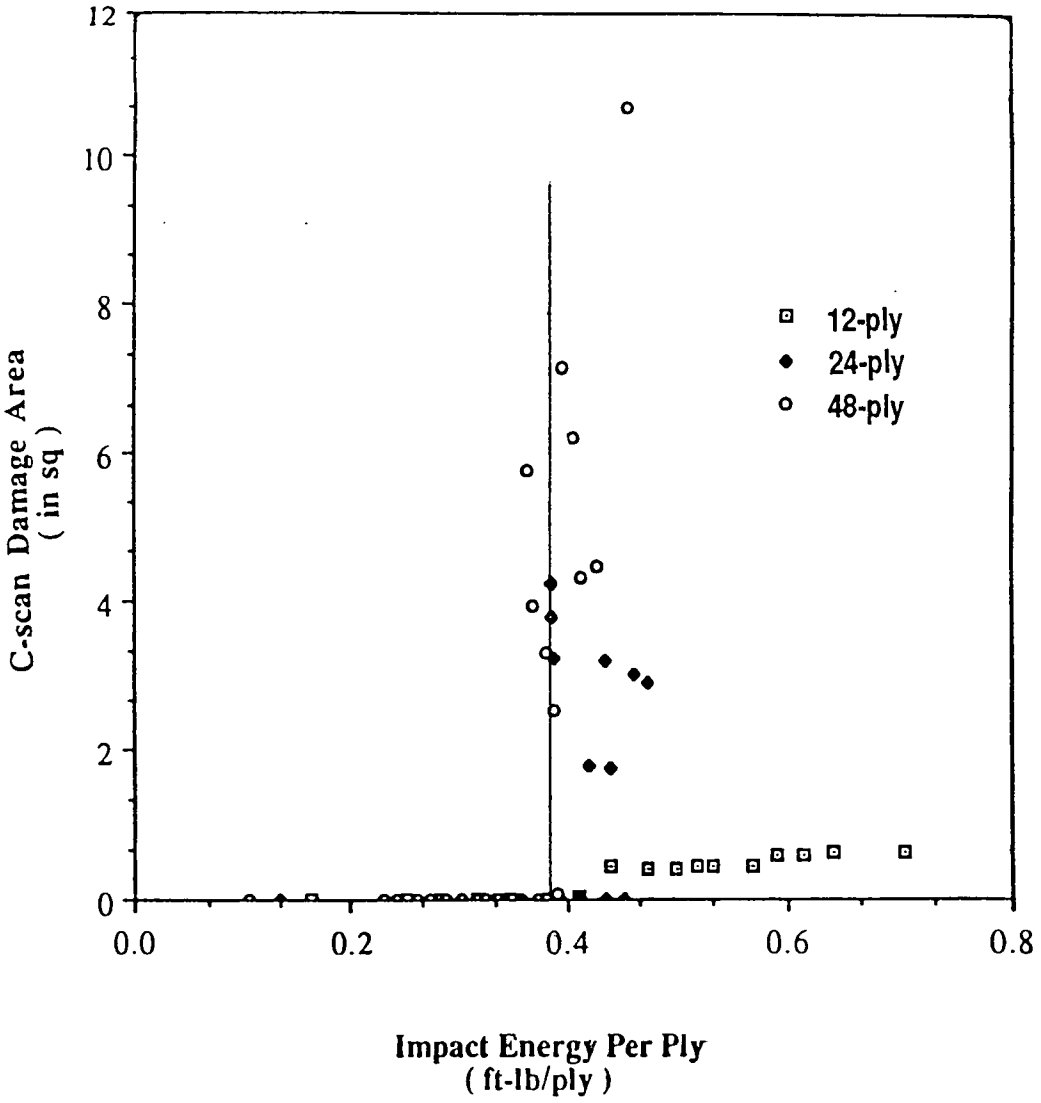

Figure 7. Delamination area vs impact energy for 12, 24, and 48-ply laminates[5].

discussion with respect to damage initiation and propagation follows.

2.3.1 The Influence of Stiffness Mismatches on Delamination

Liu[4] showed that large stiffness mismatches (a function of the angle formed by fibers between adjacent plies)

increased the potential for delamination. Stiffness mismatches were said to cause nonuniform stress distributions within the interfaces, resulting in peanut shaped delaminations. Delamination was always elongated in the lowermost ply's fiber direction. Liu tested his hypothesis by impacting six glass/epoxy plates ($[0_4/90_4]$, $[0_4/75_4]$, $[0_4/60_4]$, $[0_4/45_4]$, $[0_4/30_4]$, and $[0_4/15_4]$), each being of equal thickness and having only one favorable delamination interface. Figure 8 shows that delamination decreases with the angular difference between adjacent plies. Liu's research suggests that given some critical degree of flexure (static or dynamic), delamination will occur. Thin panels, experiencing

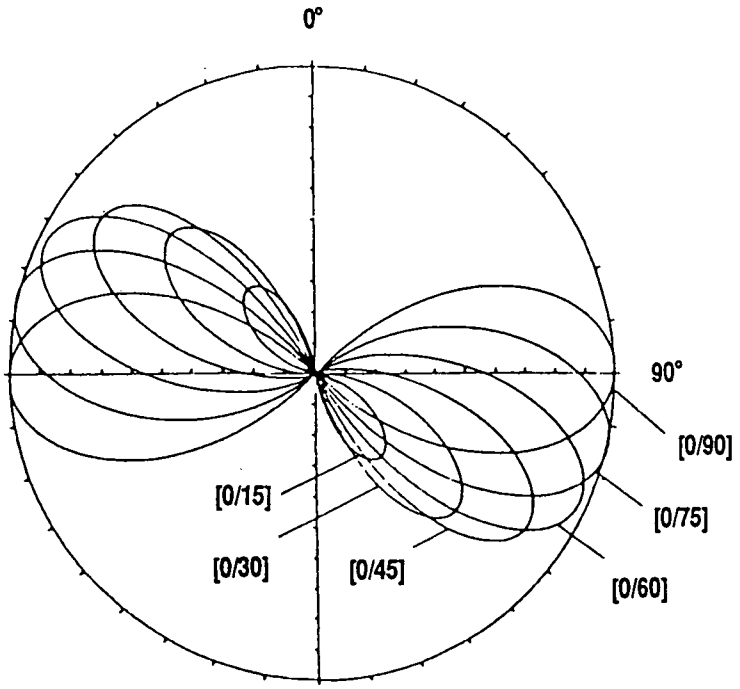

Figure 8. Normalized delamination areas as a function of the stiffness mismatch along the interface[4].

greater bending, should sustain more significant levels of delamination according to Liu's theory. However, as the author increased the thickness of his panels from $[0_4/90_4]$ to $[0_8/90_8]$ and $[0_{12}/90_{12}]$ the area of delamination was seen to increase. Foos[5] also reported that thin panels will not sustain as much delamination because energy is dissipated in flexure.

Similar to Liu, Kandalaft[18] suggests delamination is created by a combination of extensional and bending stiffness mismatches. He concluded that low matrix strength contributed to delamination initiation/growth. Liu and Malvern[14] agreed with Kandalaft's comments concerning the influence of a weak matrix and the combined extensional and bending stiffness mismatches on delamination initiation. They went further to say that fiber/matrix property mismatches contribute to matrix cracking and that interlaminar shear stresses contribute to delamination.

Avery and Grande[2] described planes of delamination which were connected by transverse interlaminar cracks to form a circular staircase. Favorable interfaces between plies were identified as those where the fiber angles are rotated in a consistent direction (CW or CCW) not more than 90°. The authors noted that when the direction of rotation was reversed (often typical of the midplanes in balanced symmetric lay-

ups), an unfavorable interface was formed and delamination did not occur.

Gosse and Mori[19] presented the K-rule as a method for predicting the spiraling distribution of delamination within an impacted laminate. Figure 9 shows a reversal of the spiral direction (CW to CCW) upon reaching symmetry at the midplane.

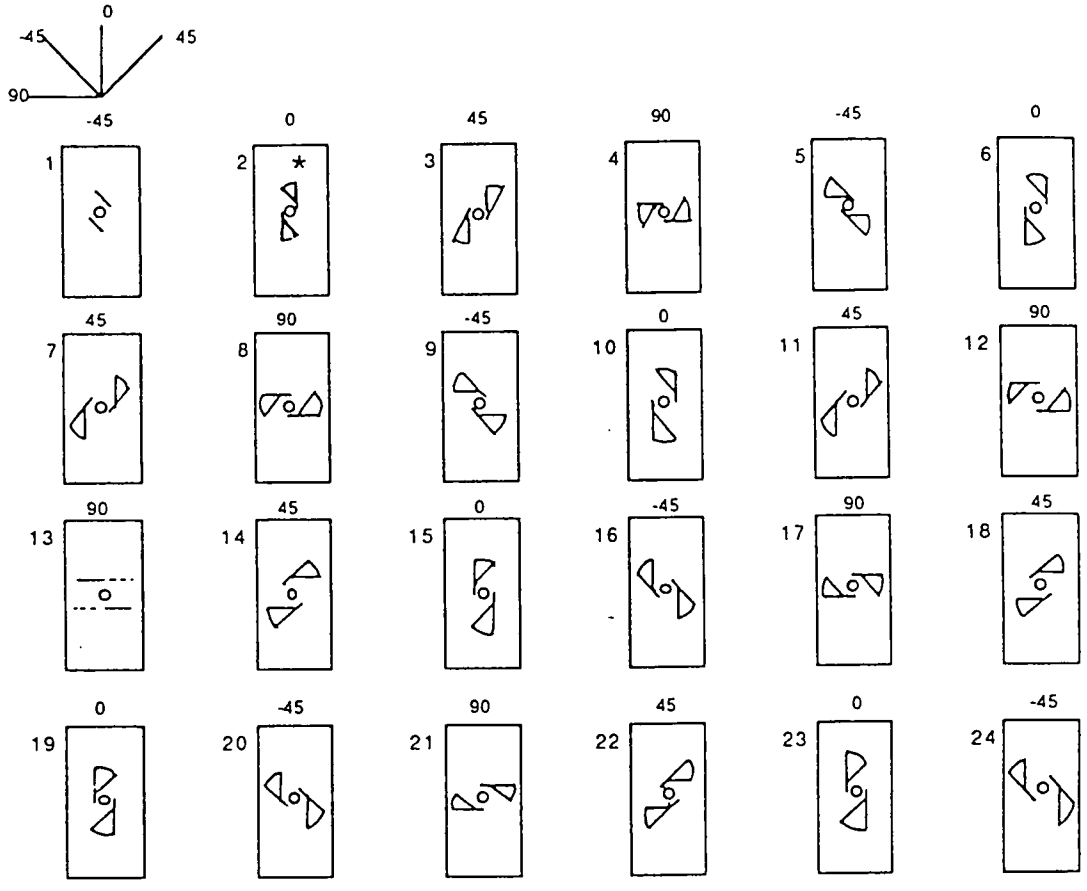

★ Delaminations shown exist between the present ply and the previous ply

Figure 9. Graphical description of damage propagation (using the K-rule) for a $[-45/0/45/90]_{3S}$ laminate[19].

Rules concerning favorable delamination interfaces and spiral reversal were not discussed.

2.3.2 The Influence of Flexure on Delamination

Hui[20] proposed that impact generated delamination may be induced by panel flexure. He credited delamination to mode II (shear) forces when the amount of flexure attained a critical value. Cordell and Sjoblom[21] proposed that bending during the impact event caused compression failures on the impacted surface and tensile failures on the laminate's rear face. Takeda et al.[22,23] suggested a large amplitude flexural wave that caused transverse cracking and delamination. Foos[5,24] believed thin laminates would fail (delaminate) in flexure, whereas thick specimens would fail (fracture) in shear. However, he noted that extreme flexure (associated with the impact of thin 12-ply laminates) resulted in little delamination.

Sun[25] found that vertical matrix cracks near the laminate's upper and lower surfaces were due to bending stresses. Slanted matrix cracks throughout the laminate were created by transverse shear stresses. His results are schematically illustrated in Figures 10 and 11. Delamination was believed to be solely the result of bending and shear induced crack propagation; not from a reflected wave.

2.3.3 The Influence of Shear on Delamination

Ramkumar and Chen[26] suggested an analysis to predict the extent of internal damage based on transverse shear stresses. Joshi and Sun[27] modeled initial stress distribution patterns for the low velocity impact case. Through-the-thickness shear stresses were believed to play a significant role in crack initiation, whereas through-the-thickness normal stresses were believed to have an insignificant effect.

Boll et al.[26] believed that most of the matrix cracking and delamination were generated from shear stresses. Tensile

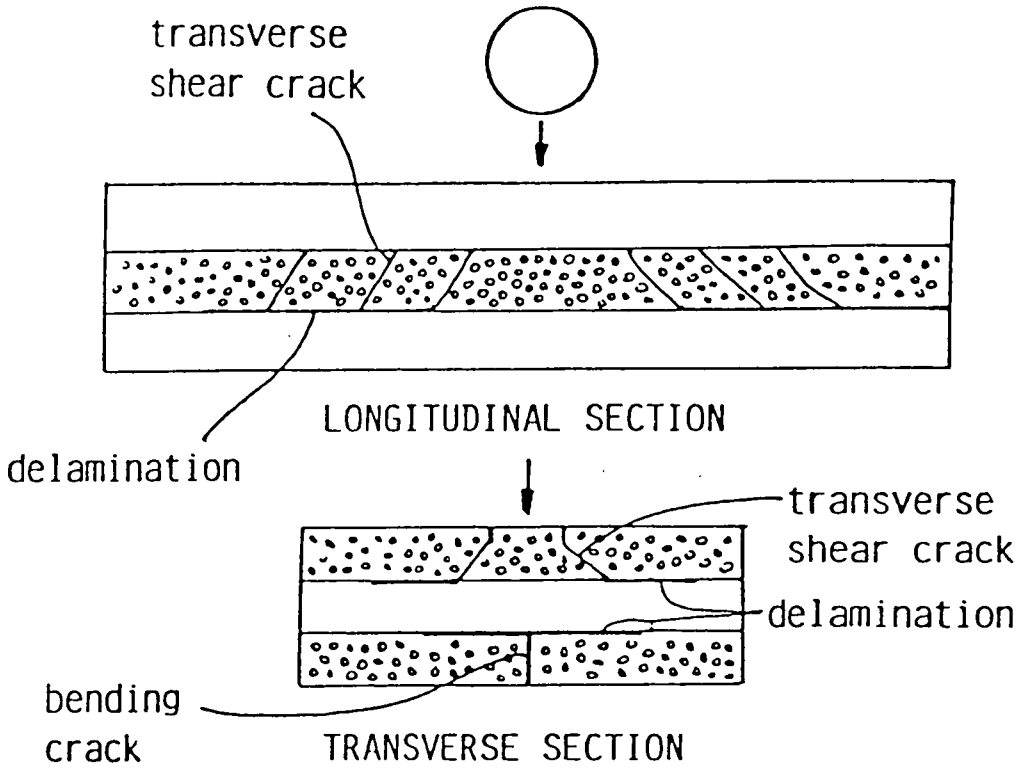

Figure 10. Failure modes in a [0/90/0] laminate[25].

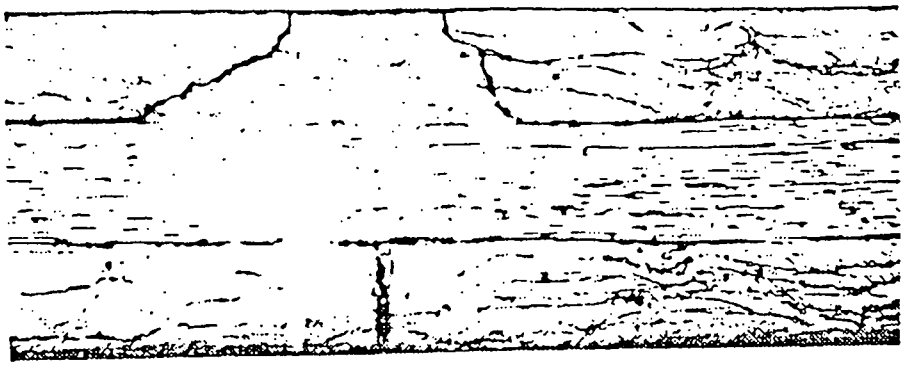

J5 N

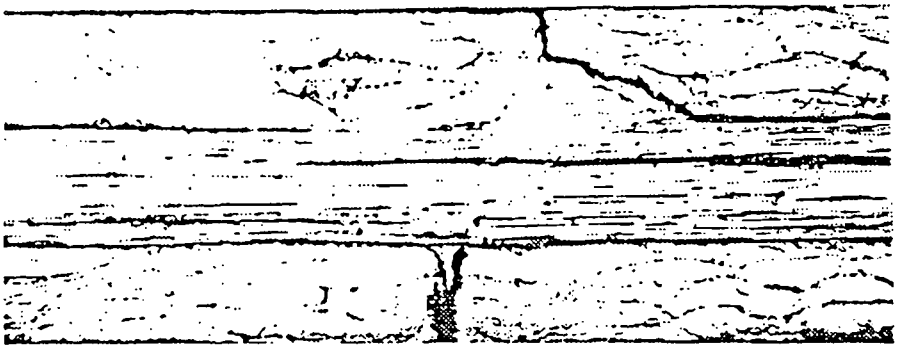

J5 F

J5 FFF

Figure 11. Transverse cross section photomicrographs showing impact induced fracture[25].

or flexural waves were believed to have sufficient magnitude to propagate delamination only to a limited extent.

2.3.4 The Influence of Tensile Stress Waves on Delamination

Several investigators[5,19,29-31] have suggested that delamination is initiated by a tensile wave rather than panel flexure. Wu and Springer[29] suggested the lateral spread of delamination is a function of the stresses at the impact location, the rate of stress change, the stress duration, the reduced stiffness difference between adjacent plies, the difference in flexural rigidities between adjacent plies, the initial flaw size, and the resistance of the material to separation. The authors rationalize their claim that delamination is caused by opposing normal forces because the K_{Ic} (fracture toughness, tension) is generally smaller than the K_{IIc} (fracture toughness, shear). Wu and Springer also noted (as did other investigators[4,7,21,22,32,33]) that delamination within each interface was elongated in the lower ply's fiber direction.

Evans and Herne[31] suggested that damage initiation coincides with stress peaks created by the propagation and reflection of stress waves within the laminate. These authors state that there is insufficient time for the damage to have been caused by quasi-static or vibrational events. They question whether damage generated during short time periods is

propagated by the slower mechanisms (i.e., flexure) or if the initial damage plays no role in, but is masked by long term quasi-static events.

Romashchenko et al.[34] modeled impact generated stress waves on a two-layer shell consisting of plastic and steel. The authors showed that a tensile unloading wave of 14.5 ksi (100 MPa) (four times yield) forms after reflection of the compression wave.

In an analysis performed by Yarve[35], impact generated tensile waves in excess of three times the laminate's ultimate through-the-thickness strength (σ_{zz}) were reported. After initial contact, a σ_{zz} compressive wave propagated toward the rear surface and eventually reflected in the form of a tensile wave. Yarve showed that the tensile wave's amplitude attenuated compressive stresses in the region of impact as shown in Figures 12 - 15. Although not discussed by the author, reverse curvature (initiating adjacent to the point of contact) formed a tensile zone that eventually propagated through the entire thickness. The tensile σ_{zz} generated from the reverse curvature was more widespread and significant than shear (τ_{xz}) stresses (also reported by Yarve).

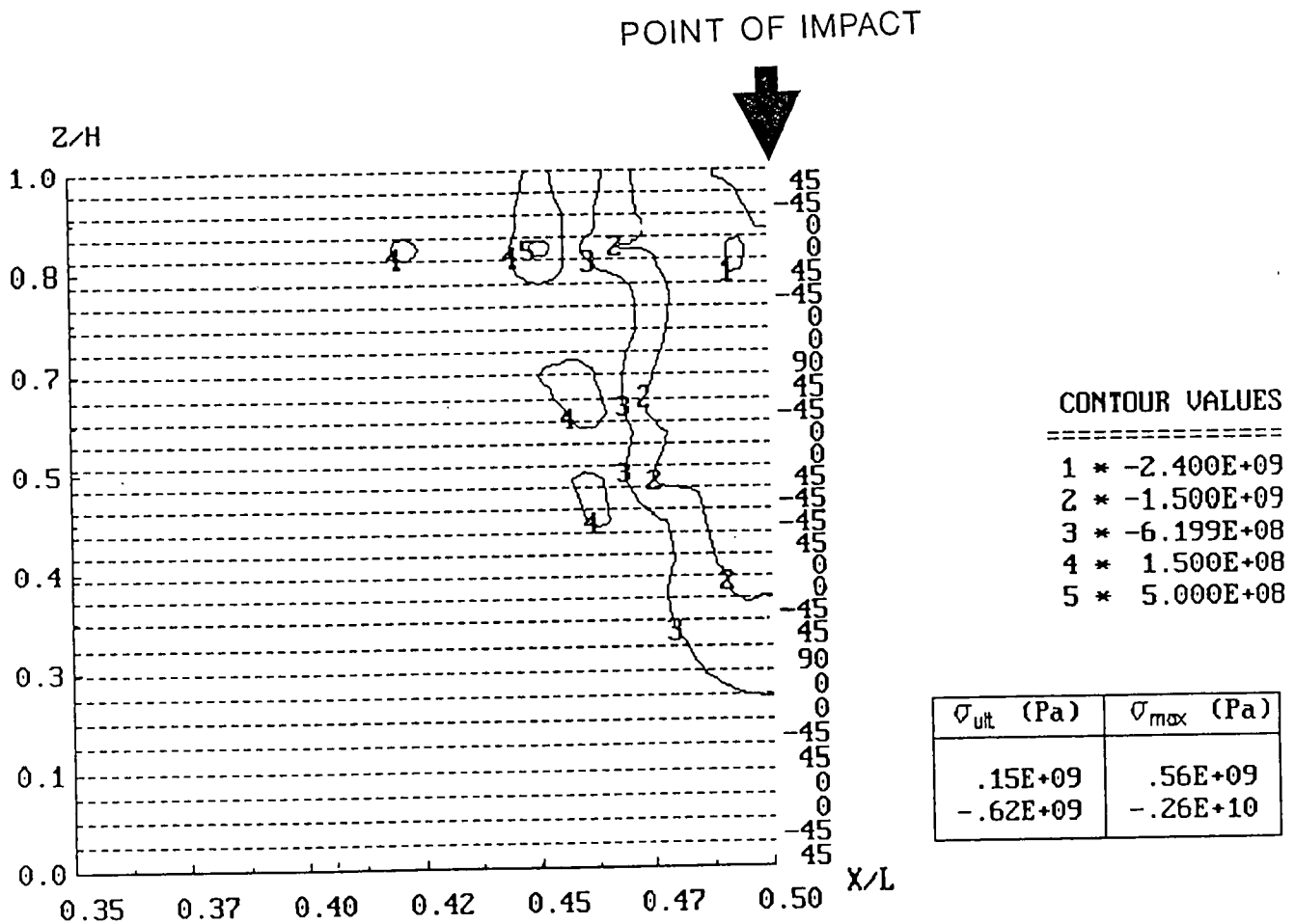

Figure 12. Transverse normal stress contours 1.13 μ-sec after impact (v = 1640 f/s)[35].

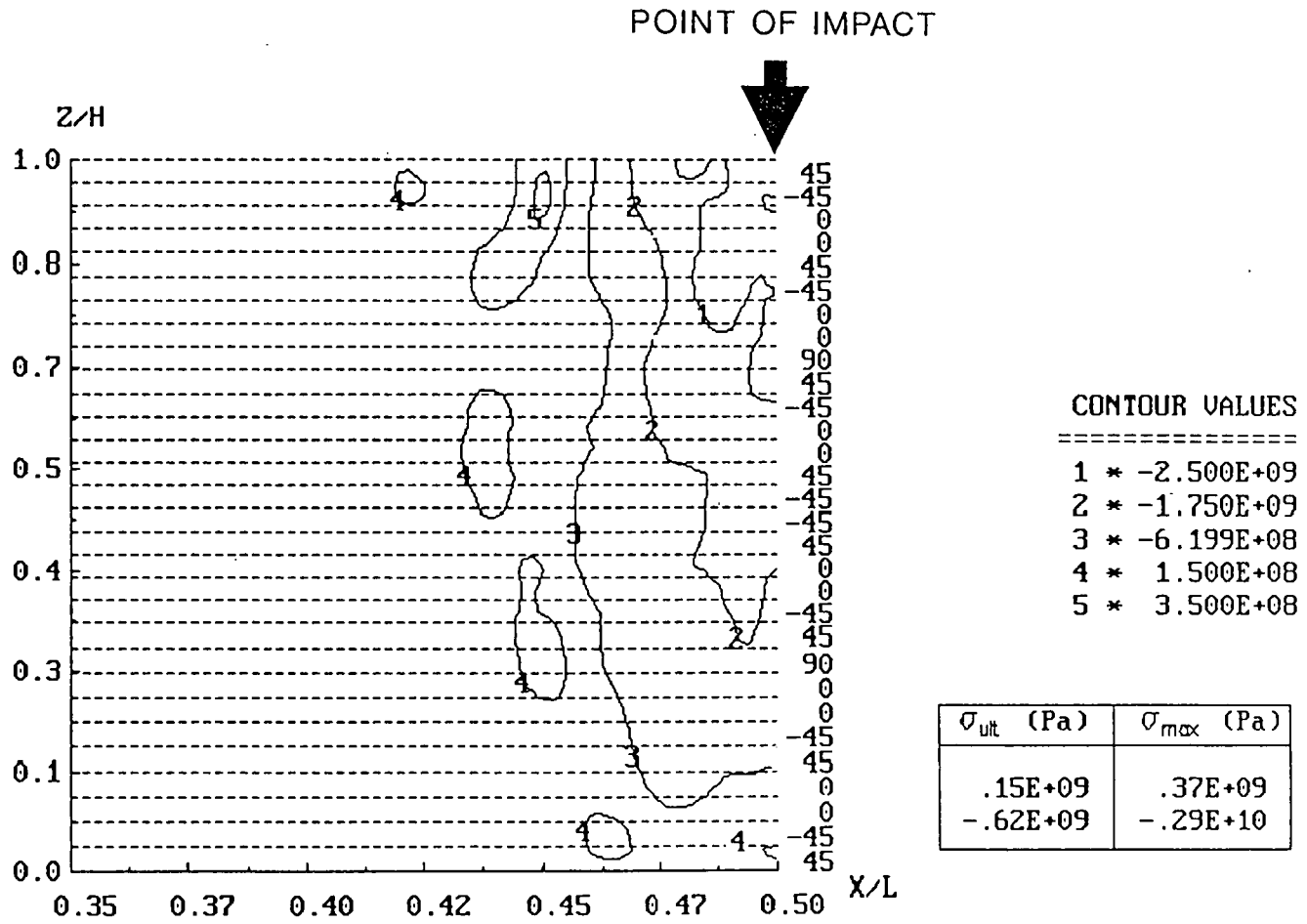

Figure 13. Transverse normal stress contours 1.81 μ-sec after impact (v = 1640 f/s)[35].

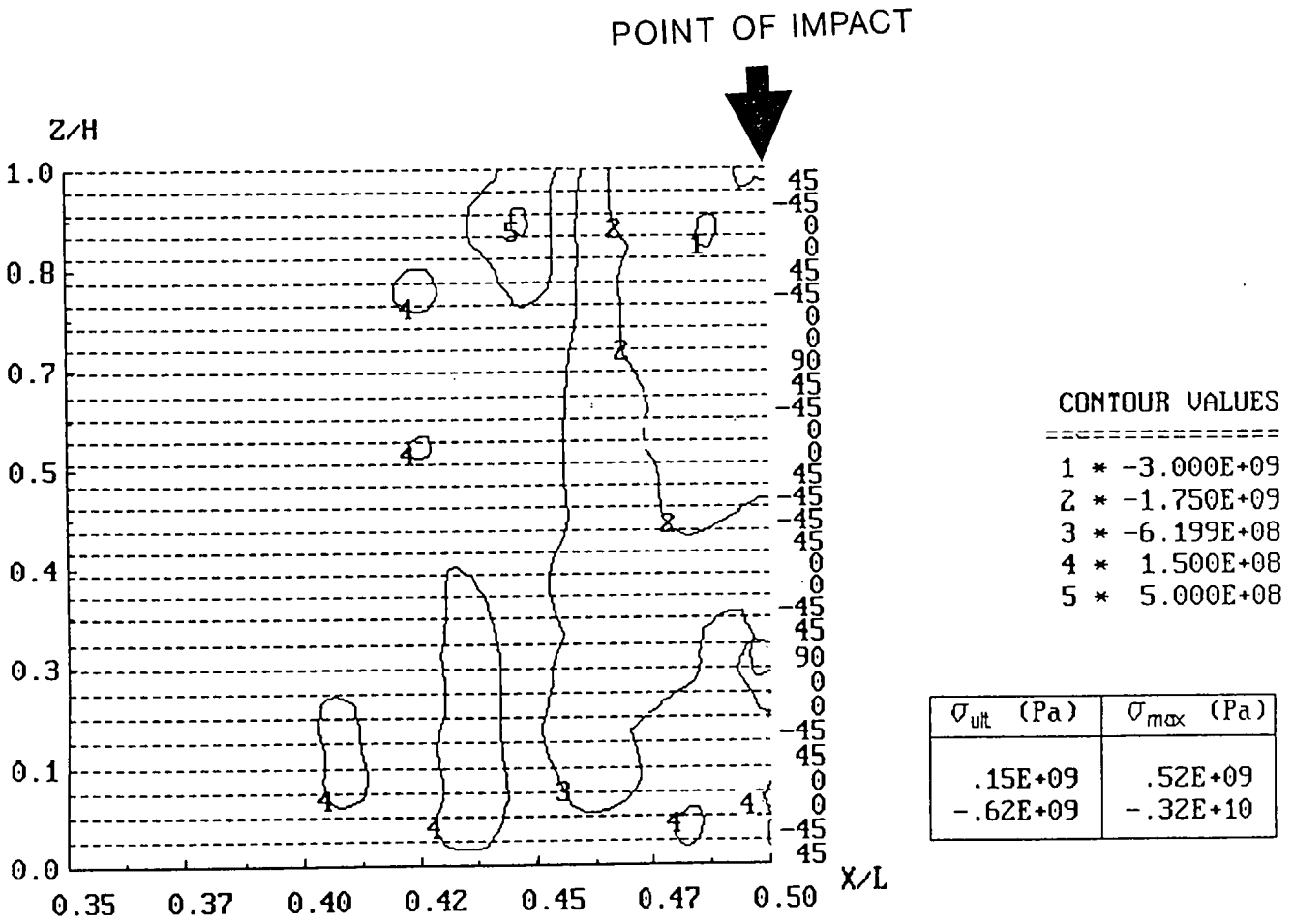

Figure 14. Transverse normal stress contours 2.26 μ-sec after impact (v = 1640 f/s)[35].

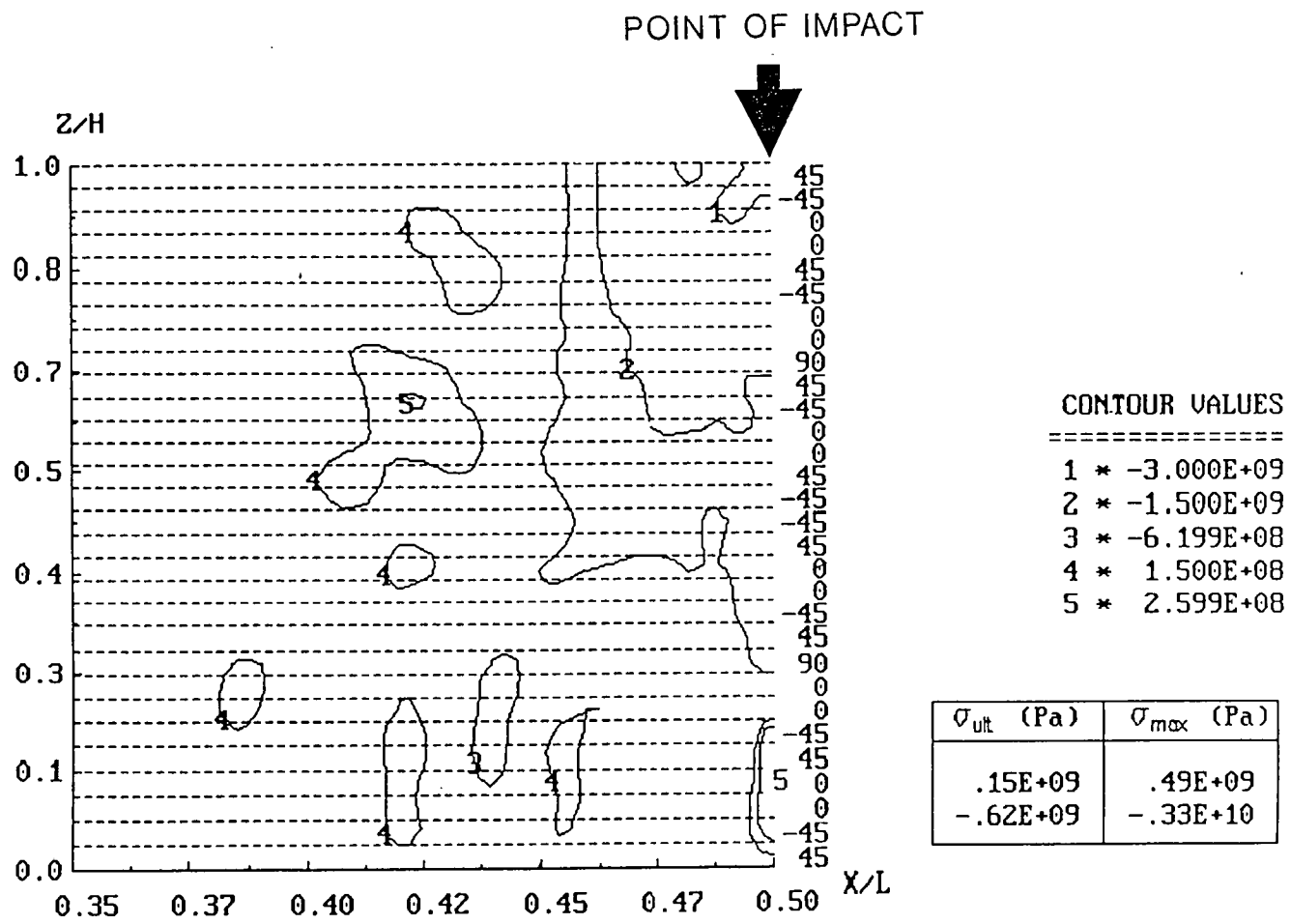

Figure 15. Transverse normal stress contours 2.83 μ-sec after impact (v = 1640 f/s)[35].

2.3.5 Other Damage Initiation Mechanisms

Sierakowski et al.[36] suggested that generator strip formation is the key factor in delamination initiation. They proposed that delamination begins when a generator strip (having a width equal to the projectile's diameter) is formed and pushes on the next ply down. The delamination process continues through the thickness of the plate. The dominate mechanism causing sequential failure is believed to change throughout the fracture process. Mechanisms include shear plugging, fiber debonding, fiber stretching, fiber fracture, fiber pull-out, delamination, matrix deformation, and matrix cracking. Two mechanisms (other than the generator strip) were said to contribute to delamination; reflected waves at the interfaces (which develop tensile stresses) and interlaminar shear waves.

Cristescu et al.[7] found that formation of the generator strip ceases when fibers within the layer are fully cut. Before being formed, the entire strip loads the next ply down and causes delamination. As the projectile's velocity is decreased during penetration, the time necessary to cut through each ply increases and the length of each successive ply's generator strip therefore grows uniformly as does the associated delamination. Delamination was believed to form only when a ply has time to resist penetration (i.e., when a generator strip has time to develop). With inadequate time

for generator strip formation, shear plugging is said to occur and was found to become more prevalent with increased projectile velocity. The authors also provided two reasons for the observed fracture mode change from shear plugging to tensile fiber failure; 1) Continued shear plugging effectively blunts the projectile's nose with an accumulation of material so that cutting can no longer occur, and 2) As the projectile is slowed, cutting may no longer be possible so stretching and breaking must occur.

Woodward and Crouch[37] modeled layered metallic laminates subjected to impact. In a two-ply model, plugging failure was studied. Results were somewhat analogous to the findings of Cristescu et al.[7] The penetrating projectile was described to accelerate a plug of material which (with continued projectile penetration) was eventually sheared from the plate. The initial stage of the penetration process ceased when the projectile and plug begin to move at the same velocity. For multi-layer laminates, the two stages of perforation are shown in Figure 16. In stage 1, a plug is accelerated ahead of the projectile as before. In stage 2 (as illustrated in Figure 16b), the projectile and a locally accelerated portion of the plug are decelerated and generate delamination as they pass through the remaining thickness of the target. Woodward commented that projectile deceleration continues after the fracture mode transition.

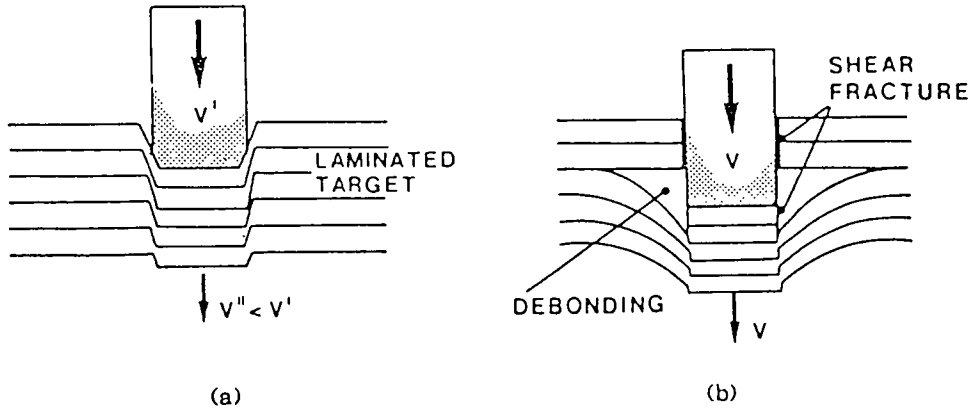

Figure 16. Penetration of a laminated target. (a) Initial shear plugging. (b) Delamination initiation[37].

2.4 Damage Propagation

Takeda et al.[23] used surface and imbedded strain gages to observe elastic waves generated during impact. Gages away from the impact location first saw an in-plane tensile wave, followed by flexural waves which tended to predominate. Transverse cracking was seen to occur before delamination initiation and propagation.

Sierakowski et al.[36] reported that flexural stress waves can propagate damage to a considerable distance from the impact site. In-plane wave speed in 0/90/0 laminates was measured to be 300 m/s in the 0° direction and 200 m/s in the 90° direction. Although the amplitude of in-plane strains generated by flexure is indeed large (albeit slow) relative to other events, out-of-plane stresses were not measured. Delamination propagation velocity was accurately observed with a high-speed camera by illuminating the rear of the plate.

Because the velocity of delamination generation was roughly the same as that of the "flexure wave", delamination is again correlated with flexure. Delamination on the upper interface stopped 100 μ-sec into the event, when flexure on the interface was at a compressive maximum. (See Figure 17.)

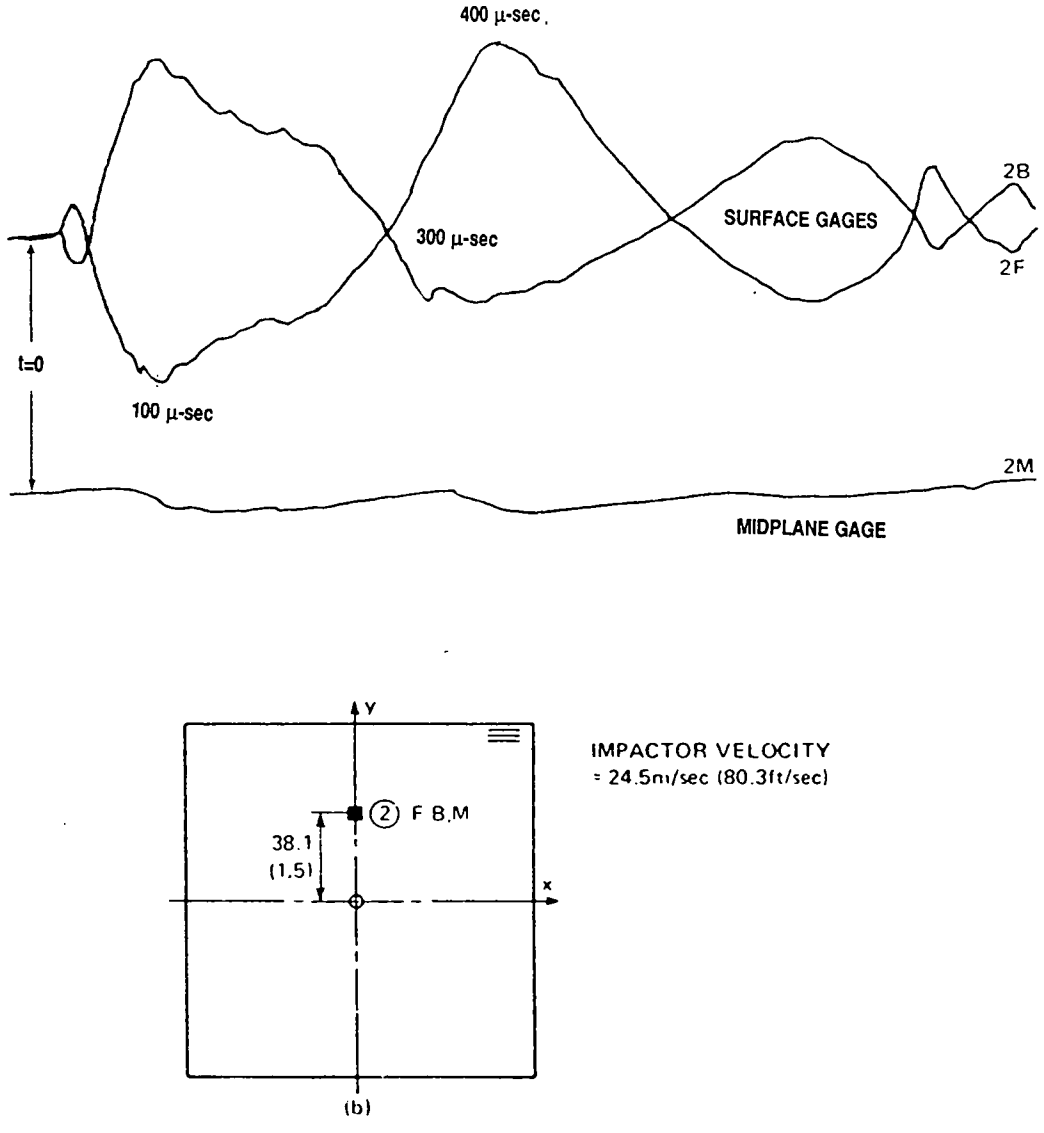

Figure 17. Output from surface and midplane strain gages on an impacted glass/epoxy laminate. (Gages were stacked 1.5-inches from the point of impact.)[36]

Delamination on the lower interface stopped 300 μ-sec after impact, when flexure on the interface was zero.

Joshi and Sun[38] performed low velocity impact tests on 15-ply laminates (having only two favorable delamination interfaces) which apparently resulted in bending induced fracture. Upon impact, a shear crack propagated through the 0° outer surface plies to the first 0/90 interface encountered. Because the crack could not continue unimpeded through the material without severing 90° fibers, the crack changed directions and continued in the form of delamination along the interfaces.

Fiber fracture was reported by Avery and Grande[2] to initiate on the front face, jump to the rear face, and then progress through the core. Figure 18 shows how fiber fracture progressed through the center of the core. (Note that the damage shown is only fiber fracture and not delamination.)

2.5 Summary of Models Describing Damage Evolution

Based on the previous research presented, several theories exist which describe the causes for impact generated damage within composite laminates. One theory suggests delamination is formed only after the target material is accelerated to match the projectile's instantaneous velocity. Another theory suggests delamination is a function of bending

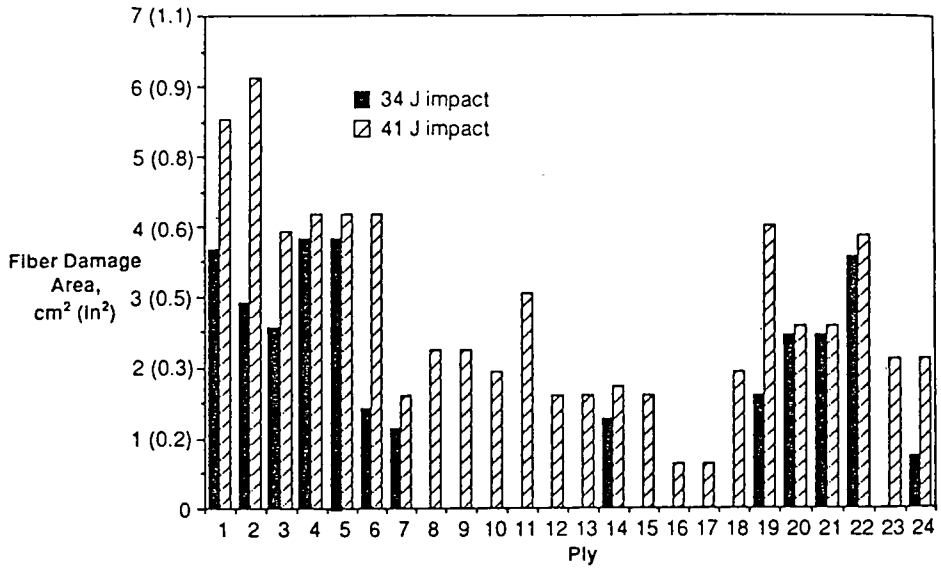

Figure 18. Fiber damage per ply for a $[45/0/-45/90_2/-45/0/45_2/0/-45/90]_s$ laminate[2].

and extensional stiffness mismatches between adjacent plies. In a third theory, flexure is identified as the primary source of delamination generation, whereas another suggests shear forces are the cause. A more mechanical explanation of delamination generation and propagation (that of generator strip formation) is presented in another theory. Finally, the laminate's tensile wave is identified as having the potential for delamination generation.

The following commentary is provided to identify anomalies encountered during the review of previous research.

2.5.1 Delamination Initiation upon Material Acceleration

As suggested by Cristescu et al.[7] and Woodward and Crouch[37], a transition from shear plugging to delamination occurs when laminated material in front of the projectile is accelerated to match the projectile's instantaneous velocity. Upon first contact with the laminate, the projectile begins to decelerate as the laminate's material is locally accelerated. Initially, the projectile's velocity is so much greater than that of the accelerating target material that penetration in the form of shear plugging occurs. Only when a plug of material within the laminate becomes fully accelerated (matching the projectile's velocity) does a transition in the fracture mode occur from shear plugging to delamination. Although this theory neglects the presence of stress waves and suggests delamination will occur simultaneously (rather than progressively from the rear face inward), the theory is compatible with observations that shear plugging continues for a considerable depth within the laminate before a transition to delamination occurs.

Complexities enter into the rationalization process when ideas presented by the forementioned researchers[7,37] are applied to high velocity penetration. At velocities just above the V_{50} (defined as the velocity where 50% of the projectiles are expected to penetrate the target), the transition from shear plugging to delamination is commonly

visible with the naked eye. For higher velocity impacts, the shear path may progress through the entire laminate as shown in Figure 19. Although in-depth analyses (via both nondestructive and destructive methods) indicate that a transition from shear plugging to delamination occurs toward the laminate's center, the projectile's velocity (combined with the delaminated material's inertial resistance) allows continued shearing through the thickness. The possibility of shear punching being continuous, despite the sudden transition to delamination, appears incompatible with this theory.

2.5.2 Lamina Stiffness Mismatches

Liu[4,14] and Kandalaft's[18] suggested that lamina stiffness mismatches were a primary factor leading to delamination. The greater the stiffness mismatch (resulting from a change in the fiber direction between adjacent plies), the greater the

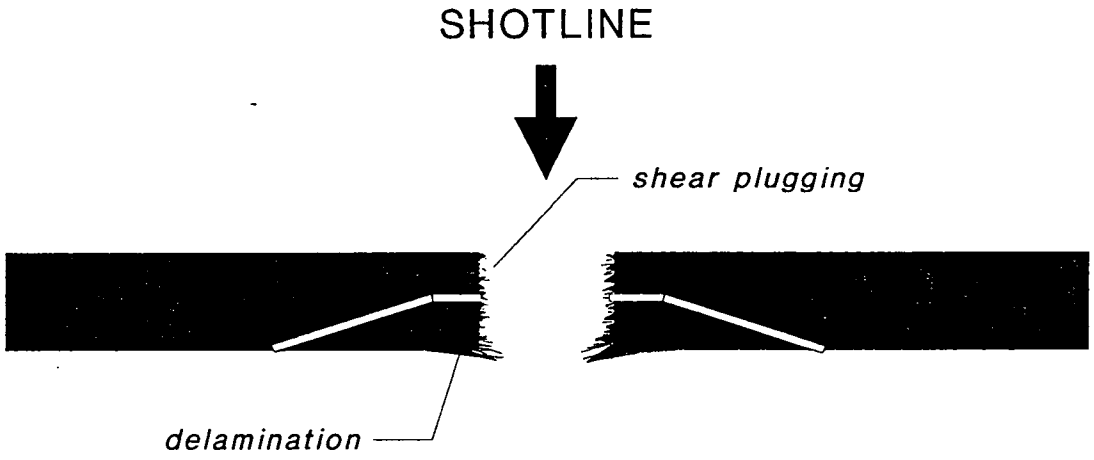

Figure 19. Dual mode fracture sustained by penetrated graphite/epoxy laminates (high velocity).

potential for delamination. Stiffness mismatches were said to result in nonuniform stress distributions along the interface in both bending and extensional loading conditions. Delaminations were identified as being somewhat peanut shaped and elongated parallel to the interface's lowermost ply. Substantiated experimentally, this theory proved that as the fiber angle between adjacent plies increased, the extent of delamination also increased. The suggestion is, given some critical degree of flexure (static or dynamic), delamination will occur. However, for reduced panel flexibility (resulting from thickness increases), the area of delamination was seen to increase. Other researchers[4,5,18,33] also found that thin panels (which experienced significant flexure) sustained relatively little delamination.

2.5.3 Flexure Assisted Damage

Perhaps based on Liu's[4,14] and Kandalaft's[18] work, others[20-24] suggested that matrix cracking and delamination were the result of flexure or flexure waves. Hui[20] credited delamination to mode II shear forces when the amount of flexure reached a critical value. Takeda, Sierakowski, and Malvern[22,23] believed flexural waves caused transverse cracking and delamination.

Although matrix cracking is likely influenced by flexure, other studies[4,5,18,33] found the degree of bending was somewhat

inversely proportional to the extent of delamination. While maintaining an equal number of favorable delamination interfaces, the laminate thickness (and therefore stiffness) was increased which resulted in greater levels of delamination. Tests such as these suggest flexure is not a cause of delamination. Perhaps at low impact velocities, the lack of inertia provided by thin laminates allows considerable energy absorption in the form of flexure. This idea is in compliance with earlier comments that flexure is only able to influence the extent of delamination in laminates thinner than 32-plies.

Sierakowski et al.[36] reported that delamination was the result of flexural stress waves. Although the recorded amplitude of in-plane strains generated by flexure was indeed large relative to other events, out-of-plane stresses were not measured. Delamination on the upper interface stopped 100 μ-sec into the event, when flexure on the interface was at a compressive maximum. (Refer back to Figure 17.) Delamination on the lower interface stopped 300 μ-sec after impact, when flexure on the interface was zero. Note however that at 400 μ-sec the upper interface is subjected to the highest flexure of the impact event and no further delamination occurs.

2.5.4 Shear Force Damage

Several investigators[24-28] have suggested that shear forces generated during impact lead to matrix cracking and subsequent delamination. Cross sections of impacted laminates seem to correlate with this idea. Only slanted shear cracking was shown to be associated with delamination. The theory suggests, however, that shear cracking propagates through the laminate from the impact point and fails to recognize any change in fracture modes along the penetration path. Delamination is not recognized to initiate adjacent to the rear face.

2.5.5 Damage Formation Through Generator Strips

One research group [7,36] suggested that delamination is propagated mechanically from the formation of a generator strip. Delamination is assumed to initiate when a generator strip (having a width equal to the projectile's diameter) is formed and pushes on the next ply down. The process then continues through the laminate's thickness. Differences in the area of delamination through-the-thickness are associated with the time necessary for the projectile to cut through each lamina. (As the projectile is decelerated, more time is available for generator strip formation.)

Delaminations form only when a ply has time to resist penetration (i.e., when a generator strip has time to

develop). With inadequate time for generator strip formation, shear plugging is said to occur and become more prevalent with increased projectile velocities. Experimental checks on the theory appear to be limited. Had a laminate been impacted at a velocity known to be slow enough for generator strip formation (i.e., the projectile's residual velocity from a test where delamination occurred), shear plugging adjacent to the impacted surface would again be present. Although the authors realized two zones of fracture are common (shear plugging and delamination), they failed to realize the true sequence of events. The influence of stress waves was never considered and delamination is believed to progress in the projectile's direction.

2.5.6 Damage Generation as a Result of the Tensile Stress Wave

Many researchers[19,30,31] have suggested that the laminate's tensile wave has a significant influence on delamination generation. Foos[5] suggested rear face delamination was the result of a tensile stress wave (a reflected compression wave) and experimentally observed delamination initiating on the rear face and propagating toward the impacted surface as impact energy was increased. Wu and Springer[29] rationalized their claim that delamination is caused by opposing normal forces because the Mode I fracture toughness (G_{Ic}) for composite materials' interfaces is generally quite small. In an analysis performed by Yarve[35], impact generated tensile

waves in excess of three times the laminate's ultimate through-the-thickness strength (σ_{zz}) were reported. The tensile σ_{zz} generated from the reverse curvature appeared more widespread and significant than τ_{xz} stresses. If matrix cracks were caused by shear and were required for delamination to occur, the σ_{zz} (already present) is expected to create delamination.

The idea of delamination progressing from the rear face inward is compatible with the experimental data showing the delamination on any interface is elongated in the direction of the interface's lowermost ply. If delamination proceeds from the bottom up, the lower ply is given the opportunity to flex downward and create delamination elongated in the lower ply's fiber direction. Delamination will only occur in the fiber direction because intraply cracking will occur before delamination can spread laterally. The upper plies remain laminated together and maintain rigidity while the lower plies separate sequentially according to the tensile wave's position and amplitude.

2.5.7 Discussion

For the literature reviewed, none of the authors described the mechanics behind transition plane formation. Similarly, through-the-thickness stress wave measurements,

such as those performed in conjunction with this thesis, have not been previously encountered.

CHAPTER III

HYPOTHESIS

This thesis investigates the validity of the hypothesis that the transition from shear plugging to delamination occurs due to the interaction between the laminate's tensile wave and a localized compression front associated with a non-planar projectile. When the projectile first contacts the laminate, two compressive stress waves are generated simultaneously. One wave propagates into the laminate and the other is attenuated within the projectile. The laminate's wave is expected to have a velocity based on the material's modulus and density. With the possible exception of matrix microcracking caused by the high rate of loading, insignificant damage is created by the laminate's compressive wave. As propagation continues, the laminate's wave is eventually reflected off the free surface and returns as tensile wave. Tensile forces applied normal to the laminate are expected to result in delamination. Because the tensile wave is initiated adjacent to the laminate's rear face and propagates toward the impacted surface, so too will the delaminations.

Energy associated with the tensile wave is attenuated as work is performed during the delamination process. With energy attenuation, the magnitude of delamination generated on each interface decreases proportionately, but remains influenced by the stiffness mismatch. The laminate's tensile wave amplitude will be fully attenuated upon coincidence with the localized compression zone formed in front of the projectile. Any release wave transferred from a non-planar projectile to the laminate should not significantly change the amplitude of the localized compression zone preceding the projectile. The tensile wave/compression zone interaction should create a well defined plane where a transition of fracture modes occurs from shear plugging to delamination. (Note: The shear plug pushed in front of the projectile may add to the apparent depth of the compression zone.) With continued penetration, the projectile passes through the transition plane and into the delaminated zone. Resistance to penetration therefore changes based on the new material state being penetrated. This change in resistance amounts to a change in the rate at which the projectile's velocity (and therefore kinetic energy) is lost.

At very high velocities, the shearing process is expected to continue through the delaminated plies, but without affecting the transition plane's position. Shearing through

previously delaminated material at high velocities is expected to result in insignificant additional structural damage.

The hypothesis presented here accurately lends itself to observations made by previous investigators. In studies performed by Foos[5], delamination was seen to initiate at the rear face and (with increased impact energy) propagate toward the impacted surface. Experiments performed by several other investigators[6,21,28,30,39] correlated with Foos' studies in that delamination was seen to be most prevalent adjacent to the rear face. In studies involving complete penetration[6,7,30], shear plugging is noted to eventually transition to a zone of delamination. Other research[4,14,18] indicated a relationship between the bending and extensional stiffness mismatches and the extent of radial delamination generated. In an unrelated in-house study[40], laminates impacted by projectiles at a high obliquity angles sustained delamination which was concentrically located around a point on the rear surface, opposite the initial point of contact. Continued penetration resulted in the laminate's material simply being pushed out of the way with little additional delamination occurring even when the projectile passed outside the initial delamination zone.

CHAPTER IV

MATERIALS, TEST METHODS, AND PROCEDURES

4.1 General Description of Approach

In this study, a series of instrumented graphite/epoxy composite laminates are impacted by steel spherical projectiles. Although several external dynamic measurements are made, imbedded within the targeted laminates are an alternating series of stress and strain gages to monitor the diverging stress wave. Rear face panel deflections are recorded optically during the impact event and are correlated with stress events. Impact and residual projectile velocities are recorded, as are changes in the specimen's weight, for energy calculations. Post-mortem investigations are limited to C-scans (to evaluate the area of delamination and approximate volume of damage) and are used to correlate fracture modes with data recorded during the impact event. Stress, strain, displacement, and NDI data are used to evidence the source of delamination initiation and propagation. Delamination is assumed to occur simultaneously with tensile stress output.

Three Taguchi L8 matrices (details of which are included in Appendix A) were established to fully investigate through-

the-thickness stress wave propagation and the wave's influence on fracture modes. Although the complete experiment will occur over a period of time beyond the scope of this thesis, several key experiments within the third Taguchi matrix (and several substantiation experiments involving penetration velocities) were performed to meet thesis goals. Experiments performed to satisfy the third L8 are underlined in Table 1.

TABLE 1. Penetration tests based on the third Taguchi L8 matrix.

SHOT NO.	TEST NO.	DENSITY (lb/in^3)	VELOCITY (f/s)	THICKNESS (plies)
1	7R	0.284	2380	32
2	8	0.284	2380	128
3	5	0.284	LOW	32
4	6	0.284	LOW	128
5	6R	0.284	LOW	128
6	2	0.099	LOW	128
7	1R	0.099	LOW	32
8	1	0.099	LOW	32
9	4R	0.099	2380	128
10	7	0.284	2380	32
11	4	0.099	2380	128
12	3	0.099	2380	32

4.2 Materials

The composite material used throughout this study is graphite/epoxy (AS4/3501-6). Two quasi-isotropic laminate thicknesses (32-ply and 128-ply) are used in the study to assist in determining flexure effects on delamination. Although the quasi-isotropic 32-ply lay-up $[(0/90/+45/-45)_4]_s$ was held constant, two different panel configurations were

established. For use in V_{50} tests, the test laminates were monolithic (fabricated in one step). For stress wave experiments, the 32-ply laminates actually consisted of four unbalanced unsymmetric sublaminates post-bonded together (after sensor installation on each of the three interfaces). Similarly, 128-ply $[(0/90/+45/-45)_{16}]_s$ laminates consist of eight sublaminates with sensors on each of the seven interfaces.

The 32-ply laminates have 30 potential delamination interfaces as compared to 126 in the 128-ply panels. Besides the -45/-45 interface along each laminate's midplane, after every four plies a nonfavorable -45/0 interface is present. (According to Avery and Grande[2], nonfavorable interfaces occur whenever the angle between fibers in adjacent plies exceeds 90° after a spiraling rotation direction is established.) The number of favorable delamination interfaces are therefore 24 for the 32-ply laminates and 96 for the 128-ply laminates. (Note: If flexure was believed the primary cause of delamination, ideally both thick and thin laminates would have the same number of favorable delamination interfaces for potentially equal energy absorption during the delamination processes. Previous studies[4,14] have evaluated laminates of differing thicknesses with an equal number of favorable delamination interfaces and found flexure related delamination was minimal.)

4.2.1 Specimen Dimensions and Boundary Conditions

All test specimens measured 8x8 inches. The dimensions were chosen to ensure radial wave propagation and reflection did not interfere with through-the-thickness stress wave measurements. Specimens were clamped around the periphery, yielding a 7x7-inch free surface. Actual edge conditions provided by the fixture were assumed to fall somewhere between fully clamped and simply supported. Care was taken to ensure an equal degree of clamping was used from specimen to specimen, even though previous researchers[14,18,32] found that boundary conditions sufficiently remote from the point of impact do not influence the damage state.

4.2.2 Specimen Bondlines

Ideally, sublaminate bondlines would have mechanical properties identical to the 3501-6 resin; however, temperature limitations of the imbedded sensors required that a room temperature curing epoxy be used. The non-toughened system selected was Hysol's RE2039 epoxy with HD3719 hardener (mixed at a 1:1 ratio) and was expected to allow delamination as readily as the 3501-6 system. Because each bondline is void of fibers (eliminating the possibility of fiber bridging), the bondline's fracture toughness is potentially lower than anywhere else in the laminate. Since fiber bridging associated with the AS4/3501-6 system is typically negligible however, the Hysol bondlines were assumed not to influence

delamination excessively. In any event, post-mortem studies (i.e., C-scanning) were performed to evaluate the bondline's influence.

4.2.3 Projectile

Spherical projectiles were chosen for this study to produce a high-amplitude short-duration wave front. Although simple spheres do not possess the complex geometry of threats commonly encountered in battlefield environments, spheres provide the necessary uniformity for repeatable testing while maintaining projectile/target interactions similar to those generated by typical blunt projectiles. All tests were performed using a 0.5-inch chromium steel sphere having a density of 0.284 lb/in^3 (7.9 g/cm^3) and modulus of 30 msi.

4.3 Specimen Instrumentation

Original plans included piezofilm sensors as the sole means of recording transverse (through-the-thickness) stress wave amplitudes. Concern over diverging stress waves and Poisson's effects forced a shift to a combination of more conventional gages. (Piezofilm sensors would have indicated an unknown combination of in-plane and normal stresses.) In an attempt to differentiate between radial and transverse wave amplitudes, carbon stress gages (relatively insensitive to in-plane stresses) and constantan strain gages (relatively insensitive to normal stresses) were chosen for the study.

(Carbon stress gages had an active area of 0.05x0.06 inch, whereas the active are of constantan strain gages was 0.1x0.1 inch.) All gages were dispersed throughout each panel in an alternating fashion (Figure 20) and used to track the stress wave's progress and pin-point the transition plane's location.

All sensors were positioned along the shotline in the geometric center of the panel. Sensors located on the midplane were sandwiched between a pair of -45° plies (a nonfavorable delamination interface), whereas the other sensors were mounted on "favorable" 0/-45 interfaces.

Significant reductions in the measured stress wave amplitude were correlated with damage generated, as observed during post-mortem studies. To eliminate the effect of flexure and provide a direct observation of stress wave's dilatation and Poisson's effects, strain gages were positioned on the panel's centerline. (Calibration procedures for the imbedded stress and strain gages are discussed in Appendix B.)

In addition to the imbedded sensors, an external PVDF (piezofilm) sensor was installed on the specimen's surface and used to mark the projectile's time of first contact.

Rear surface displacements were obtained at 200 KHz via fiber optic means. To avoid damaging the fiber optic wand,

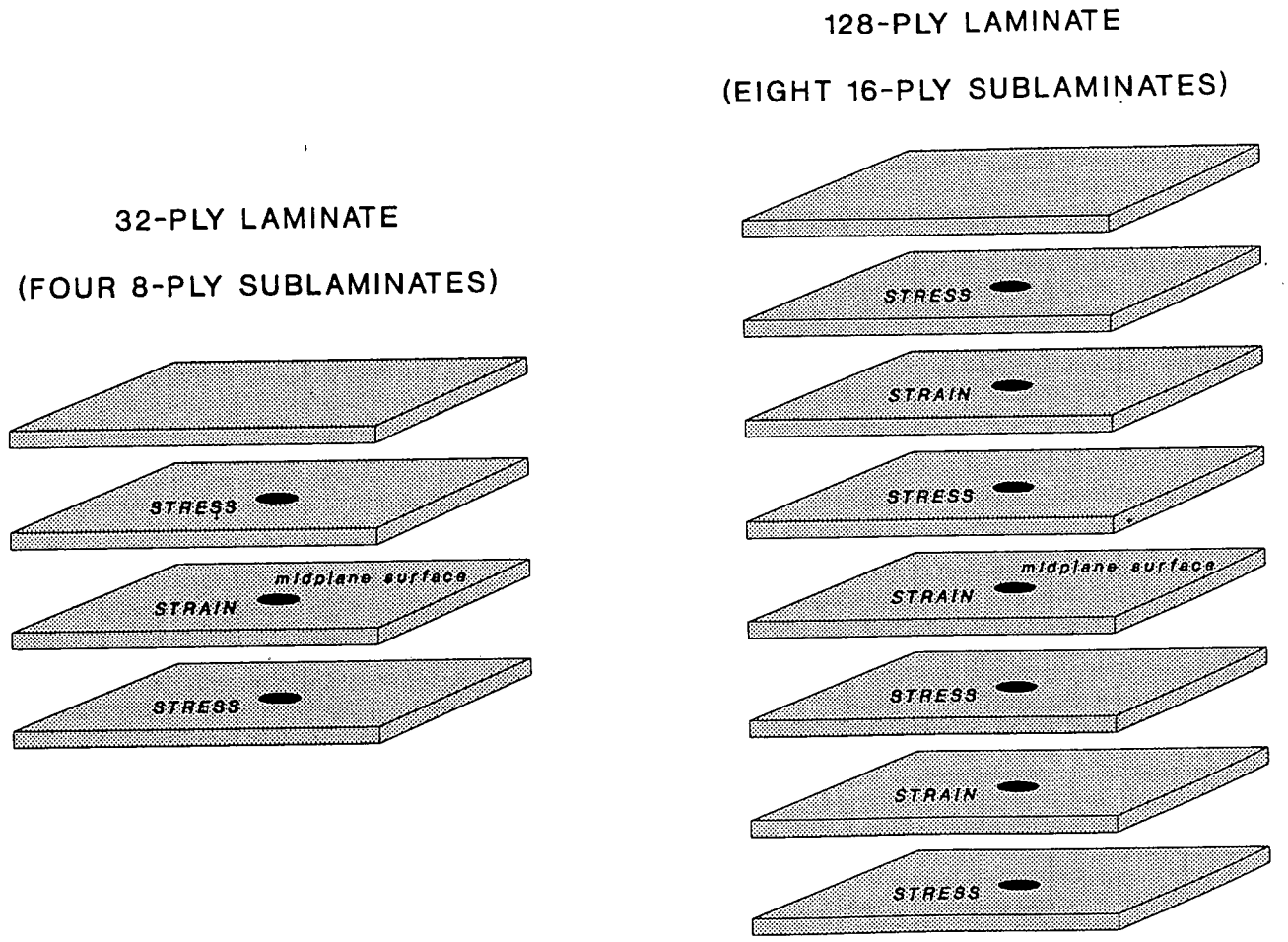

Figure 20. Gage stacking sequence within 32 and 128-ply laminates.

the sensor was positioned 1.5 inches off-center from the shotline as shown in Figure 21. (The calibration procedure for fiber optic displacement sensors is discussed in Appendix B.)

4.4 Experimental Facility

The range setups for V_{50} and stress wave tests are shown in Figures 22 and 23, respectively. Projectile impact velocities were determined from light-screens which were

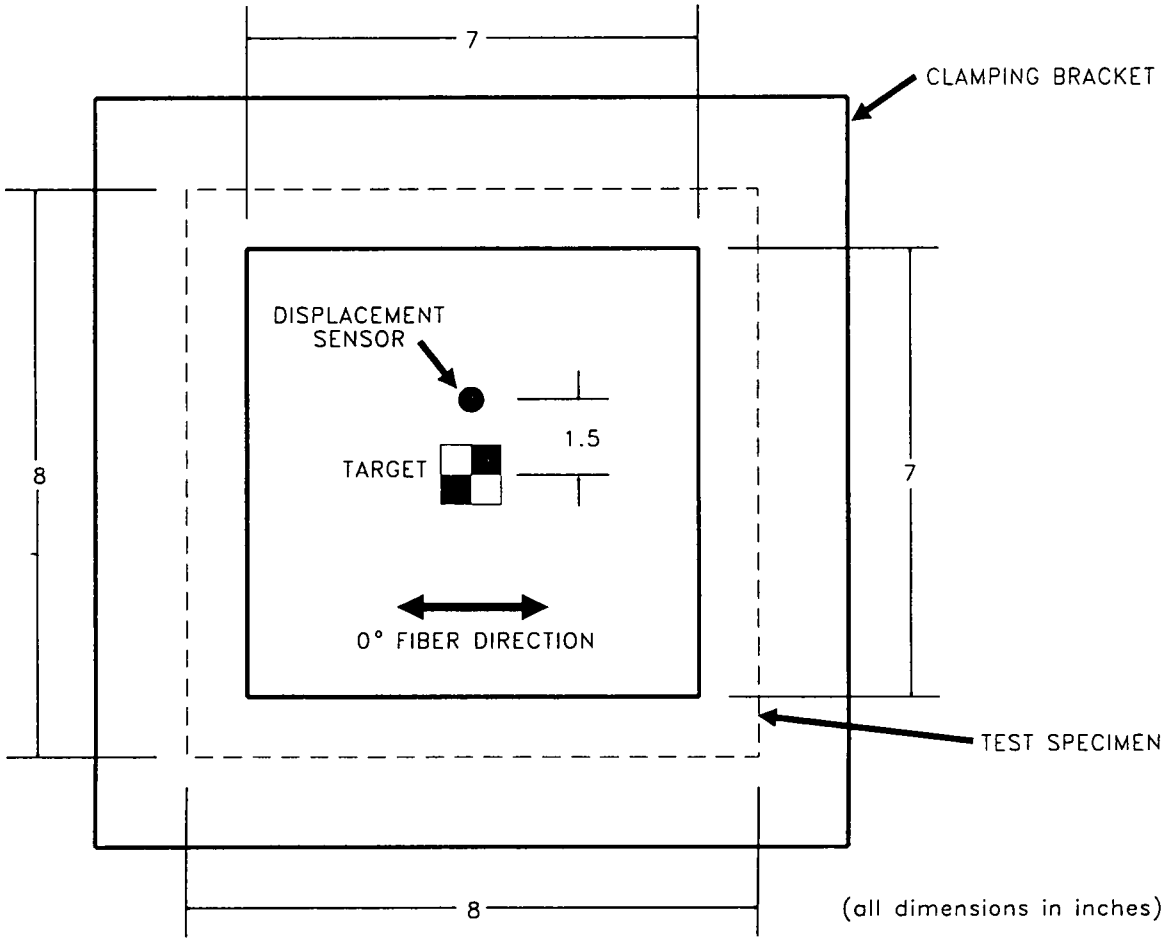

Figure 21. Location of rear surface displacement sensor.

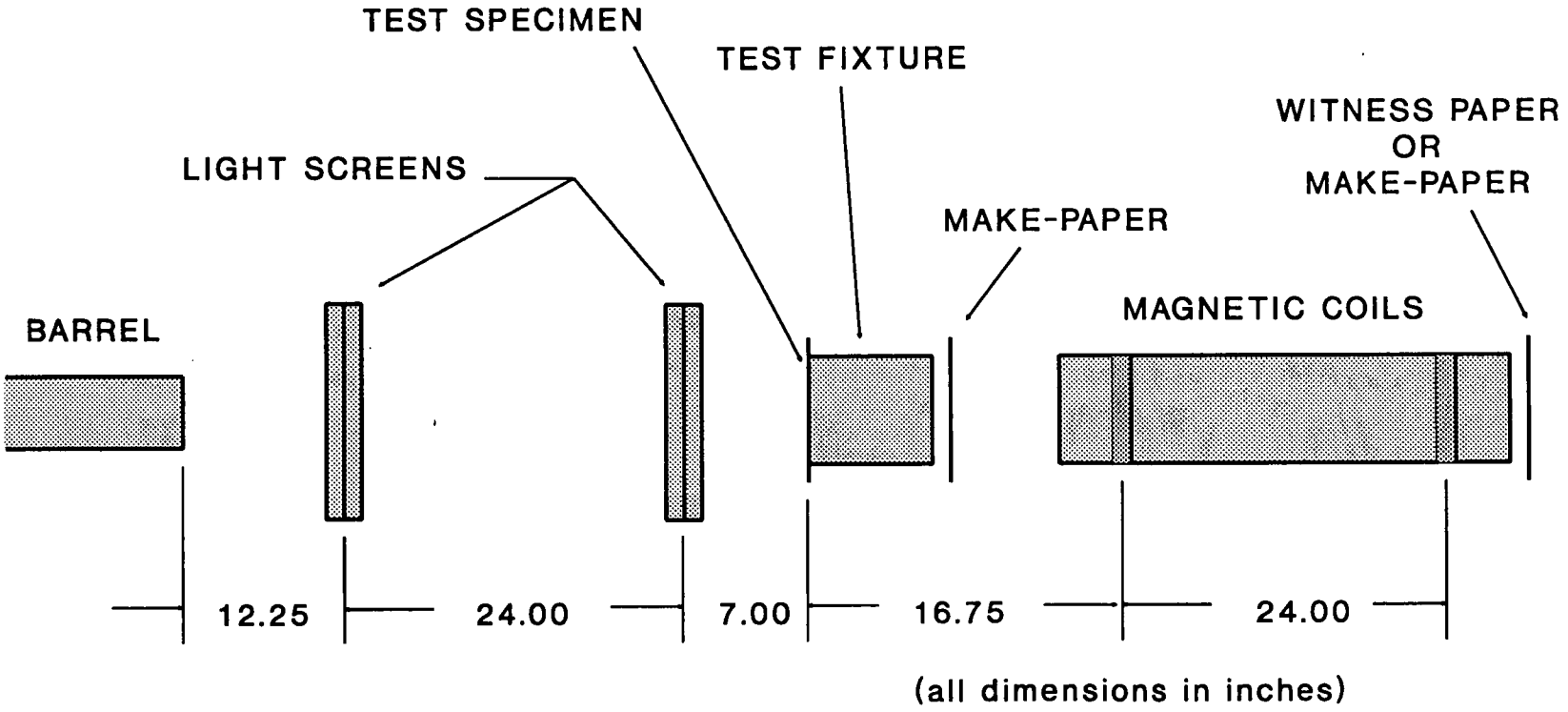

Figure 22. V_{50} range setup.

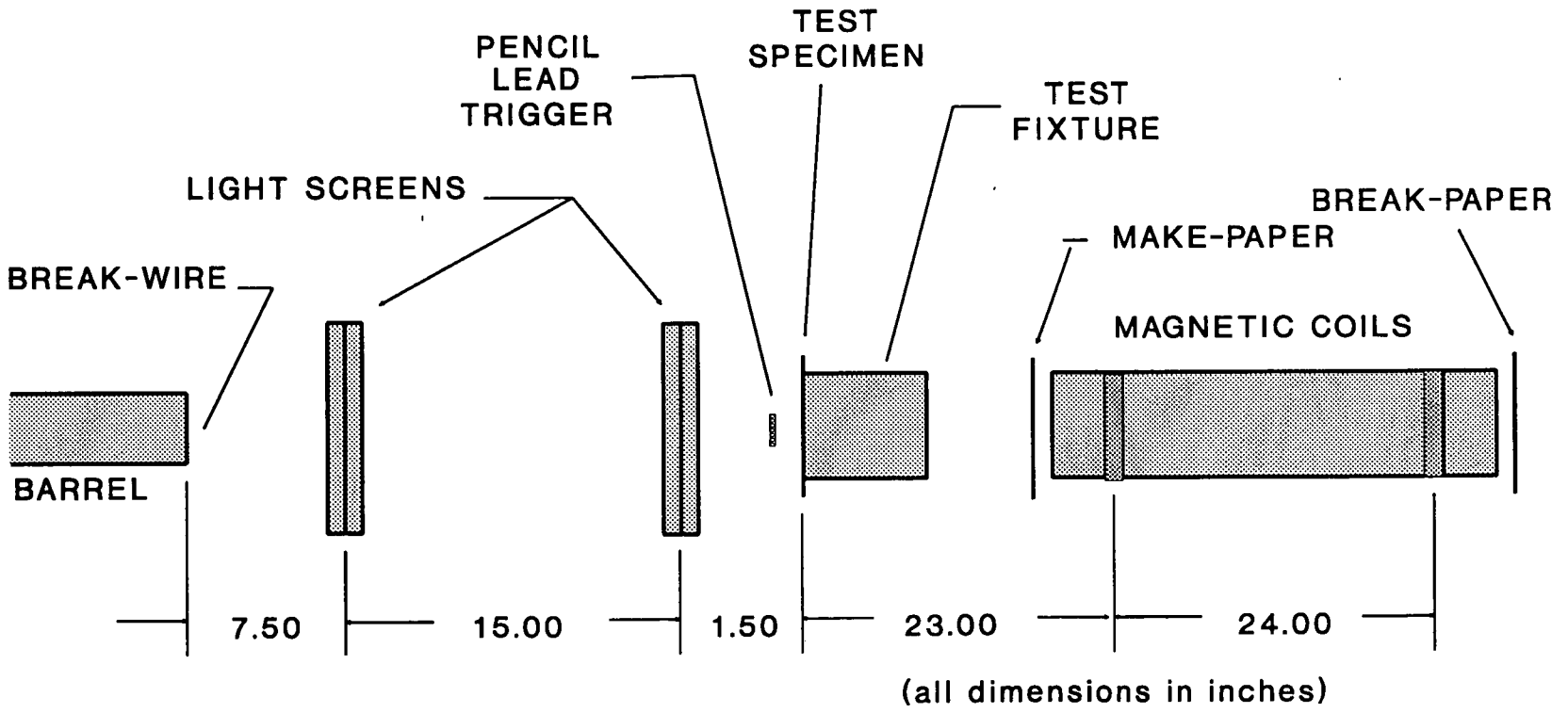

Figure 23. Normal range setup for non-V_{50} tests.

modified to also allow measurement of rebound (residual) velocities. A redundant system for measuring impact velocities was provided by a pair of break-wires (one at the muzzle and one immediately in front of the piezofilm sensor bonded to the targeted surface). The break-wire adjacent to the specimen doubled as a triggering mechanism for the data acquisition system and pulsed power supply (serving the imbedded sensors).

Residual velocities (in the case of complete penetration) were measured by a pair of electromagnetic coils aft of the test specimen. The electromagnetic coils proved capable of discriminating between the projectile and composite spall (which often precedes the projectile for a considerable distance downrange). As a backup to the coils, make-papers were designed and also proved capable of discriminating between the projectile and composite spall.

The test fixture consisted of a steel box beam to which a clamping assembly was welded. (See Figures 24 and 25.) Three built-in shims (ledges) were used to consistently register the location of the test specimen's lower left corner.

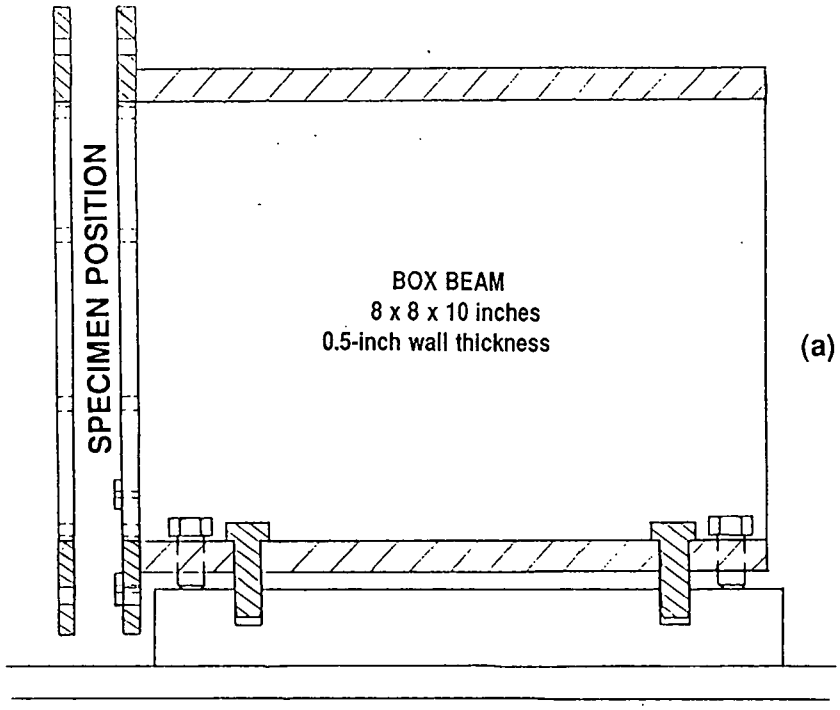

Figure 24. Test fixture.

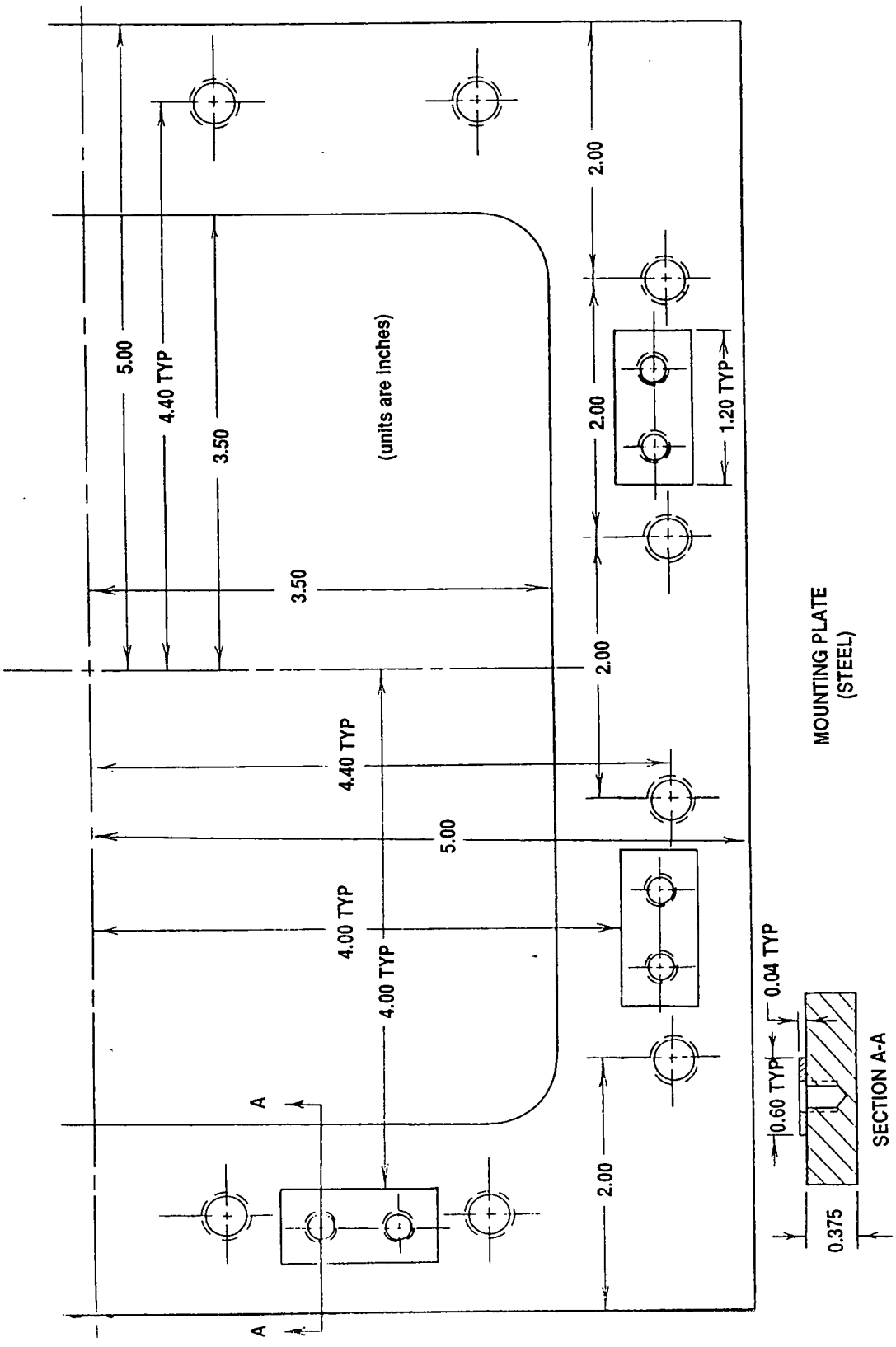

Figure 25. Clamping assembly.

4.5 Data Acquisition

Stress, time-of-contact, and velocity data were acquired via a Kontron transient recorder operating 20 independent channels at 20 MHz each and 10 additional channels at 50 MHz sampling rates. Relatively rapid phenomena (i.e., stress wave motion) were recorded using the full capability of the 50 MHz channels. All channels had 8-bit resolution.

Displacement data were acquired at 200 KHz. The lower sampling rate was a function of the integral fiber optic device. Output of displacement data was recorded in real-time into an open 20 MHz channel on the Kontron system. Doing so allowed the timewise correlation of displacement data with time-of-contact and stress data.

The Kontron data acquisition system was triggered by the projectile severing the break-wire closest to the laminate. Upon being triggered, 256,000 data points (divided such that 28% were before the trigger) were recorded by each channel. Simultaneously (using the same trigger), the pulsed power supply sent a 120 μ-sec square wave voltage to each of the imbedded sensors. Timing for delivery of the pulse was obviously critical.

4.6 Experimental Procedures

Prior to defining velocities for the experimental program, several pretests had to be performed. One of the first requisites was to determine the required distance between the test specimen and the muzzle. The maximum distance was defined to provide the desired accuracy of impact location to within ±0.04-inch (1mm). Such accuracy ensured the impact would occur directly over the stack of imbedded sensors. Other pretests involved developing and validating reliable procedures for measuring the initial, rebound, and residual projectile velocities. Another basic requirement was modifying the light gas gun to provide the desired high velocities and developing pressure vs velocity curves for each of the projectile densities.

Critical to velocity definition for the experimental design was determining V_{50}'s. The upper velocity bound in the first L8 and lower velocity bound in the second L8 was based on the V_{50} obtained when 32-ply laminates were impacted by steel projectiles. The upper velocity bound in the second L8 and the lower velocity bound in the third L8 was based on the V_{50} obtained when 128-ply laminates were impacted by aluminum projectiles. Verification that high mass steel projectiles would provide a lower V_{50} than aluminum projectiles, and establishing a relationship between the V_{50} and projectile mass was the subject of still other pretests.

4.6.1 Accuracy Tests

Initial pretests involved determining the distance the specimen had to be from the muzzle while maintaining a point-of-impact accuracy of ±0.04-inch (1mm). A thick aluminum plate was anchored 16.21 feet downrange from the muzzle and used as a witness plate for projectile impacts. While maintaining a constant impact velocity, 16 shots were fired into the aluminum plate with each impact creating a slight indenture. The maximum center to center distance between indentures measured 9/16-inch, requiring that the test specimen be positioned two feet from the muzzle.

4.6.2 Velocity Measurement

Other pretests involved developing and validating velocity measurement systems suitable for this study. Five velocity measurement techniques were evaluated: break-wires, break-papers, make-papers, light-screens, and electromagnetic coils.

Break-wires are small diameter wires placed across the shotline and spaced at known distances. The time of each wire's breaking is assessed to the projectile and used to obtain a velocity. Because break-wires are severed on the projectile's first passing, rebound velocities (in the case of nonpenetration) can not be measured. [Note: Rebound velocities (like residual velocities, in the case of

penetration) are desirable measurements for energy calculations.]

Break-papers consist of a continuous grid of conductive paint applied to vellum paper. Although break-papers can be used to obtain initial velocities, the relatively large grid is commonly applied to situations where the projectile may deviate from the shotline. Similar to break-wires however, the break-paper's grid is severed on the projectile's first passing.

Make-papers consist of pairs of fully conductive papers spaced at a distance roughly 1/4 the projectile's length. The conductive projectile is used to complete (make) a circuit between each pair of papers. Unlike break-papers, make-papers may mark the passing of multiple projectiles to include spall.

Light-screens are screens of light through which the projectile passes. With light-screens spaced at a defined distance, the times of the projectile's passing are obtained and used in velocity calculations. Because light-screens can be configured to register the passing of multiple projectiles, this velocity measurement system is well suited for recording both initial and rebound velocities. The system's usefulness for residual velocities can be hampered however by the presence of high-velocity spall.

Electromagnetic coils can be used to obtain the passing of both ferrous and nonferrous projectiles. Projectiles passing through the center of charged coils generate a flux in the magnetic field, appearing as a sine wave. Although coils can be used to obtain rebound velocities, the coils are especially useful for obtaining residual velocities in that discrimination between the projectile and spall can be achieved.

For launches below the speed of sound, when compressed air within the barrel (in front of the projectile) was not a factor, initial projectile velocities were accurately obtained within two feet of the muzzle using a variety of measurement techniques. Because some techniques (i.e., break-papers and the break-wire combination) would not provide rebound velocities (in the case of nonpenetration), and electromagnetic coils restricted access to the muzzle, light-screens were chosen as measurement means. For launches above the speed of sound (where a dense slug of air from the barrel preceded the projectile downrange), reliable initial projectile velocities could only be measured using electromagnetic coils and the break-wire combination. Again, to maintain unrestricted access to the muzzle, the break-wire combination was relied upon as the primary measurement means.

Although rebounds would not occur at impact velocities approaching the speed of sound, a means of measuring the residual projectile velocity had to be determined. Previous work (performed by Pettit[40]) demonstrated that composite spall fragments can precede the projectile downrange and render conventional break-papers and useless. Other velocity measurement systems such as light-screens were also believed to produce erroneous measurements by triggering on spall fragments rather than the projectile. Pretests proved, however, that electromagnetic coils were capable of discriminating between the spall and projectile. As a back-up system (primarily when nonferrous projectiles were used), an experimental system was developed whereby make-papers were also found capable of discriminating between the projectile and spall.

4.6.3 Gas Gun Pressure vs Velocity

The gas gun system proved capable of launching projectiles repeatedly at velocities accurate to within 0.3% This degree of repeatability proved especially valuable during V_{50} determinations.

4.6.4 Post-Mortem Investigations

Post-mortem investigations were limited solely to time-of-flight C-scans. The time-of-flight technique was used to directly observe the diameter and area of delamination. From

the C-scan plots, the diameters (which appear later in this document) are actually averages of diameters in the 0° and 90° fiber directions. Delamination areas, on the other hand, were precisely obtained through a pixel counting procedure. The time-of-flight NDI technique was also employed to indirectly calculate the total volume of delamination. Again, this was achieved through a pixel counting procedure. Most importantly, the NDI technique was later used to identify the depth of the delamination interface closest to the impacted surface.

4.7 Determination of V_{50}

4.7.1 V_{50}'s on 32-Ply Monolithic Laminates

Preliminary to determining V_{50}'s for L8 velocity definition, V_{50}'s (using steel spheres) were obtained on monolithic 32-ply specimens. These laminates were essentially identical (minus three bondlines) to the post-bonded 32-ply laminates used subsequently in this study. (See paragraph 5.7.3.) The goal was to approximate the V_{50} for post-bonded panels and determine differences in the V_{50} between standard monolithic 32-ply laminates and 32-ply laminates post-bonded together from four 8-ply sublaminates. Light-screens were used to obtain initial velocities, with magnetic coils used to discriminate between the projectile and composite spall during residual velocity determination. A witness paper was used aft of the coils to verify laminate penetration and the presence

of spall. V_{50} tests using 1/2-inch diameter steel spheres were performed in the order shown in Table 2.

Several observations were made during this series of tests. No discrepancies occurred between penetration and nonpenetration velocities, indicating the V_{50} was a precise velocity rather than a range of velocities. Based on the data in Table 2, the V_{50} for the 32-ply specimens was estimated to be 375 ±1 f/s. Residual velocities proved to decay rapidly with small decreases in impact velocity as the V_{50} is approached.

TABLE 2. V_{50} tests performed on monolithic laminates.

Panel	Initial Velocity	Residual Velocity	Comment
E73-1	366 f/s	0 f/s	No penetration.
E74-1	392	125	
E75-1	382	60<	Penetration, but an accurate residual velocity was not obtained because the window was too short for the complete signal. The estimated residual velocity was discarded.
E76-1	380	106	
E77-1	376	84	
E78-1	367	0	No penetration.
E79-1	-	0	No penetration. (Light-screens weren't plugged in to get the initial velocity.)
E80-1	374	0	No penetration.

Observing the uniformity of steel spheres, 15 were weighed, producing the following results:

Average projectile weight = $\bar{X}$ = 0.0189 lb

Standard deviation = σ = 0.0001 lb

Coefficient of variation = $\sigma/\bar{X}$ = 0.0063

4.7.2 Residual Velocity Decline as the V_{50} is Approached

Additional pretests were performed at and above the V_{50} using 1/2-inch steel spheres to produce data substantiating the fact that linear regression of residual velocities inaccurately predicts the V_{50}. Data from the V_{50} tests seemed to indicate that the residual velocity decreases rapidly (as the impact velocity is decreased slightly) near the V_{50}. Data from these experiments can be found in Table 3. As noted in Table 3, two shots were off-center. This was apparently caused by a rebounding projectile which peened the barrel's crown. Projectiles rubbing the peen upon exit from the muzzle

TABLE 3. Additional experiments performed at and above the V_{50} (centered impact, except as noted).

Panel	Initial Velocity	Residual Velocity	Comments
E73-3	377 f/s	0 f/s	No penetration.
E74-3	375	119.5	Off-center impact.
E75-3	379	0	No penetration. Off-center impact.
E76-3	377	96.5	
E77-3	537	385.5	
E78-3	1014	884.5	
E79-3	2380	2132.0	

were deflected up to an inch before striking the target. Data from off-center impacts deviated from the norm and were therefore discarded from further consideration. The variation in impact location (with respect to the edge constraints) apparently affects the range of velocities over which the V_{50} occurs. (Note: After completion of test E78-3, the muzzle was repaired.)

Velocities from Tables 2 and 3 were combined with the appropriate energies to produce the data set in Table 4. Linear regression of the velocity terms in this data set predicts a value for V_{50} of 168 f/s (which is less than the actual V_{50} of 375±1 f/s). As shown in Figure 26, the impact vs residual velocity data are extremely nonlinear near the V_{50}. An accurate V_{50} could be predicted using energy terms however. (See Figure 27.) Initial and residual energies can in fact be used to accurately predict a V_{50} based on as few as two shots (using differing velocities above the V_{50}).

TABLE 4. Summation of impact tests performed at and above the V_{50} on monolithic graphite/epoxy laminates.

PANEL NO.	INITIAL VELOCITY (f/s)	INITIAL ENERGY (ft-lbs x 10^3)	RESIDUAL VELOCITY (f/s)	RESIDUAL ENERGY (ft-lbs x 10^3)
V_{50}	375	1337	0	0
E77-1	376	1337	84.0	68
E76-3	377	1345	96.5	88
E76-1	380	1366	106.0	106
E74-1	392	1454	125.0	148
E77-3	537	2728	385.5	1406
E78-3	1014	9728	884.5	7401
E79-3	2380	53582	2132.0	42997

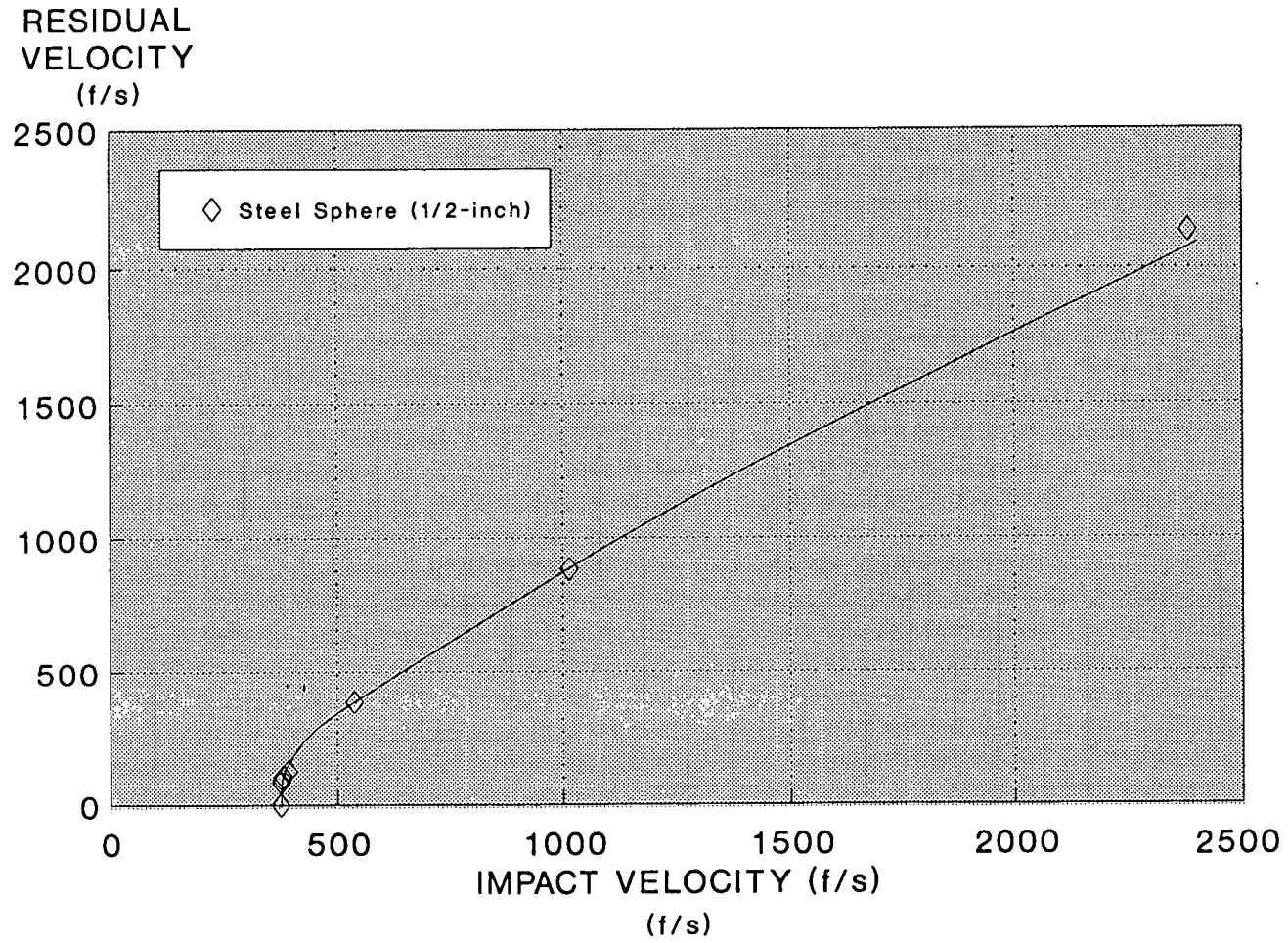

Figure 26. Impact vs residual velocity for monolithic 32-ply quasi-isotropic laminates.

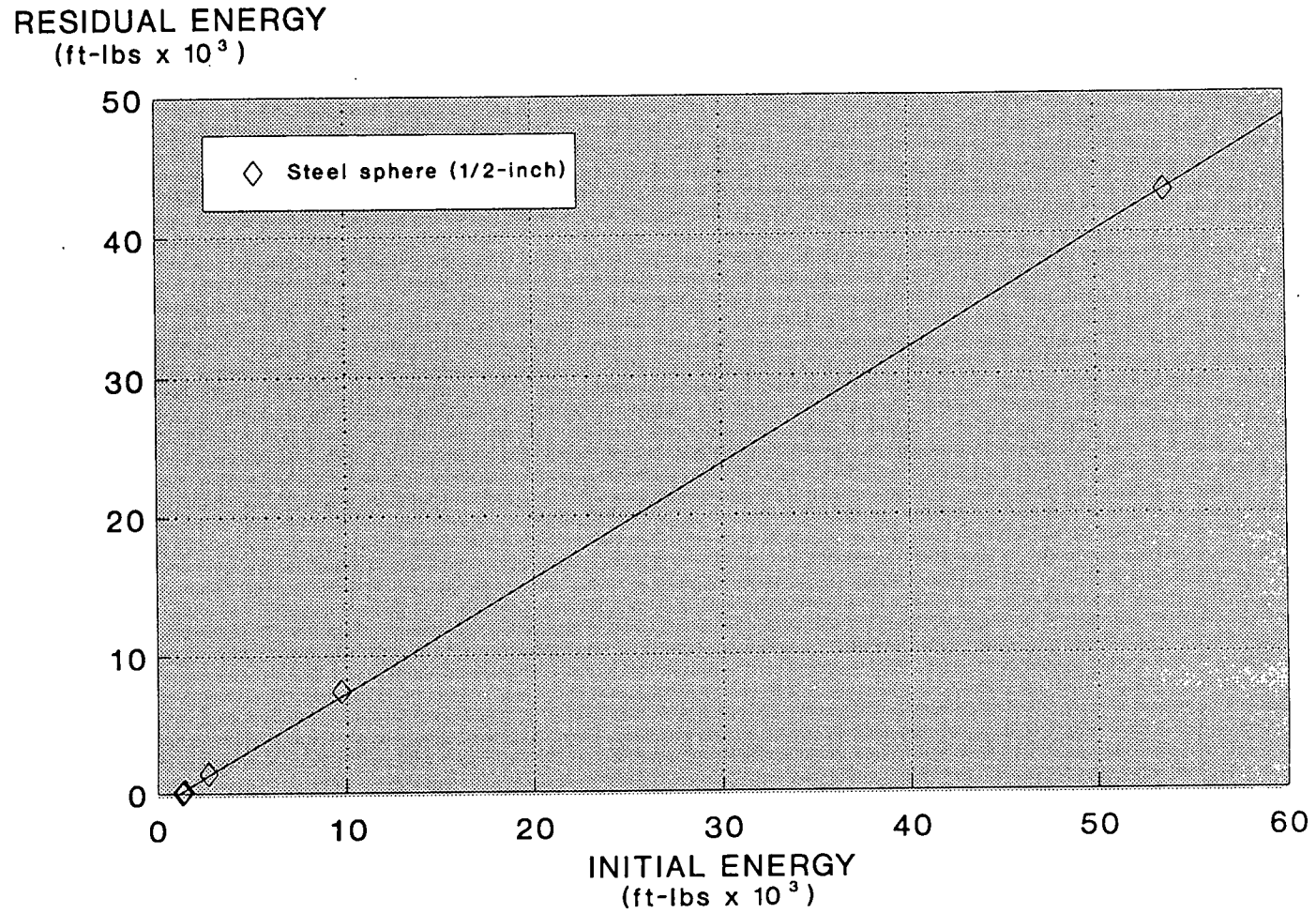

Figure 27. Initial vs residual energy for monolithic 32-ply quasi-isotropic laminates.

A compilation of damage data (delamination diameter, area, and damage volume) associated with impacted monolithic laminates is presented in Table 5 along with measured velocities and calculated energies. Inspection of these data indicated delamination areas and damage volumes behave similarly with respect to the impact velocity. Both measures of damage decrease sharply as the V_{50} is surpassed and quickly become constant with increased velocity. (See Figures 28 and 29.)

4.7.3 V_{50}'s on 32-Ply Post-Bonded Laminates

Noninstrumented 32-ply laminates (fabricated from four 8-ply sublaminates) were subjected to V_{50} testing (using spheres identical to those of the previous tests) to define the upper bound velocity of the first L8 and lower bound velocity of the second L8. (See Appendix A.) For the three tests performed and summarized in Table 6, a V_{50} of 377±4 f/s was estimated which is close to that obtained during V_{50} testing on monolithic laminates. Damage sustained by post-bonded sublaminates proved to be greater than their monolithic counterparts. However, excess damage remained confined to the post-bonded sublaminate's three bondlines. The lack of direct correlation between sublaminate and monolithic configurations is not expected to influence the validity of this study. The location of the fracture mode transition plane is expected to be a function of the stress wave velocity and development of

TABLE 5. Test data from monolithic laminates.

PANEL NO.	INITIAL VELOCITY (f/s)	INITIAL ENERGY (ft-lbs x 10^3)	NORMALIZED IMPACT VELOCITY RELATIVE TO V_{50}	RESIDUAL VELOCITY (f/s)	RESIDUAL ENERGY (ft-lbs x 10^3)	AVERAGE DELAM. DIA. (in)	DELAM. AREA (in^2)	DAMAGE VOLUME (in^3)	REMARKS
E73-1	366	1267	0.9760	-	-	2.19	3.92	0.343	No penetration
E78-1	367	1274	0.9787	-	-	2.42	4.76	0.358	No penetration
E80-1	374	1323	0.9973	-	-	2.11	3.49	0.307	No penetration
E77-1	376	1337	1.0027	84	68	2.19	3.55	0.287	Penetration
E73-3	377	1344	1.0053	-	-	2.11	4.34	0.364	No penetration
E76-3	377	1345	1.0053	97	88	2.42	3.32	0.297	Penetration
E76-1	380	1366	1.0133	106	106	2.34	4.01	0.343	Penetration
E75-1	382	1380	1.0187	?	-	2.04	3.13	0.295	Penetration
E74-1	392	1454	1.0453	125	148	2.19	3.86	0.326	Penetration
E77-3	537	2728	1.4320	386	1406	1.51	1.81	0.192	Penetration
E78-3	1014	9728	2.7040	885	7401	1.81	2.17	0.216	Penetration
E79-3	2380	53582	6.3467	1951	42997	1.51	1.69	0.179	Penetration

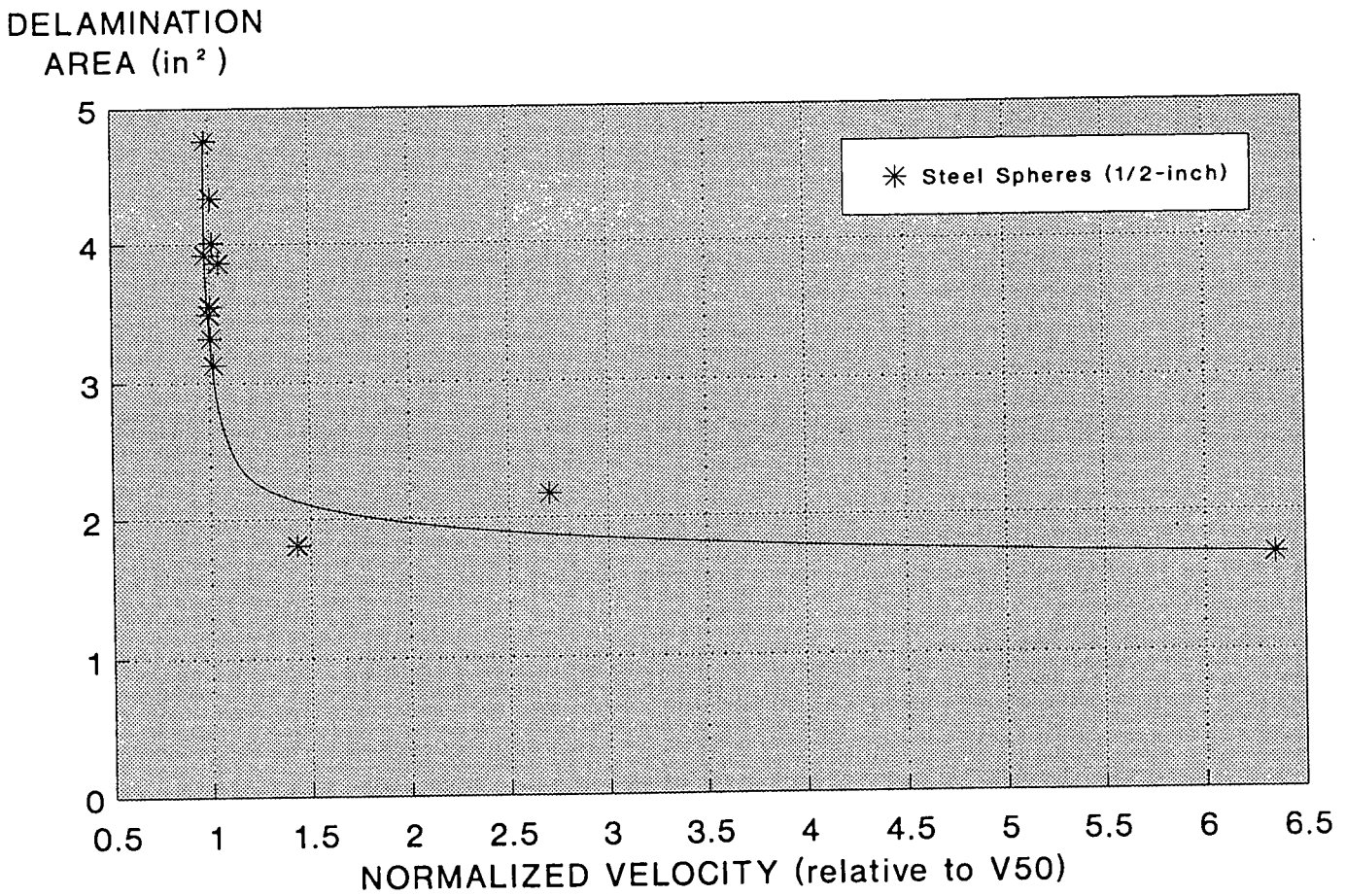

Figure 28. Delamination area vs impact velocity for monolithic 32-ply quasi-isotropic laminates.

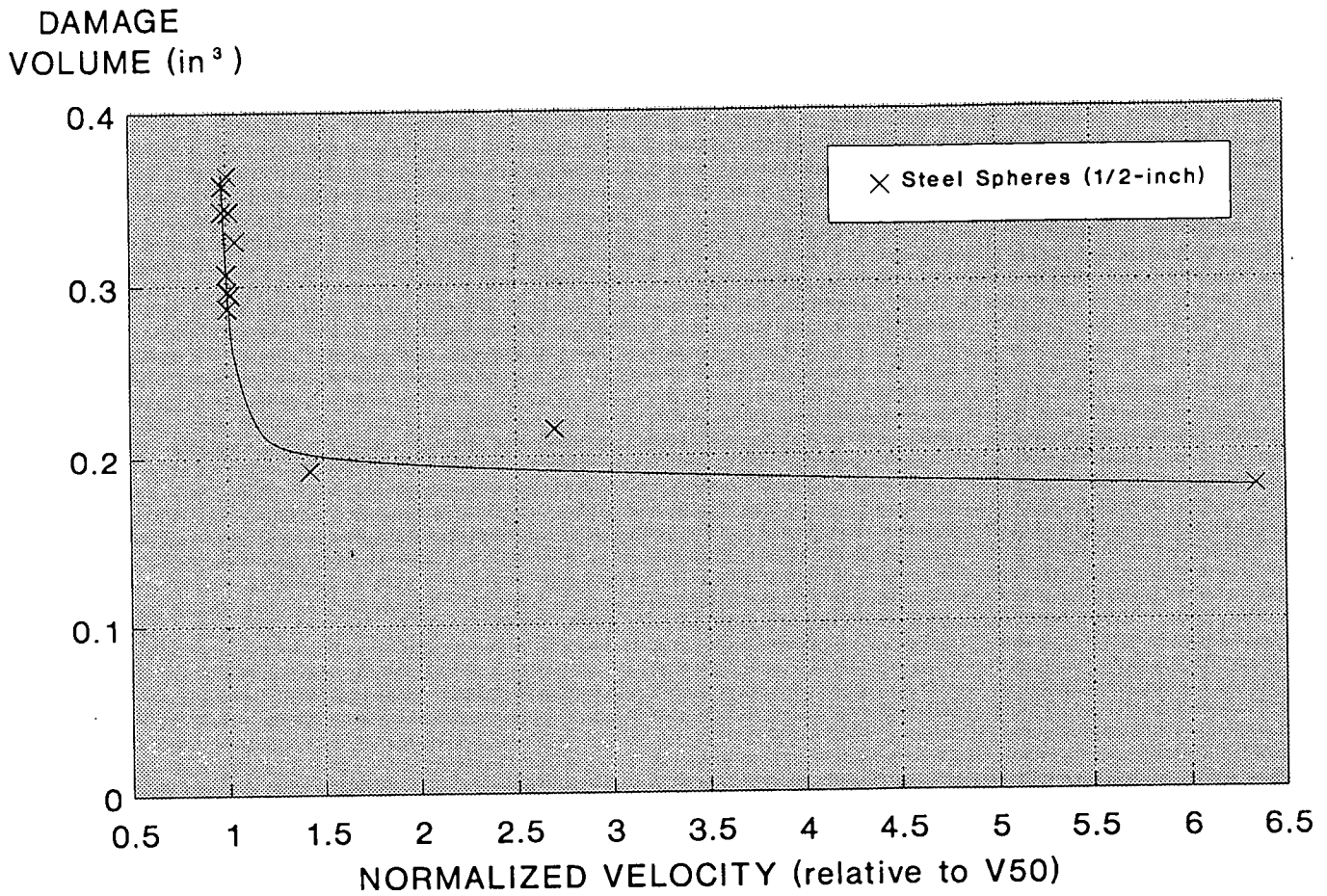

Figure 29. Damage volume vs impact velocity for monolithic 32-ply quasi-isotropic laminates.

TABLE 6. Damage sustained by post-bonded graphite/epoxy laminates impacted by 1/2-inch diameter steel spheres.

PANEL NO.	INITIAL VELOCITY (f/s)	INITIAL ENERGY (ft-lbs x 10^3)	NORMALIZED IMPACT VELOCITY RELATIVE TO V_{50}	REBOUND/ RESIDUAL VELOCITY (f/s)	RESIDUAL ENERGY (ft-lbs x 10^3)	AVERAGE DELAM. DIA. (in)	REMARKS
B4.3	368	1281	0.9813	78	58	2.84	No penetration
B4.1	373	1316	0.9947	77	56	2.97	No penetration
B10.1	381	1373	1.0160	slow	-	4.08	Penetration

a compressive zone (in front of the penetrating projectile), rather than the extent of damage generated, or excess energy available.

4.8 Data Reduction

The total volume of delamination is determined via C-scan to substantiate correlations between delamination and deflection/wave amplitudes. Integration of the damage volume is then correlated with the projectile's change in kinetic energy. Significant reductions in the measured stress wave amplitude (from interface to interface) is also correlated with damage generated, as observed during post-mortem studies. Measurements of the tensile wave and Hertzian compression are used to predict the fracture mode transition from shear plugging to delamination. The transition location (depth) is evidenced through time-of-flight C-scan results. Based on stress wave measurements and post-mortem results, modeling the impact generated stress wave is achieved through an equation

of motion and an accompanying z-t diagram. Using these tools, prediction of the fracture mode transition is attained.

CHAPTER V

IMPACT GENERATED STRESS WAVES

5.1 Complexities Associated with Non-Planar Wave Propagation

Flyer plate impacts are designed to produce an easily understood planar wave in both the target and projectile. Eventual superposition of the tensile waves (after reflections occur) can result in the formation of a spall plane. (Because wave amplitudes are additive, the extremely high tensile stress generated can cause material separation along this plane.) In the case of spherical impactors, several complexities ensue. Nonplanar diffusing waves are generated and a spall plane is not expected to form. Immediately after impact, the laminate's compression wave begins to diffuse radially. Although the wave's velocity through the laminate's thickness is expected to remain constant, the amplitude will be reduced at a rate which can be determined experimentally (i.e., through an array of imbedded stress gages). Similarly, after reflection off the rear face, the tensile wave's amplitude will be attenuated not only due to continued radial diffusion, but due to remnants of the compressive wave.

Compressive wave diffusion is also expected to occur within the spherical projectile. Unlike that within the

laminate, the projectile's dilating wave is immediately influenced by the boundary's proximity and spherical geometry. With time, wave interactions within the projectile become increasingly complex and self-attenuating. Because any projectile release wave passing into the laminate is expected to be effectively attenuated by a localized compressive zone preceding the projectile, effects of the projectile release wave are believed negligible.

5.2 Stress Wave Propagation

For the one-dimensional case, the stress wave velocity (c_L) is solely a function of the material's density (ρ) and elastic modulus (E) in the wave direction (equation 1), whereas Poisson's ratio (μ) is included in the three-dimensional case (equation 2)[41]. The transverse (through-the-thickness) stress wave velocity generated within a plate (as a result of normal impact) is most accurately described according to equation 2. The expected compression and tension transverse wave velocities through a pure resin plate (ignoring the fiber's effect) can be easily calculated.

$$c_L^2 = \frac{E(g)}{\rho} \qquad \text{(one-dimension)} \tag{1}$$

$$c_L^2 = \frac{E(1-\mu)(g)}{\rho(1+\mu)(1-2\mu)} \qquad \text{(three-dimension)} \tag{2}$$

Note: Acceleration due to gravity (g) is included.

Given a 3501-6 resin system (ρ=0.0457 lb/in^3, E_c=0.66x10^6 lb/in^2, E_t=0.62x10^6 lb/in^2, and μ=0.34), the associated compression and tension wave velocities (c_{Lc} and c_{Lt}, respectively) are calculated as follows:

$$c_{Lc}^2 = \frac{660{,}000\ (1 - 0.34)\ (386.4)}{0.0457\ (1 + 0.34)\ [1 - 2\ (0.34)]} = 8.59\text{x}10^9$$

$$c_{Lc} = 92{,}678 \text{ in/sec } (2.35 \text{ km/s})$$

$$c_{Lt}^2 = \frac{620{,}000\ (1 - 0.34)\ (386.4)}{0.0457\ (1 + 0.34)\ [1 - 2\ (0.34)]} = 8.07\text{x}10^9$$

$$c_{Lt} = 89{,}826 \text{ in/sec } (2.28 \text{ km/s})$$

Note: $g = 386.4$ in/sec^2.

If fibers are present in the matrix, micro-impedance differences are expected to influence the stress wave's velocity, amplitude, and length. In this study, through-transmission (an ultrasonic NDI technique) was used to obtain the wave's transverse velocity so that an effective through-the-thickness modulus could be calculated. Sound velocity measurements were obtained through the thickness of monolithic 8, 16, 32, 48, and 64-ply laminates. All thicknesses of panels (8-64 ply) exhibited a through-the-thickness wave

velocity of 118,000 in/s (3 km/s). (This correlates well with through-the-thickness stress wave velocities of 114,200 in/s (2.9 km/s) measured by Dutta[42], but differs slightly from the 92,900 in/s (2.36 km/s) suggested by Kim and Moon[43] and the 139,400 in/s (3.54 km/s) suggested by Yarve[35].) With the density of the AS4/3501-6 laminate being 0.055 lb/in^3, the elastic modulus in the z-direction was calculated according to equation 3 (the inverse of equation 1), i.e.,

$$E_z = \frac{\rho (c_L^2)}{g} \qquad (3)$$

$$E_z = \frac{(0.055)\ (118{,}000^2)}{386.4}$$

$$E_z = 1.982 \text{ msi}$$

where c_L is the wave velocity in in/sec, E_z is the transverse modulus in lbs/in^2, g is the acceleration due to gravity in in/sec^2, and ρ is the density in lbs/in^3.

If the depth of the localized compression zone in front of the projectile is ignored and one assumes the fracture mode transition plane is formed by an interaction between the laminate's tensile wave and the projectile, the following equation can be used to determine the depth of the transition plane:

$$z = \frac{v_p\ (2t - z)}{c_L} \qquad (4)$$

where z is the distance from the laminate's impacted surface to the proposed change in fracture modes, v_p is the average projectile velocity (in the laminate) until the tensile wave is encountered, t is the laminate's thickness, and c_L is the laminate's stress wave velocity (assumed constant in both tension and compression). Parameters of the equation are graphically shown in Figure 30.

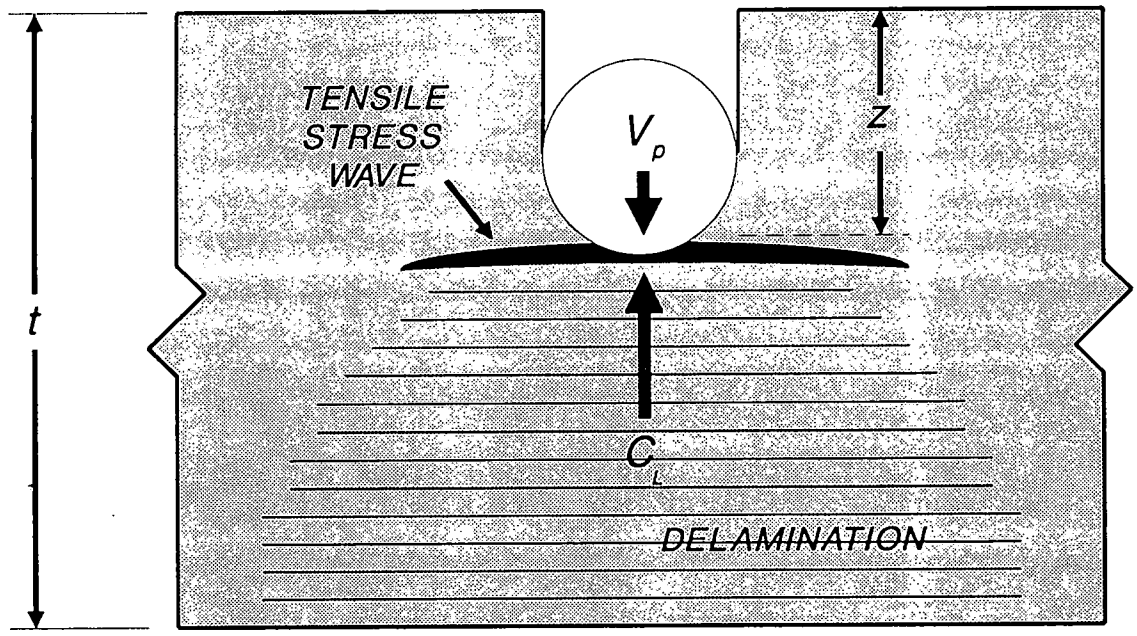

Figure 30. Parameters associated with equation 4.

CHAPTER VI

RESULTS AND DISCUSSION

As discussed in Chapter IV, several laminates were impacted to partially fulfill requirements of the third L8. Because high velocity was the desired test parameter for this preliminary investigation, all tests chosen involved a high velocity. Higher velocities were believed to provide the greatest stress wave magnitude, having the most probability of a significant reflection from the laminate's rear surface. Steel projectiles were chosen for convenience. Table 7 summarizes the test matrix for the instrumented specimens impacted at high velocities. Table 8 relates the type of data

TABLE 7. Penetration test matrix for instrumented laminates impacted by 1/2-inch diameter steel spheres at high velocities.

PANEL NO.	SHOT NO. (from L8 no. 3)	TEST NO. (from L8 no. 3)	NO. OF PLIES	IMPACT VELOCITY (f/s)	RESIDUAL VELOCITY (f/s)
D13.1	2	8	128	2313	1515
B9.1	1	7R	32	2373	2111
B8.3	1	7R	32	2382	2097
B1.3	10	7	32	2382	2111
B2.3	-	-	32	1825	1667

TABLE 8. Identification of data recorded vs Kontron channel number for each test.

DATA RECORDED	CHANNEL FOR SPECIMEN NO. B9.1	B8.3	B1.3	B2.3
Muzzle breakwire	S09	S09	S09	S01
First light-screen	S10	S10	S10	S02
Second light-screen	S11	S11	S11	S03
Piezofilm time-of-contact trigger	S19	S16	S16	-
Pencil lead trigger	-	S17	S17	S04
Pulse from the power supply	-	S18	S18	S09
Strain gage (position no. 2)	-	-	S22	S11
Stress gage (position no. 3)	-	-	S21	S12
Displacement sensor (off-center)	S14	S14	S14	S06
First electromagnetic coil	S12	S12	S12	S07
Second electromagnetic coil	S13	S13	S13	S08

collected by the data acquisition system to the channel number.

Detailed signals recorded by the Kontron data acquisition system are presented in Figure 31 and are considered typical of all tests performed. Although pulses generated by the light-screens (channels S10 and S11 in Figure 31) are numerous, the first pulse produced by each screen is created by the projectile's passing. Flexure is seen to be a relatively slow event which occurs over a prolonged period as compared to the stress wave data. The signal provided by each electromagnetic coil was a single sinusoidal pulse (channels 12 and 13 in Figure 31). Times used to determine the residual velocity were commonly measured from the peak of one coil's output to the corresponding peak on the second coil.

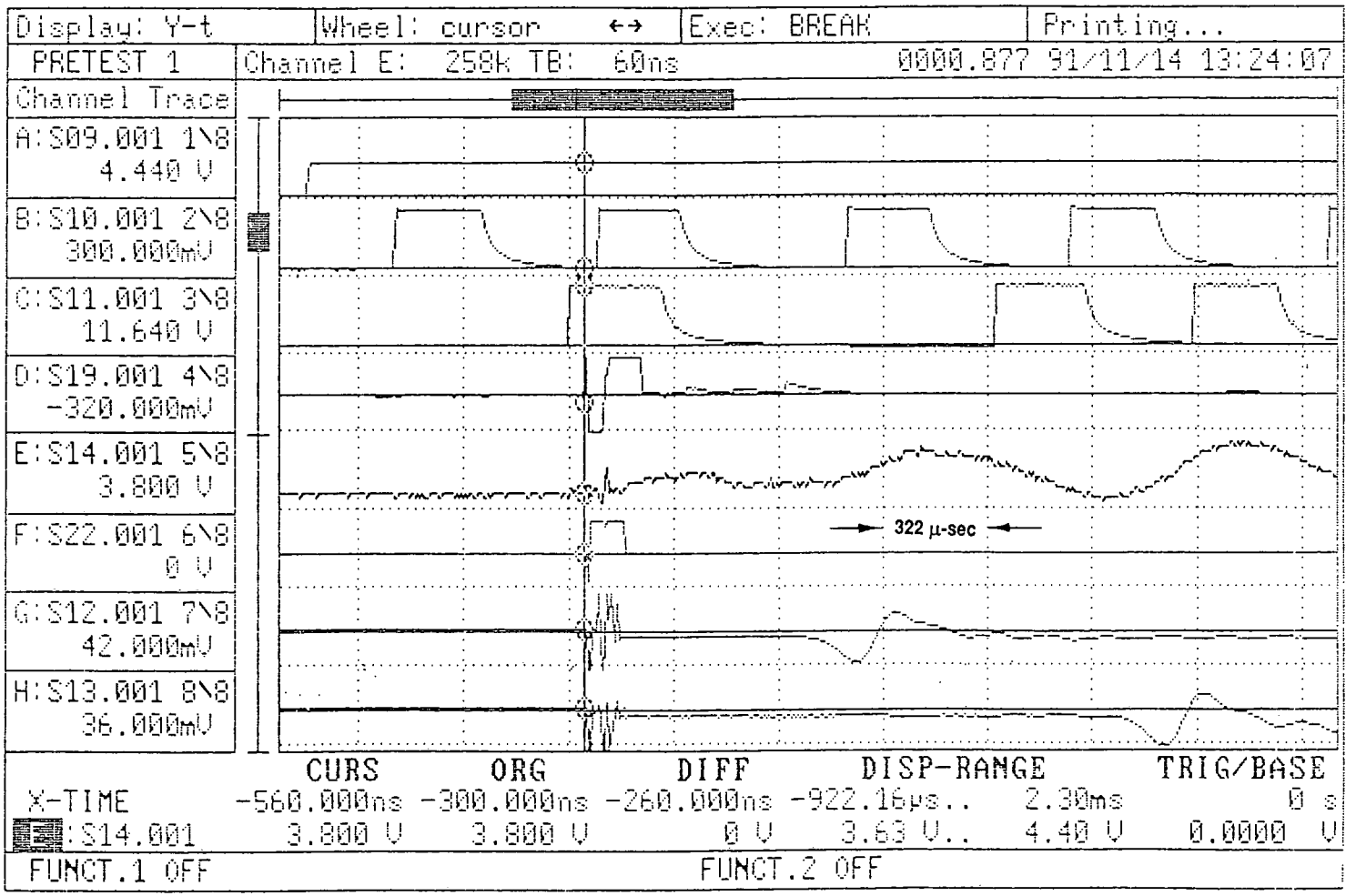

Figure 31. Typical data recorded during the impact of instrumented laminates (specimen B9.1).

6.1 Stress Wave Velocity Determination

A 128-ply specimen (D13.1) was impacted with a 1/2-inch diameter steel sphere at 2313 f/s. Active stress gages were mounted in positions 1 and 7, whereas active strain gages were in positions 2, 4, and 6. Based solely on the initial response of each stress gage (see Figure 32), the elastic compressive stress wave was calculated to have a velocity of 120,888 in/s. Strain gages did not respond immediately to the stress wave's passing, presumably due to the low amplitude in-plane signal generated. (Note: The 120,888 in/s elastic stress wave velocity correlates well with the 118,000 in/s acoustic wave velocity reported earlier in Chapter V.) For the remaining 32-ply experiments, the stress wave velocity is assumed to be 120,888 in/s.

An estimated time-of-contact, based on the first stress gage response and the known stress wave velocity is believed accurate to within 100 n-sec. This degree of resolution is based on the signal's clarity (decisive initial change in voltage) and the 20 n-sec data acquisition rate, and an approximate 10 n-sec gage response time.

6.2 Instrumented 32-Ply Laminate Tests

6.2.1 PVDF Sensor Response

Typical PVDF sensor data is shown in Figure 33. The piezofilm time-of-contact sensor registered a signal at point

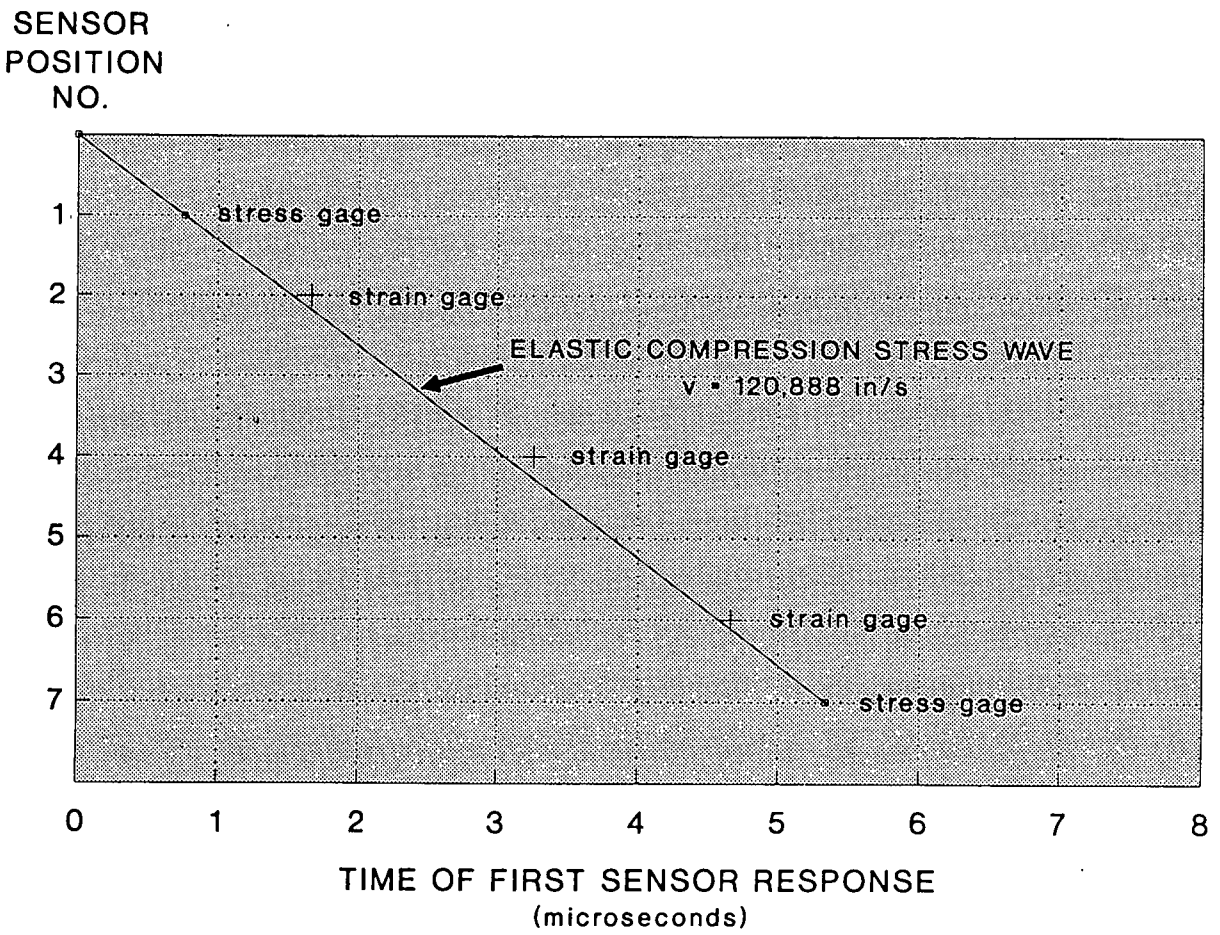

Figure 32. Stress wave velocity based on first sensor response times (panel D13.1).

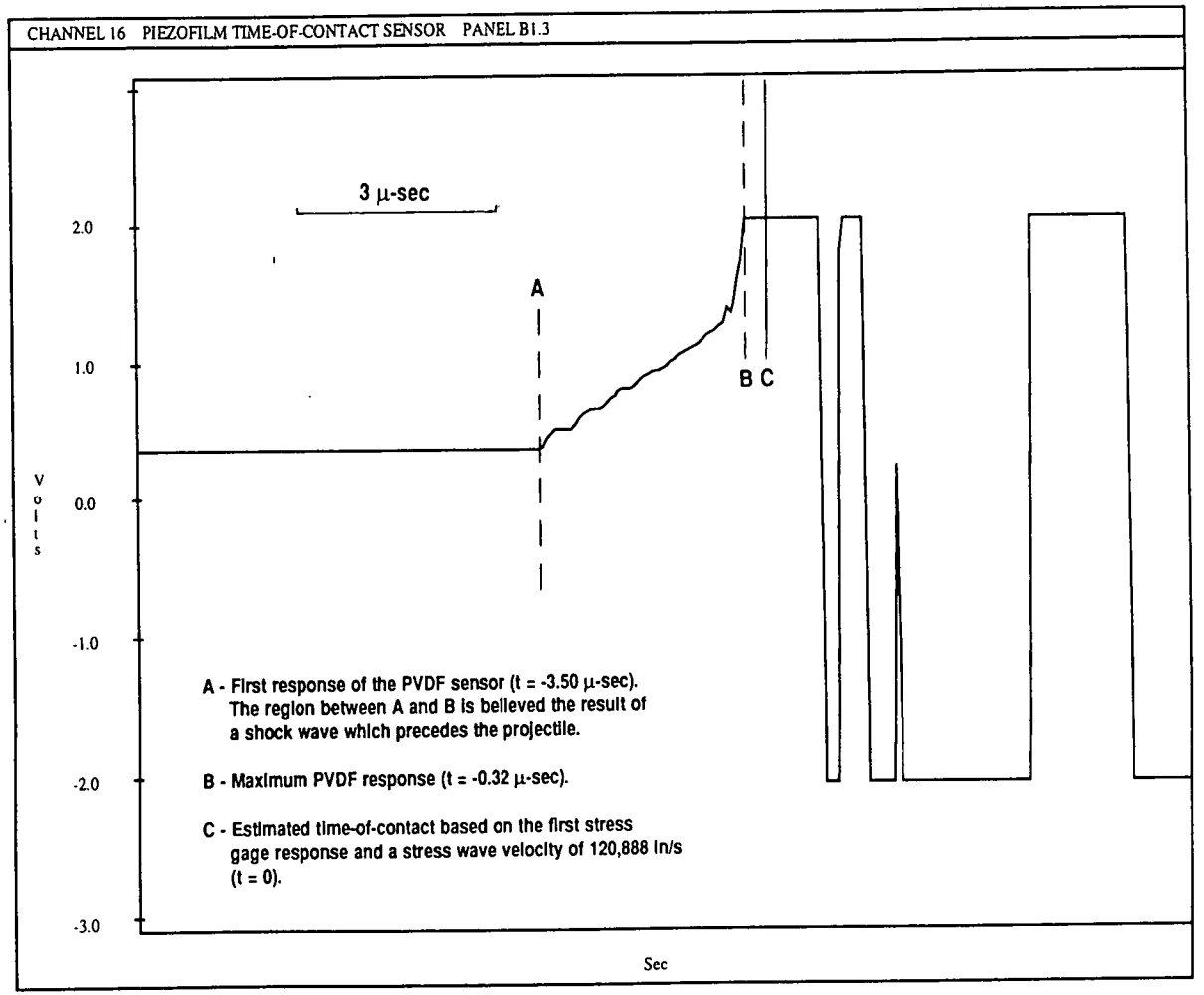

Figure 33. Typical PVDF sensor data (specimen B1.3).

A, 7 μ-sec before the imbedded gages produced an initial response. Knowing that no more than one micro-second should have elapsed between the time-of-contact and the first gage response, the early PVDF signal is believed created by a shock wave which precedes the projectile. A presumed time of contact is plotted as point C (based on a stress wave velocity of 120,888 in/s), with a possibility of the actual time-of-contact falling between points B and C.

6.2.2 Flexure Measurements

A typical flexure response recorded at the off-center position is shown in Figure 34. The estimated time-of-contact is indicated by point A (t = 0). Only after 145 μ-sec does flexure begin to increase significantly (point B), indicating a flexure wave velocity of 862 f/s. Between points B and D, a displacement offset of 0.141 V occurs, therefore the displacement amplitude at point C is questionable. Once the offset is established, displacement amplitudes of 0.015 and 0.018-inch (at points D and E, respectively) are obtained.

Based on the data in Table 9, flexure wave velocities were noted to vary between 862 and 1666 f/s and generated a maximum displacement at the off-center location of 0.025-inch. Differences in the flexure wave velocities probably resulted from difficulties in detecting the initial flexure.

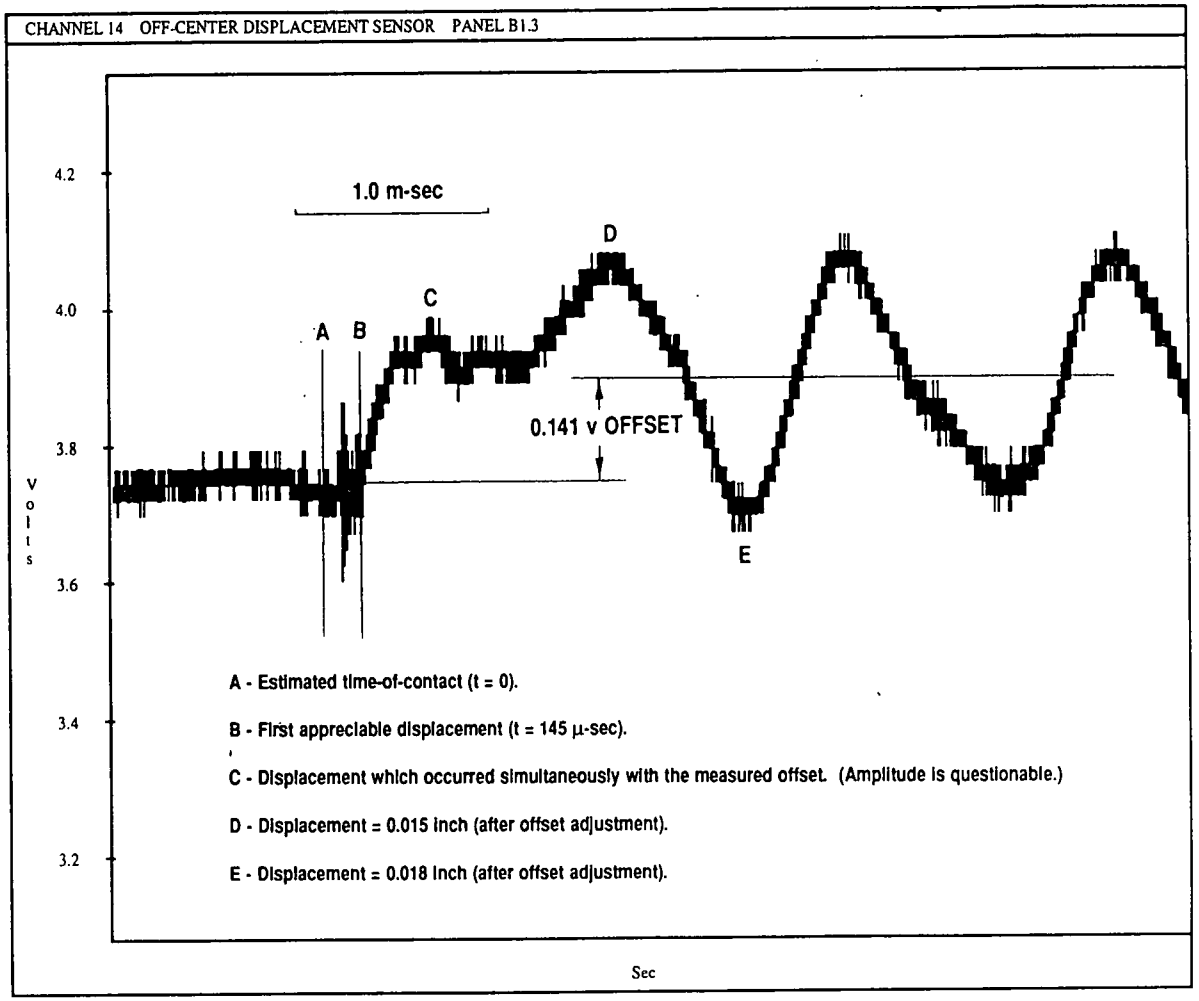

Figure 34. Typical off-center displacement as a function of time (specimen B1.3).

Table 9. Summation of flexure data from instrumented 32-ply laminates.

TEST PANEL NO.	IMPACT VELOCITY (f/s)	MAXIMUM DISPLACEMENT (in)	FLEX. WAVE VELOCITY (f/s)
B9.1	2373	0.025	1238
B8.3	2382	0.020	1600
B1.3	2382	0.018	862
B2.3	1825	0.015	1666

6.2.3 Transverse Stress Wave Amplitude Measurements

Figure 35 shows typical stress gage output (taken from the specimen B2.3 results for stress gage position 3). The pulsed power supply had the gages powered in a steady state condition 30 μ-sec prior to the projectile contacting the test specimen. The estimated time-of-contact, based on the first stress gage response and a stress wave velocity of 120,888 in/s (as measured from point B), is identified by point A (t = 0). Note that even though the gage is powered, the output voltage remains at zero until contacted by the stress wave at point B (t = 1.19 μ-sec). The definitive initial gage response is compressive, as expected, and attains a maximum stress amplitude of 232 ksi at point C (t = 1.83 μ-sec). Relaxation of the compressive stress is noted to correspond closely to the time which the stress wave is expected to return to the gage location (reference point D, t = 1.98 μ-sec). The gage's tensile response (point E, t = 5.97 μ-sec) is of unknown amplitude, but is believed sufficient to cause substantial delamination adjacent to the rear surface. The fastest time

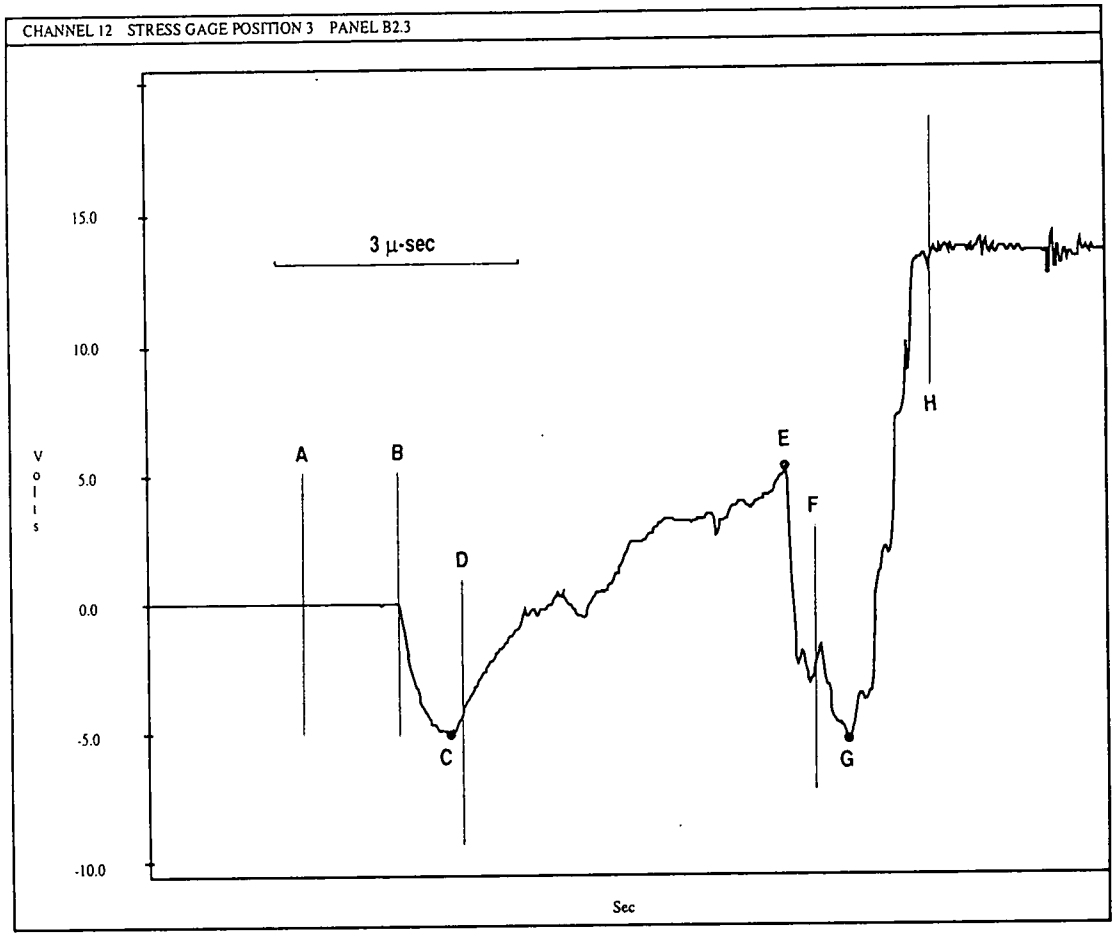

A - Estimated time-of-contact based on the first stress gage response and a stress wave velocity of 120,888 in/s as measured from point B (t = 0).

B - Initial stress gage response (t = 1.19 μ-sec).

C - Maximum out-of-plane compression amplitude produced by the passing stress wave (-5.04 V, σ = 232 ksi), t = 1.83 μ-sec.

D - Estimated time-of-arrival for the return tensile wave based on a stress wave velocity of 120,888 in/s (t = 1.98 μ-sec).

E - Maximum tension (amplitude unknown), t = 5.97 μ-sec.

F - Fastest time that the projectile could arrive at the gage to insure failure (based on a rigid specimen and an initial projectile velocity of 1825 f/s), t = 6.54 μ-sec.

G - Initiation of gage failure (-5.16 V, σ = 246 ksi), t = 6.75 μ-sec.

H - Slowest time that the projectile would arrive at the gage to insure failure (based on the specimen flexing 0.015-inch and the residual projectile velocity of 1652 f/s), t = 7.79 μ-sec.

Figure 35. Typical stress gage output (specimen B2.3, stress gage position 3).

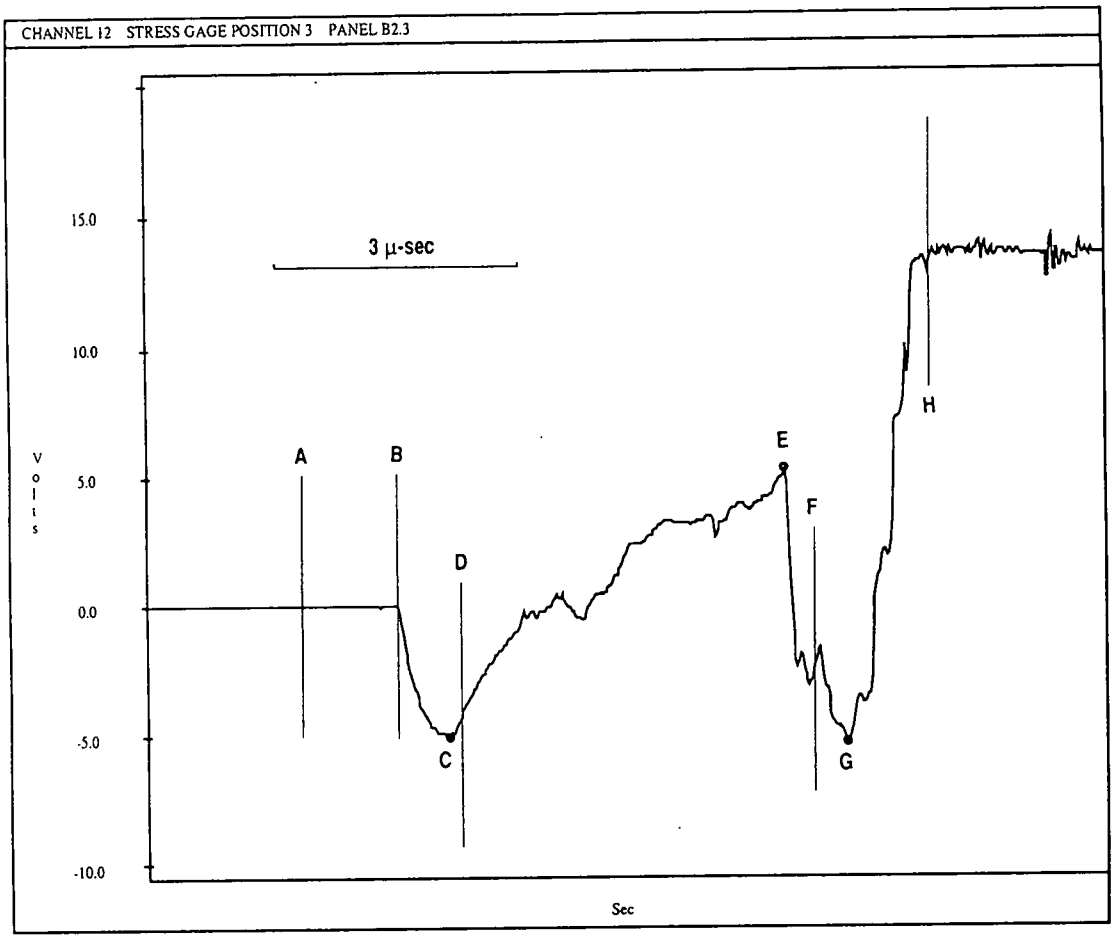

A - Estimated time-of-contact based on the first stress gage response and a stress wave velocity of 120,888 in/s as measured from point B (t = 0).

B - Initial stress gage response (t = 1.19 μ-sec).

C - Maximum out-of-plane compression amplitude produced by the passing stress wave (-5.04 V, σ = 232 ksi), t = 1.83 μ-sec.

D - Estimated time-of-arrival for the return tensile wave based on a stress wave velocity of 120,888 in/s (t = 1.98 μ-sec).

E - Maximum tension (amplitude unknown), t = 5.97 μ-sec.

F - Fastest time that the projectile could arrive at the gage to insure failure (based on a rigid specimen and an initial projectile velocity of 1825 f/s), t = 6.54 μ-sec.

G - Initiation of gage failure (-5.16 V, σ = 246 ksi), t = 6.75 μ-sec.

H - Slowest time that the projectile would arrive at the gage to insure failure (based on the specimen flexing 0.015-inch and the residual projectile velocity of 1652 f/s), t = 7.79 μ-sec.

Figure 35. Typical stress gage output (specimen B2.3, stress gage position 3).

that the projectile could arrive at the gage to ensure failure (based on a rigid specimen and an initial projectile velocity of 1825 f/s) is identified by point F (t = 6.54 μ-sec). Initial gage failure is believed to occur at point G (t = 6.75 μ-sec), after which the signal becomes purely tensile (indicative of gage failure). The slowest time that the projectile would arrive at the gage to ensure failure (based on the specimen flexing 0.015-inch and a residual projectile velocity of 1652 f/s) is marked by point H (t = 7.79 μ-sec).

Prior to performing stress wave experiments on instrumented laminates, estimates of stress wave amplitude vs depth were prepared for an impact condition of 125 f/s. The estimates were developed for use as a lower bound check on measured stress wave amplitudes within this study. (Calculations used to achieve the estimates are included in Appendix C.) Although extrapolations above an impact velocity of 125 f/s were not attempted, higher velocity impacts would surely result in higher stresses.

A summary of stress data measured during the impact of the four 32-ply tests, together with the predicted lower bound values, is presented in Table 10. Measured stresses were not obtained for laminates B9.1 and B8.3 as a result of triggering difficulties. With the transverse tensile strength ($\sigma_{zz\,ult}$) of AS4/3501-6 estimated to be 7 ksi[35], and tensile stress

Table 10. Summation of transverse compressive stress data from instrumented 32-ply laminates (position 3).

TEST PANEL NO.	IMPACT VELOCITY (f/s)	MEASURED MAXIMUM STRESS (ksi)	ESTIMATED LOWER BOUND STRESS (ksi)
B9.1	2373	-	112
B8.3	2382	-	112
B1.3	2382	239	112
B2.3	1825	232	112

amplitudes believed roughly identical to those of compression, the tensile stress had ample opportunity to generate fracture early in the impact event.

6.2.4 In-Plane Strain Measurements

Figure 36 shows typical strain output (this data curve is from the test of specimen B2.3, strain gage position 2). The estimated time-of-contact based on the first stress gage response (position 3) and a 120,888 in/s stress wave is indicated by point A (t = 0). The first in-plane strain response (point B, t = 1.11 μ-sec) created by the passing stress wave is tensile. This tensile response is believed the result of a combination of Poisson's effects and wave dilatation. The tensile strain eventually reaches a maximum of 0.040 in/in at point C. Point D (t = 2.37 μ-sec) represents the estimated time-of-arrival (at the gage location) for the returning tensile stress wave. This is followed closely by an extreme tensile response between points

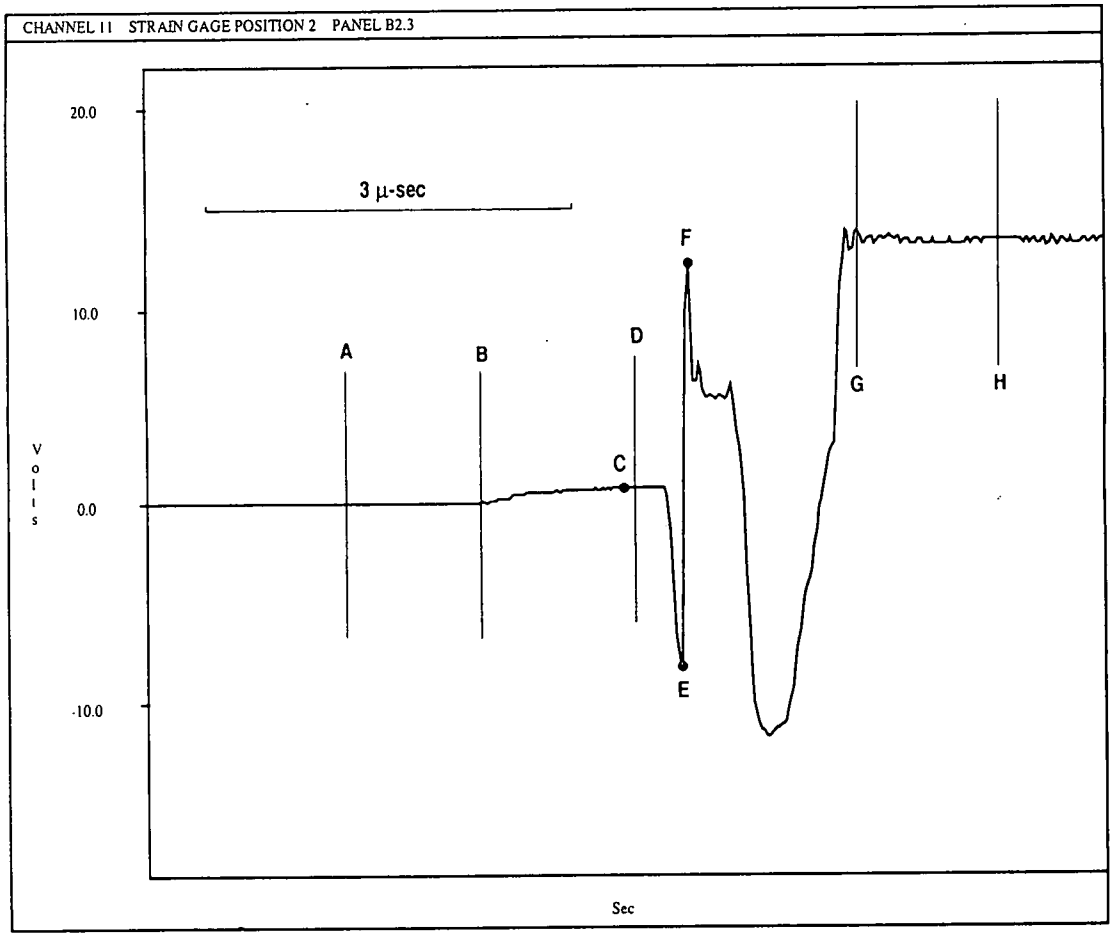

A - Estimated time-of-contact based on the first stress gage response and a stress wave velocity of 120,888 in/s (t = 0).

B - Initial strain gage response (t = 1.11 μ-sec).

C - Maximum in-plane tensile amplitude produced by the passing compression stress wave (0.84 V, ε = 0.040).

D - Estimated time-of-arrival for the return tensile wave based on a stress wave velocity of 120,888 in/s (t = 2.37 μ-sec).

E - Initiation of gage failure (-8.04 V, ε = 0.41), t = 2.76 μ-sec.

F - Tensile strain response at failure (12.24 V, ε = 1.02), t = 2.82 μ-sec.

G - Fastest time that the projectile could arrive at the gage to insure failure (based on a rigid specimen and an initial projectile velocity of 1825 f/s), t = 4.36 μ-sec.

H - Slowest time that the projectile would arrive at the gage to insure failure (based on the specimen flexing 0.015-inch and the residual projectile velocity of 1652 f/s), t = 5.20 μ-sec.

Figure 36. Typical in-plane strain output generated by the passing stress wave (specimen B2.3, strain gage position 2).

E and F which is likely indicative of the gage's failure. After some electronic shorting, the projectile passes through the strain gage position to ensure failure (as bounded by points G and H).

A summary of the maximum tensile strains measured during the impact of 32-ply laminates is presented in Table 11. Strain output was not obtained for laminates B9.1 and B8.3 as a result of triggering difficulties.

Table 11. Summation of in-plane tensile strain data from instrumented 32-ply laminates.

TEST PANEL NO.	IMPACT VELOCITY (f/s)	MAXIMUM STRAIN (in/in)
B9.1	2373	-
B8.3	2382	-
B1.3	2382	0.055
B2.3	1825	0.040

6.2.5 Summary of Results

Amplitudes of stress, strain, and displacement sustained by each of the 32-ply laminates are reviewed in Table 12 along with flexure wave velocities. Again, it is important to note that the time of initial flexure was difficult to resolve, so the flexure wave velocities should be considered approximate.

TABLE 12. Review of stress, strain, and flexure measurements.

TEST PANEL NO.	MAXIMUM STRESS (ksi)	MAXIMUM STRAIN (in/in)	MAXIMUM DISPLACEMENT (in)	FLEX. WAVE VELOCITY (f/s)
B9.1	-	-	0.025	1238
B8.3	-	-	0.020	1600
B1.3	239	0.055	0.018	862
B2.3	232	0.040	0.015	1666

6.3 Fracture Mode Transition

6.3.1 Effect of Bondlines

Significant disbonds along the three bondlines in the 32-ply laminates precluded observation of the fracture mode transition via NDI techniques. An example C-scan (specimen B1.3), showing the extensive disbonding, is presented in Figure 37. This can be compared to the typical delamination observed in a monolithic 32-ply laminate (E79-3) in Figure 38.

6.3.2 Post-Impact C-Scan Summary of Monolithic Panels

Rather than performing a fractographic study, it proved more convenient to observe the fracture mode transition via C-scans of monolithic 32-ply specimens. C-scan cross sections of panels E79-3, E78-3, E74-1, and E76-1 (having impact velocities of 2380, 1014, 392, and 380 f/s, respectively) are presented in Figures 39 - 42. Test results relative to these laminates were listed earlier in Table 5. (Note: The 32-ply monolithic configuration was 0.185-inch thick, whereas the instrumented laminates were 0.191-inch thick.)

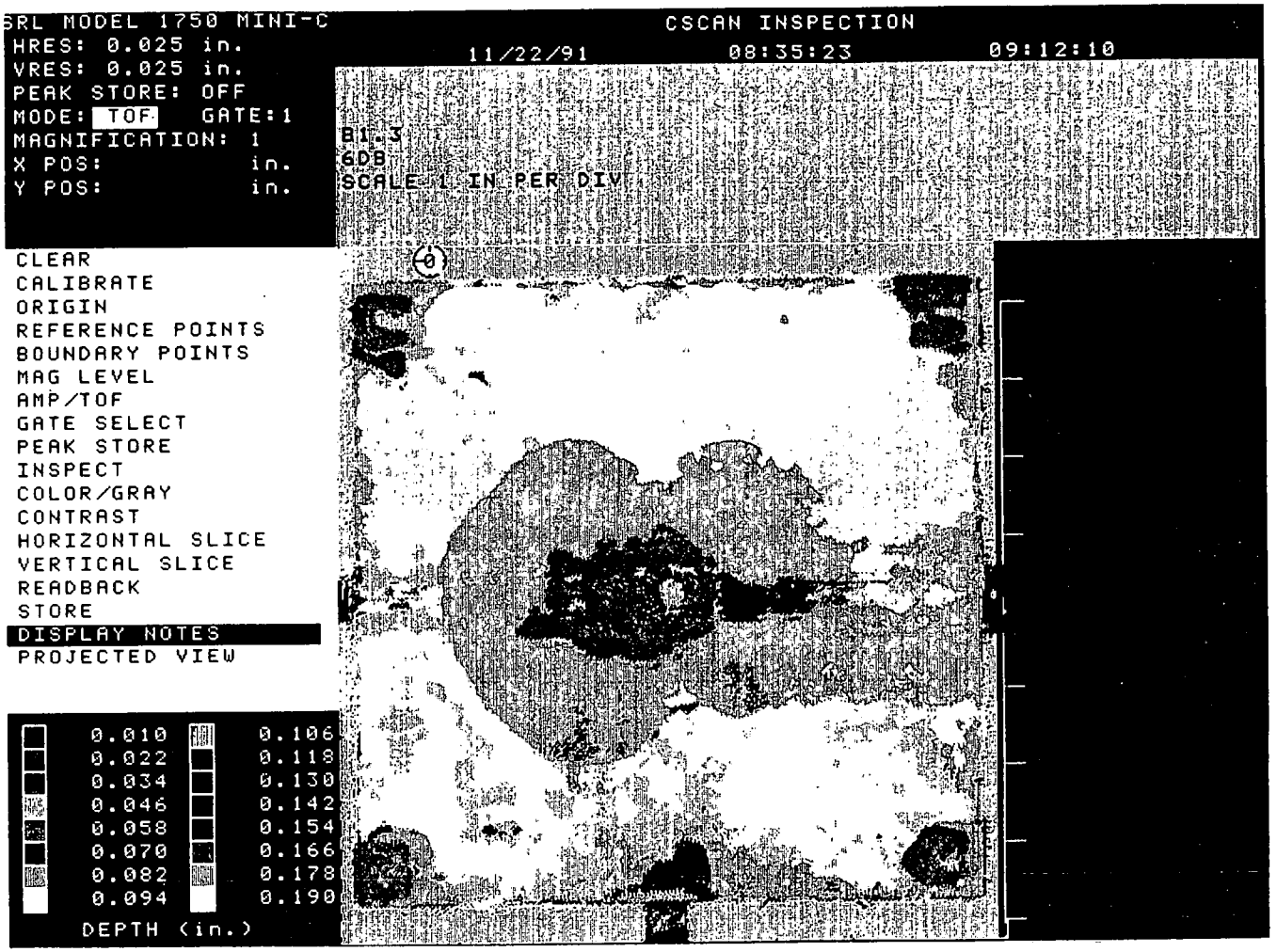

Figure 37. Typical time-of-flight C-scan (indicating delamination depth) of a post-bonded instrumented laminate (specimen B1.3).

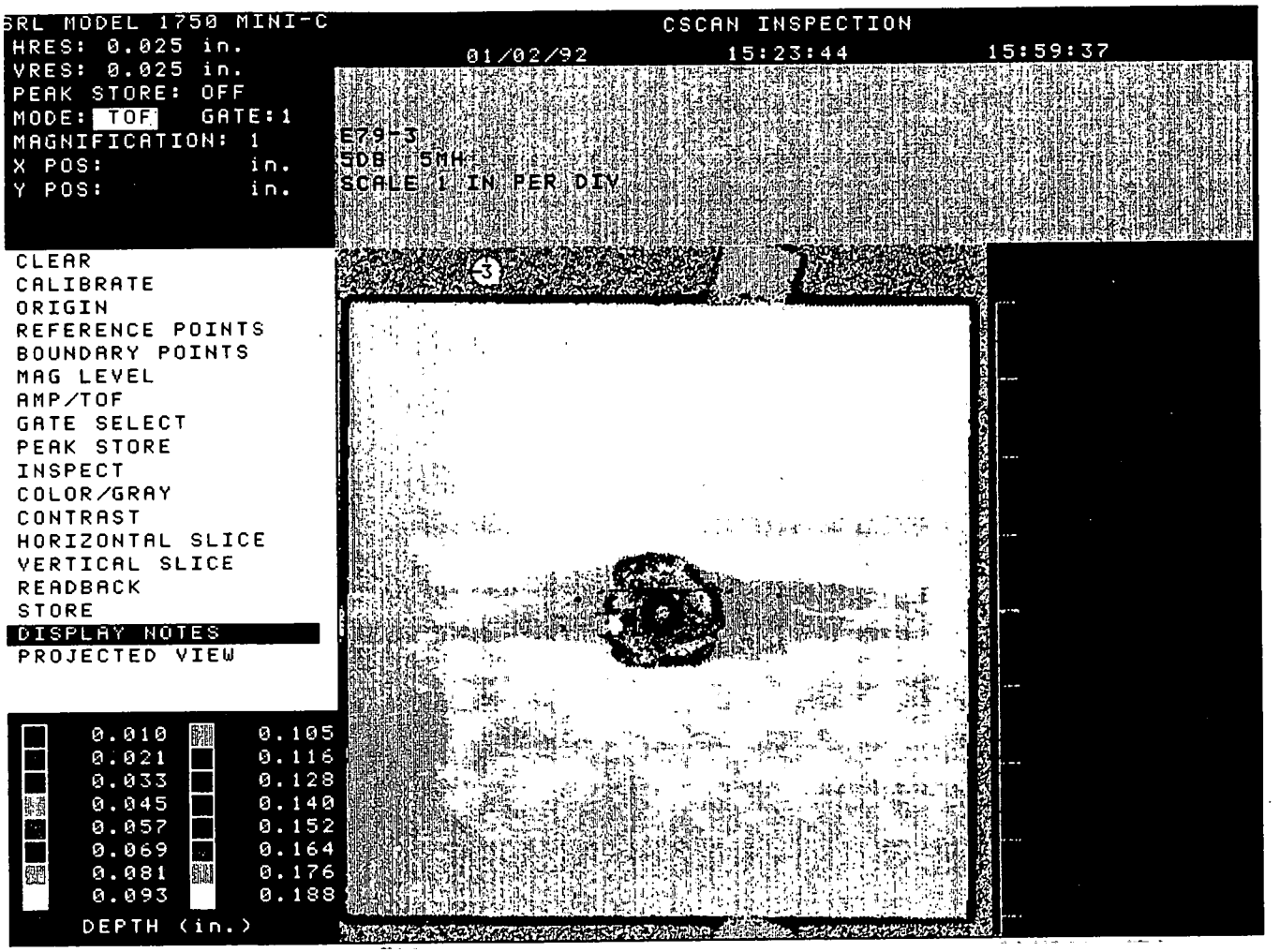

Figure 38. Typical time-of-flight C-scan (indicating delamination depth) for a monolithic laminate (specimen E79-3).

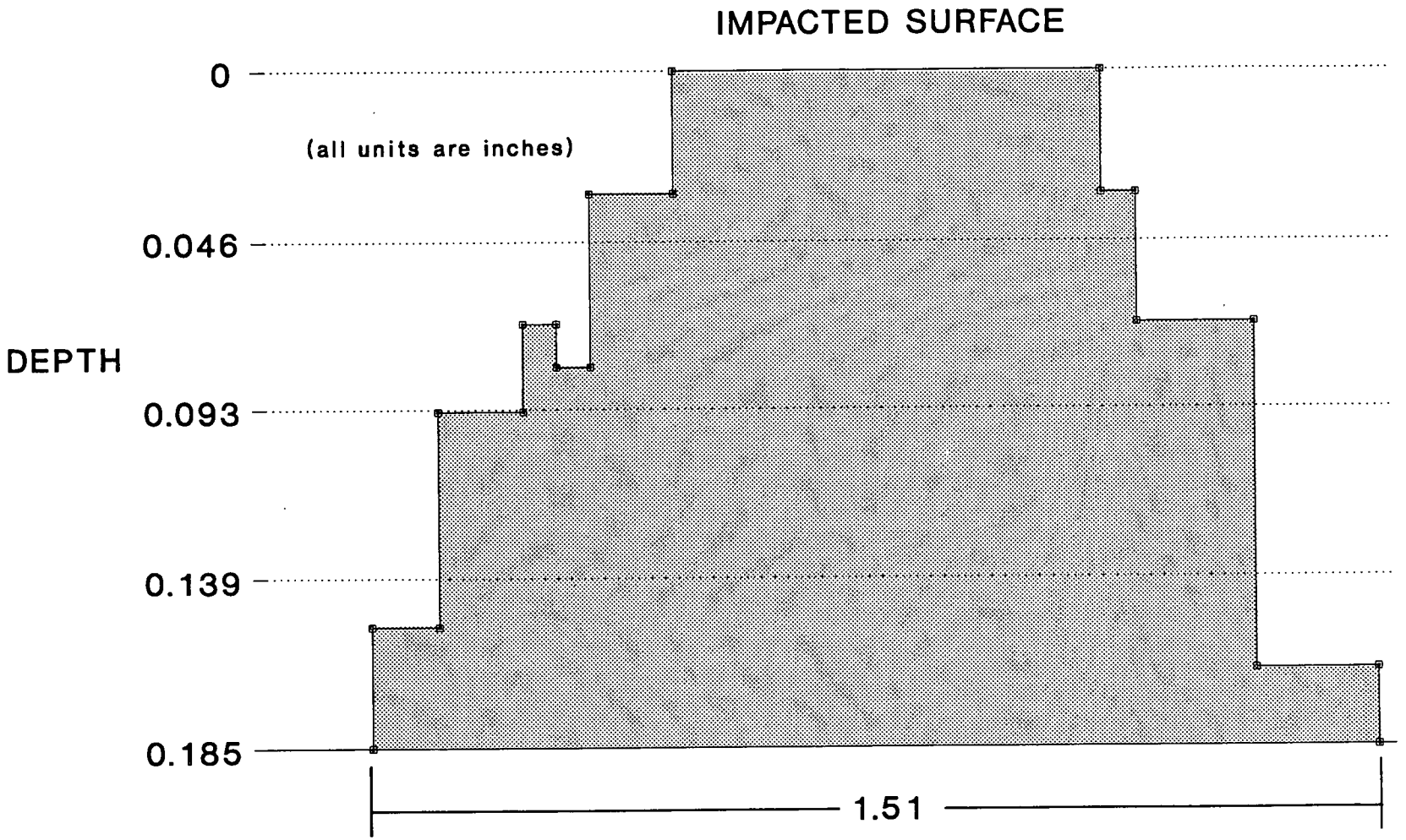

Figure 39. Cross section of through-the-thickness damage sustained by panel E79-3, a 32-ply monolithic laminate impacted by a 1/2-inch diameter steel sphere at 2380 f/s.

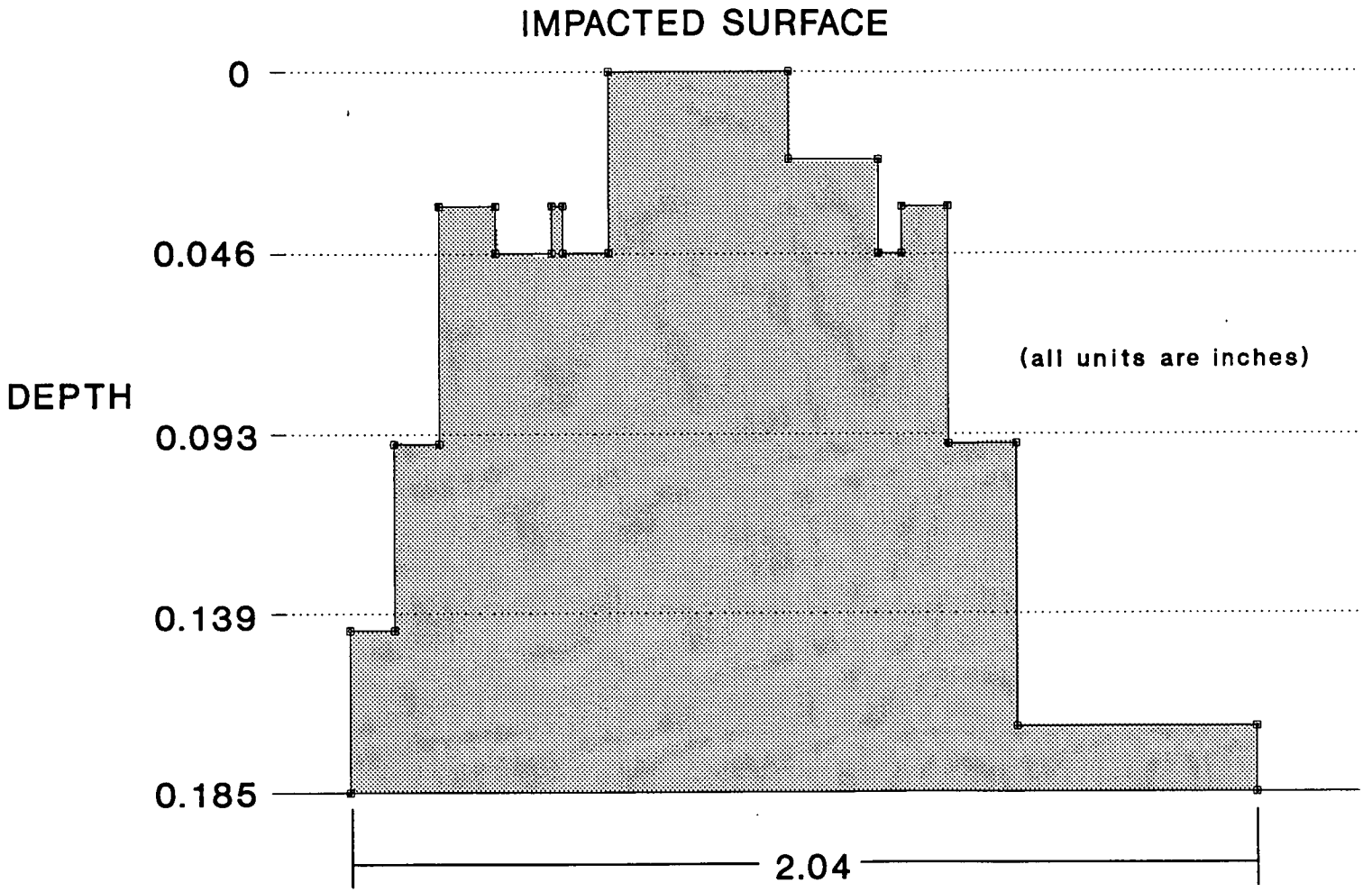

Figure 40. Cross section of through-the-thickness damage sustained by panel E78-3, a 32-ply monolithic laminate impacted by a 1/2-inch diameter steel sphere at 1014 f/s.

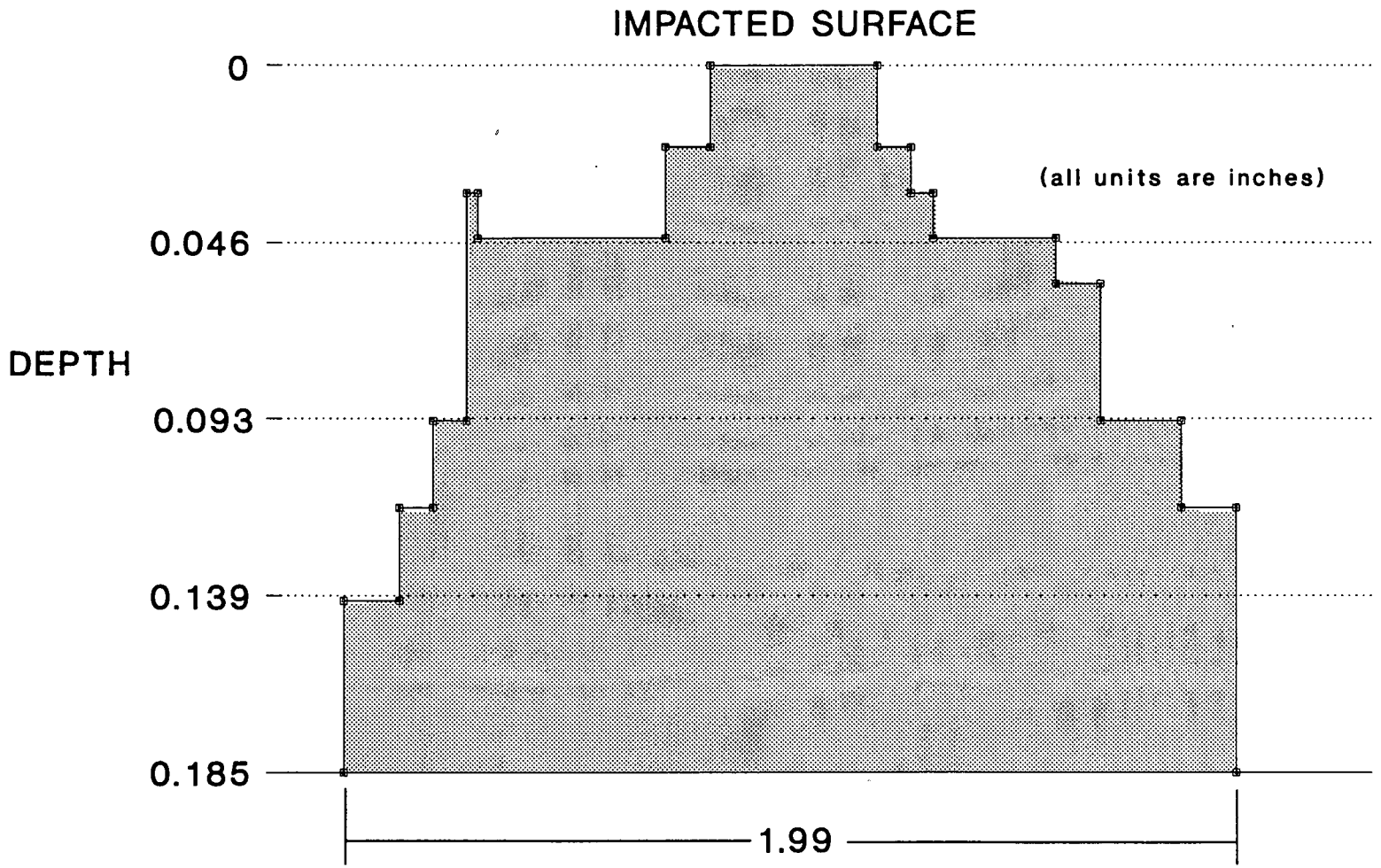

Figure 41. Cross section of through-the-thickness damage sustained by panel E74-1, a 32-ply monolithic laminate impacted by a 1/2-inch diameter steel sphere at 392 f/s.

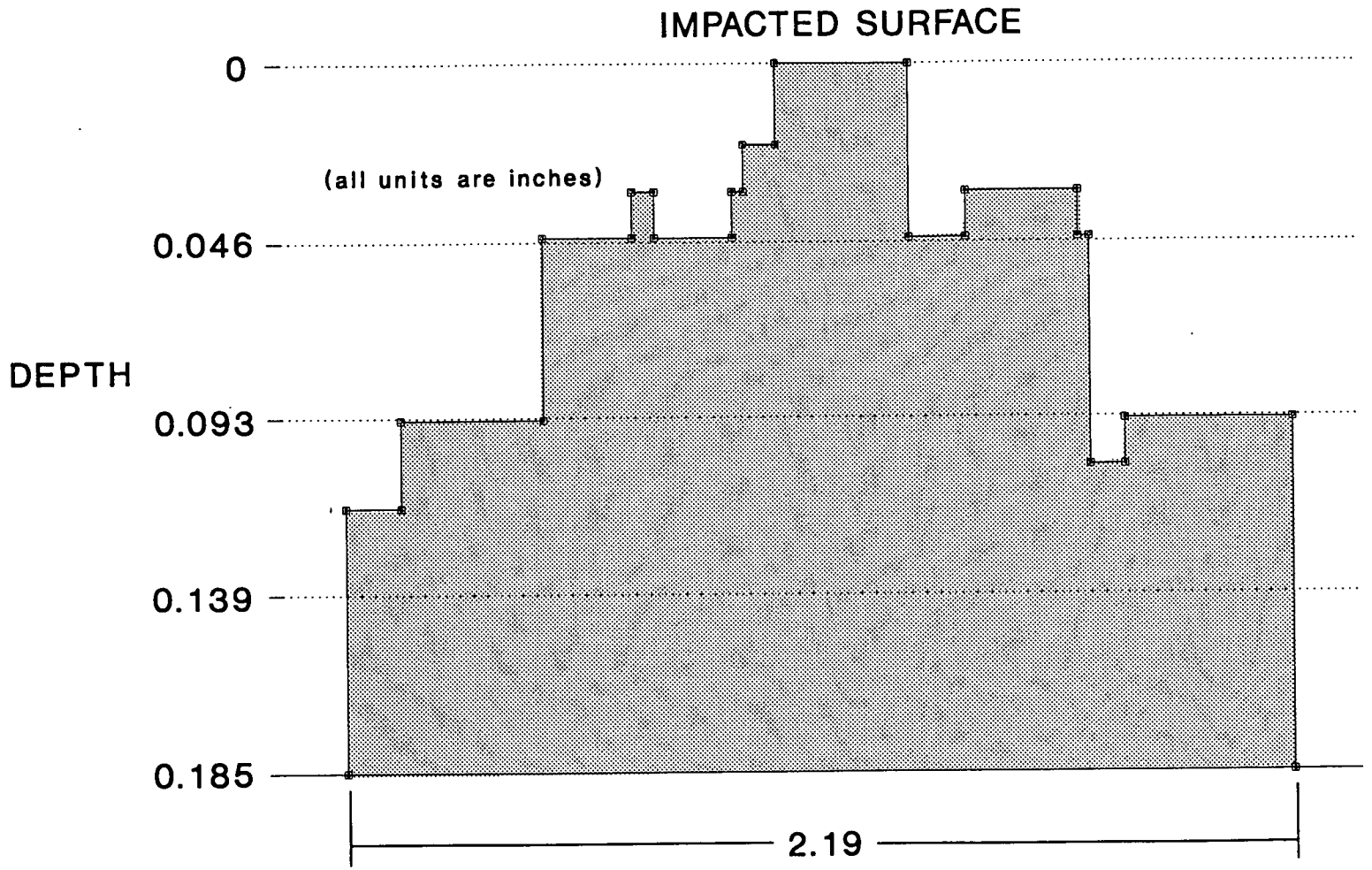

Figure 42. Cross section of through-the-thickness damage sustained by panel E76-1, a 32-ply monolithic laminate impacted by a 1/2-inch diameter steel sphere at 380 f/s.

The three laminates impacted at lower velocities (see Figures 40-42) display a clear transition from shear plugging to delamination at a depth of approximately 0.046-inch. In fact, as the impact velocity is decreased, the fracture mode transition appears more pronounced. Only in the C-scan cross section of panel E79-3 (see Figure 39) is the fracture mode transition not identifiable. Rather than showing an abrupt transition from a narrow shear path to wide spread delamination, the damage spread seems to expand somewhat uniformly with depth.

6.3.3 Estimating the Depth of Transition

Applying equation 4 (repeated here for convenience) to the impact events of panel E78-3, the predicted fracture mode

$$z_{\text{LOWER BOUND}} = \frac{v_p\ (2t - z)}{c_L} \qquad (4R)$$

transition occurs at a depth (z) of 0.034-inch and is considered a lower bound. This depth is compared to that of the actual transition in the form of a z-t diagram as illustrated in Figure 43. (Note: The predicted depth is based on the projectile's preimpact (initial) velocity because the transition occurs so near the impacted surface.) The deeper actual transition is believed the result of a localized zone of compressed material which precedes the projectile

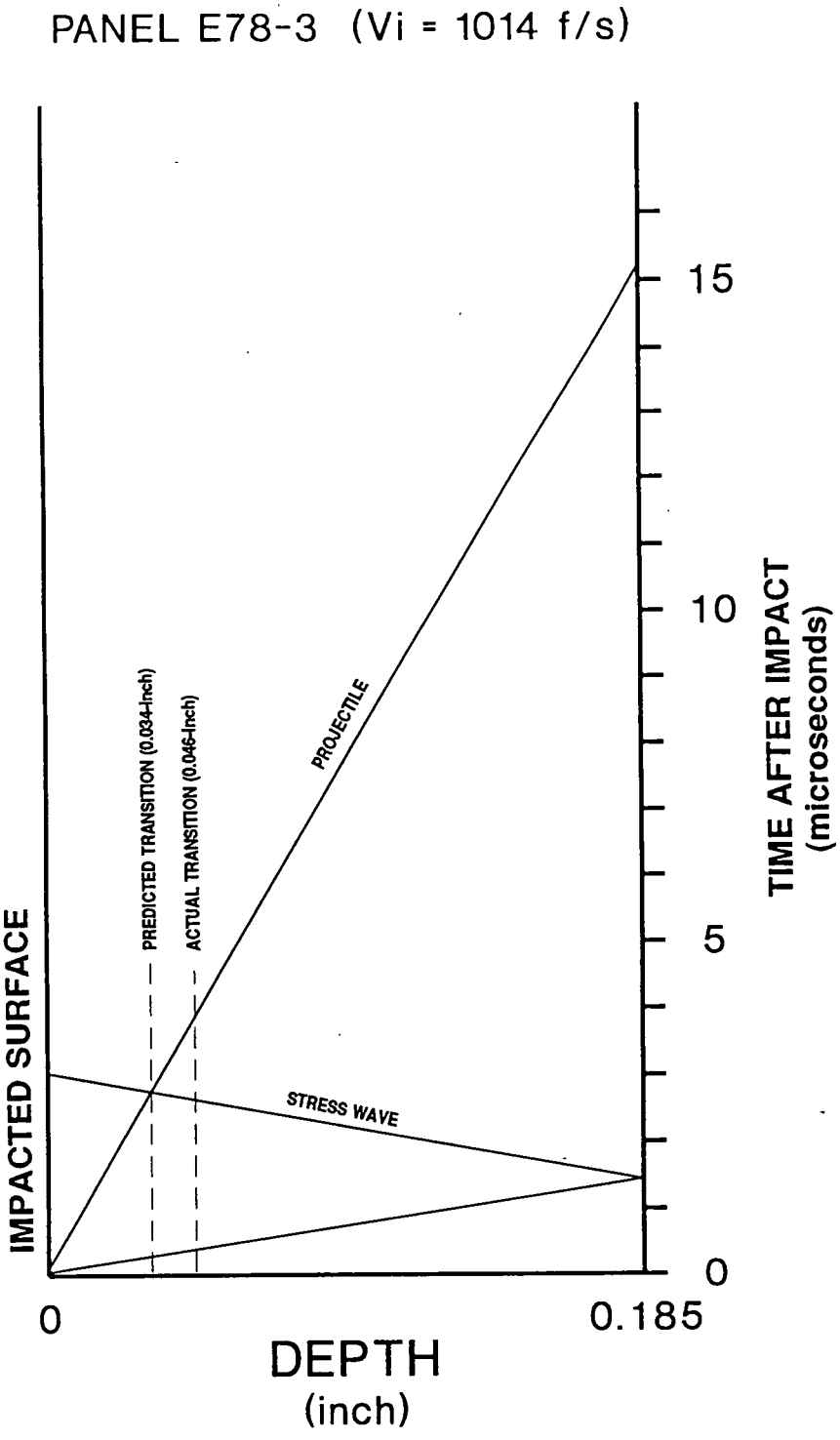

Figure 43. Typical z-t diagram of the tensile return wave's interaction with the projectile (panel E78-3).

through the laminate. Based on the times at which gages (of known depth) were influenced by the localized compression zone and the estimated projectile depth, the thickness of the compression zone was quantified[44]. Figure 44 describes a summary of observations that encompass impact velocities from 1300 to 2380 f/s. While the behavior may not be appropriate for use at velocities near the V_{50}, the velocities are comparable to those used in this investigation. An empirical modification to equation 4 is included in equation 5, which is simplified to become equation 6.

$$z_{\text{UPPER BOUND}} = z_{\text{LOWER BOUND}} + 0.015 + 0.338\ (z_{\text{LOWER BOUND}}) \quad (5)$$

$$z_{\text{UPPER BOUND}} = 1.338\ (z_{\text{LOWER BOUND}}) + 0.015 \quad (6)$$

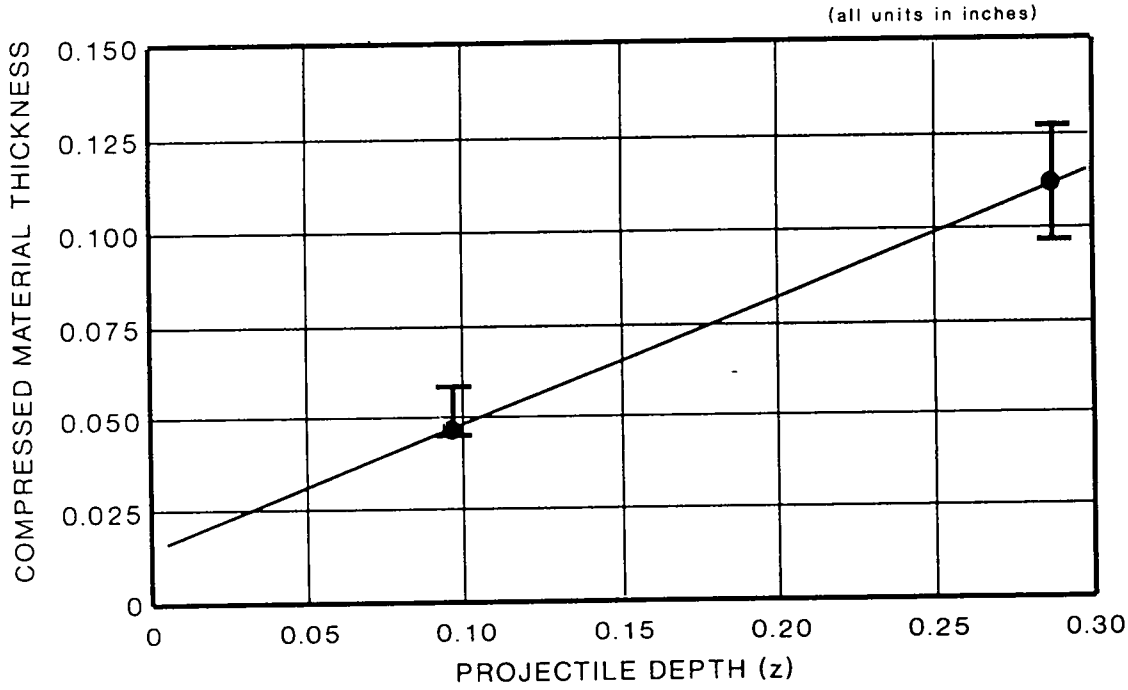

Figure 44. Thickness of compressed material (which precedes the projectile) as a function of projectile depth[44].

Based on equation 6, the upper bound transition for panel E78-3 is expected to be at 0.060-inch. The z-t diagram for panel E78-3 is modified in Figure 45 to show upper and lower bounds of the fracture mode transition as compared to the actual transition. Table 13 lists a summary of the relationships between the actual transition and the upper and lower bounds. For the lowest velocities (well beyond the limits of data used to establish Figure 44), the actual transition occurred slightly outside the upper bound. For the range of velocities markedly above the V_{50} however, equations 4R and 6 appear to establish accurate bounds on the fracture mode transition and lend credibility to the hypothesis.

Table 13. Summary of fracture mode transition data for selected monolithic laminates.

PANEL NO.	IMPACT VELOCITY (in)	LOWER BOUND FRACTURE MODE TRANSITION (in)	UPPER BOUND FRACTURE MODE TRANSITION (in)	ACTUAL FRACTURE MODE TRANSITION (in)
E79-3	2380	0.071	0.110	?
E78-3	1014	0.034	0.060	0.046
E74-1	392	0.013	0.032	0.044
E76-1	380	0.013	0.032	0.044

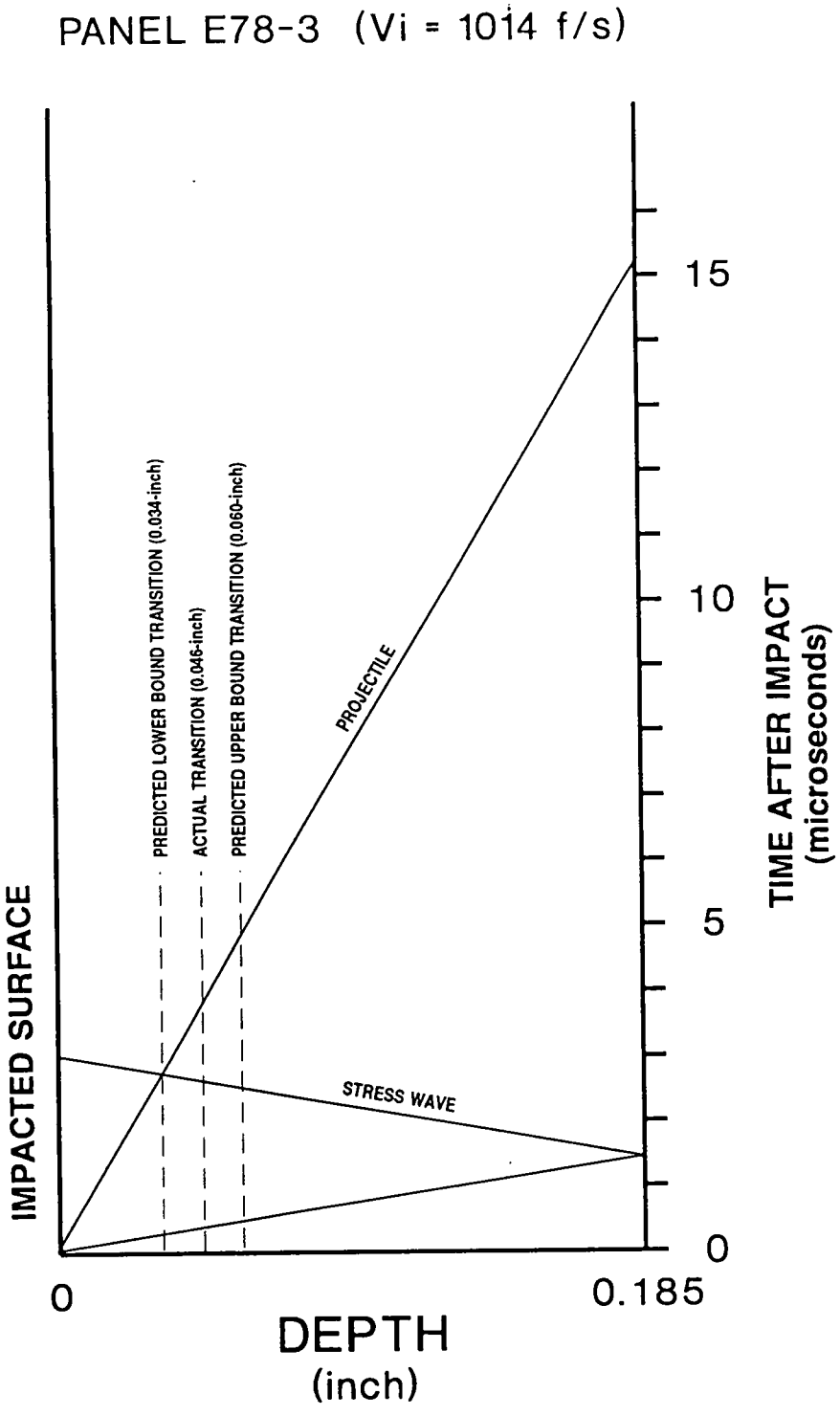

Figure 45. Z-t diagram showing the relationship between the actual fracture mode transition and the upper and lower bounds.

CHAPTER VII

SUMMARY AND CONCLUSIONS

7.1 Summary

An experimental procedure was developed to observe transverse stress wave propagation through impacted composite laminates. Impact experiments were performed on instrumented graphite/epoxy (AS4/3501-6) laminates in an effort to determine the basis for delamination initiation and propagation. In doing so, an explanation for the fracture mode transformation from shear plugging to delamination was established. When high-velocity steel spheres (1/2-inch diameter) contacted the quasi-isotropic laminate, two compressive non-planar stress waves were generated. One wave propagated into the laminate and the other into the projectile. The laminate's compressive stress wave was recorded by imbedded stress and strain sensors to have progressed through the laminate and reflected at the rear surface. The resulting tensile wave was demonstrated to have been attenuated by localized compression associated with the on-coming projectile. Inspection of time-of-flight C-scans did not reveal a direct correlation between the predicted location of tensile wave attenuation and the last interface delaminated. A slight adjustment to the method of prediction

(which accounts for the compressed material ahead of the projectile) lends itself to an accurate explanation for the fracture mode transition from shear plugging to delamination. The laminate's tensile wave is identified to have sufficient energy to initiate and propagate delamination from the rear surface toward the point of impact. The transition from shear plugging to delamination is therefore identified to occur when the locally compressed material, adjacent to the projectile's leading edge, overpowers the tensile stress wave.

7.2 Conclusions

An experimental procedure was developed and applied to attain transverse stresses and in-plane strains generated by high velocity impacts. The compressive stress wave had sufficient amplitude such that with reflection from the rear surface, delamination would easily occur. Stress wave events proved to have greater significance early in the impact sequence than flexure events. Based on experimental results, and accounting for material compressed in front of the projectile, the hypothesis appears reasonable.

Electromagnetic coils provided accurate residual velocity measurements and proved capable of discriminating between the steel projectile and accompanying composite spall. Steel spheres penetrating monolithic 32-ply quasi-isotropic laminates proved to sustain a drastic reduction in residual

velocity as the V_{50} was approached. Significant increases in energy absorption (synonymous with significant reductions in residual velocity near the V_{50}) resulted in similar increases in both delamination area and damage volume. As the projectile's residual velocity increased uniformly above the V_{50}, the damage volume decreased sharply and quickly attained a constant.

The V_{50} of monolithic quasi-isotropic graphite/epoxy laminates proved to be a well defined velocity which can be predicted accurately from a linear regression of the initial vs residual energy terms. Post-bonded quasi-isotropic laminates (consisting of four unbalanced unsymmetric sublaminates) proved to absorb the same amount of impact energy (based on V_{50} test results) as their monolithic counterparts.

An inspection of the penetration path through composite laminates revealed a form of shear plugging adjacent to the impacted surface which transitioned into a region of delamination adjacent to the rear surface. Disbonds (generated during the impact event) in post-bonded laminates proved to mask this typical form of impact-generated damage.

Impact-generated transverse (through-the-thickness) stress wave propagation can be monitored by imbedded carbon stress and constantan strain gages when used in combination with a pulsed power supply and high speed data acquisition system. The fact that the tensile wave amplitude is established quickly and has an amplitude exceeding that required to create delamination, together with the fact that flexure is a relatively slow event, suggests delamination is initiated and propagated by the tensile return wave.

The impact-generated compression stress wave velocity is approximately 121,000 in/s. This velocity correlates closely with the material's acoustic wave velocity (118,000 in/s) as determined via NDI techniques. Initial indications are that the stress wave amplitude varies with the impact velocity. Measured through-the-thickness stress wave amplitudes are in excess of 230 ksi for the test cases presented.

The time of projectile contact with the laminate proved to be a difficult measurement. An estimated time-of-contact, based on the first stress gage response and the known stress wave velocity is believed accurate to within 100 n-sec.

Although the flexure wave velocity proved erratic (likely due to limitations associated with the flexure sensor), the maximum out-of-plane flexure (as measured at the far-field

location) proved to remain roughly constant at 0.015-0.020 inch.

The combined in-plane stress wave divergence and Poisson's effects (as measured by the strain gages) proved difficult, but resolvable within the 8-bit (120 mV) resolution provided by the data acquisition system.

A direct relationship between the tensile wave's interaction with the on-coming projectile, and the fracture mode transition's depth could not be established with so few tests as were conducted. Only by assuming that a thin zone (approximately 0.03-inch) of compressed material exists in front of the penetrating projectile can the above explanation be modified to accurately predict the fracture mode transition plane.

At impact velocities above 1000 f/s, shear plugging is not readily evident in C-scan cross sections. This suggests another mode of fracture may be occurring adjacent to the impacted surface (i.e., in-plane stress waves coupled with ply-to-ply stiffness mismatches). Because damage areas and volumes do not change to any significant degree above 1000 f/s, the effect is believed localized to the impacted surface.

7.3 Recommendations

The hypothesis (that the fracture mode transition occurs as a result of an interaction between the returning tensile stress wave and the localized compressive zone associated with the projectile) remains viable and requires further validation. Although initial results support the hypothesis, insufficient data were obtained during this investigation to provide conclusive proof. Other theories encountered relative to this subject appear inaccurate, however.

A piezofilm sensor should not be used to mark the projectile's time of contact if submicro-second accuracy is desired. A devise nonsensitive to the shock wave (preceding the projectile) needs to be used.

Future testing should be achieved using an on-center (replaceable tipped) fiber optic displacement sensor. Such a devise will allow direct correlation between rear surface flexure and the transient stress waves.

To fully appreciate the effects of the tensile return wave, from sub-penetration through penetration impact velocities, future testing should take the form of the three L8's (Taguchi test matrices) detailed in Appendix A.

Bondlines within the laminate should be achieved with a highly toughened room-temperature epoxy. Although delamination along toughened bondlines may not occur as readily as other interfaces, substantial extraneous damage (disbonding) will be avoided.

For further proof that delamination can be achieved by a tensile wave, another type of test can be performed. Using a single Hopkinson bar, a short duration planar compressive stress wave can be sent through the bar and into a two-piece laminate. (See Figure 46.) As the wave reflects from the

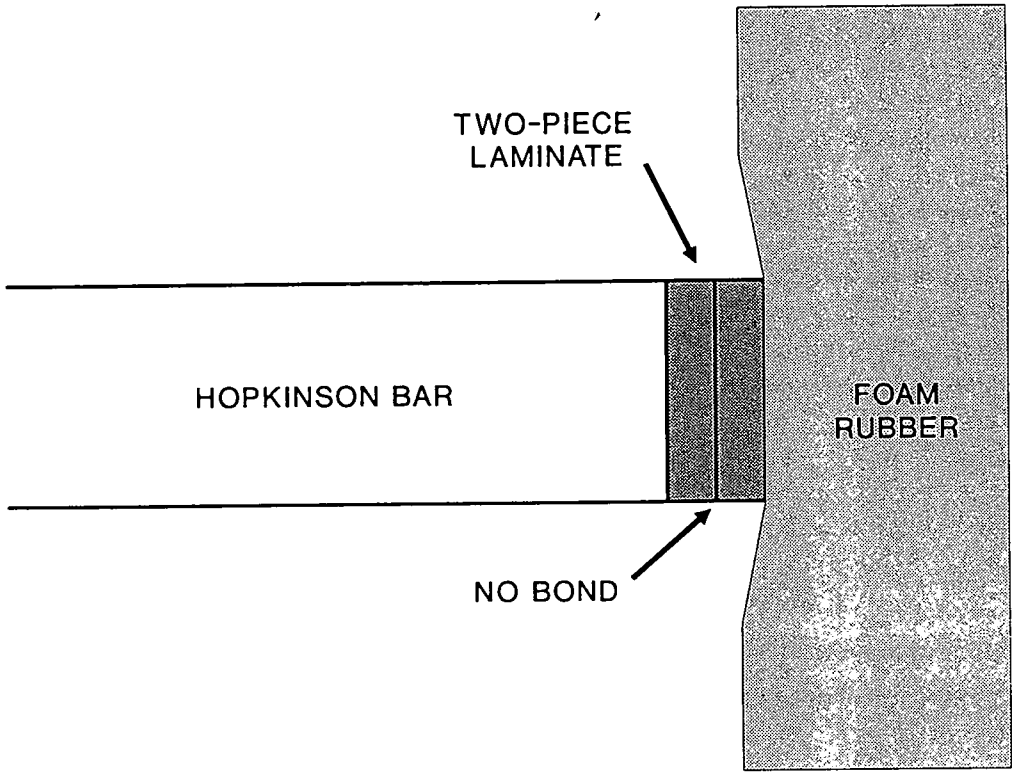

Figure 46. Proposed test configuration for future evaluation of the tensile wave's effect on delamination generation.

laminate's rear surface, the tensile stress will begin to delaminate the rearmost half of the specimen. Without a bondline between specimen halves, the tensile wave will not be transmitted to the remainder of the specimen.

APPENDIX A

Global Test Plan

A.1 General

Work directly associated with this thesis is considered preliminary to a more extensive in-house investigation of through-the-thickness stress wave propagation and its influence on fracture modes. Published literature relative to low velocity impacts on composites is abundant as compared to high velocity penetration studies. Research linking low and high velocity regimes is extremely rare. In the impending study, impacts in the low velocity range will be transitioned through the V_{50} into velocities well beyond those required for perforation.

A.2 Taguchi Experimental Setup

Although objectives presented in this thesis were achieved using a limited number of tests, a more detailed investigation of the impact generated stress wave's influence on delamination initiation and propagation will be achieved through a series of experiments designed according to Taguchi[45] methodology. Because nonlinearities in the laminate's response are expected to occur across the velocity spectrum (especially through the V_{50}), the full effects of velocity will be determined by performing three sequential L8 test series (the design of which is shown in Table A-1). Columns marked AB, AC, and BC are reserved for the interactions between factors. The last column in the L8 design is reserved for error accumulation and is used to determine if a significant

TABLE A-1. L8 matrix.

TEST NO.	A	B	AB	C	AC	BC	error
1	1	1	1	1	1	1	-
2	1	1	1	2	2	2	-
3	1	2	2	1	1	2	-
4	1	2	2	2	2	1	-
5	2	1	2	1	2	1	-
6	2	1	2	2	1	2	-
7	2	2	1	1	2	2	-
8	2	2	1	2	1	1	-

	Level 1	Level 2
A = density	low	high
B = velocity	low	high
C = thickness	low	high

factor, affecting the test results, has been omitted. Any tests not determined to be fair (i.e., the impact was not in the panel's geometric center, or significant amounts of test data failed to be recorded) are repeated.

Significant factors (i.e., density, velocity, and thickness) and interactions between factors (i.e., AB, AC, and BC) are obtained using Taguchi methodologies. The AB interaction is significant if delamination is a strong function of stress wave amplitude. The BC, and to a lesser extent, the AC interactions are significant if delamination is a strong function of panel deflection. A level of confidence is established for each significant factor/interaction using Analysis of Variance (ANOVA) techniques.

The first L8 will involve nonpenetration projectile velocities ranging from 100 f/s up to the V_{50} for 32-ply laminates impacted by 1/2-inch diameter steel spheres. The second L8 test series will consist of velocities bracketing the V_{50}'s for 32-ply laminates (impacted by steel projectiles) and 128-ply laminates (impacted by aluminum projectiles). The third L8 will involve penetrating projectile velocities ranging from the V_{50} for 128-ply laminates (impacted by aluminum spheres), up to 2,380 f/s. The first L8 performed will be verified by a 1/2 replication using an L4 (four tests). Results from the L8 will be compared to those of the 12 combined tests. The value of replications for the remaining two L8's will be based on this comparison. Randomized versions of the three L8's (with replications) are listed in Tables A-2 through A-4.

TABLE A-2. Nonpenetration tests (L8 no. 1).

SHOT NO.	TEST NO.	DENSITY (lb/in^3)	VELOCITY (f/s)	THICKNESS (plies)
1	4	0.099	250	128
2	7	0.284	250	32
3	1R	0.099	100	32
4	5	0.284	100	32
5	6	0.284	100	128
6	3	0.099	250	32
7	4R	0.099	250	128
8	2	0.099	100	128
9	7R	0.284	250	32
10	6R	0.284	100	128
11	1	0.099	100	32
12	8	0.284	250	128

(The R designations refer to tests which may be repeated to achieve a half repetition.)

TABLE A-3. V_{50} tests (L8 no. 2).

SHOT NO.	TEST NO.	DENSITY (lb/in^3)	VELOCITY (f/s)	THICKNESS (plies)
1	7	0.284	HIGH	32
2	1	0.099	350	32
3	3	0.099	HIGH	32
4	5	0.284	350	32
5	2	0.099	350	128
6	8	0.284	HIGH	128
7	6	0.284	350	128
8	1R	0.099	350	32
9	4R	0.099	HIGH	128
10	6R	0.284	350	128
11	7R	0.284	HIGH	32
12	4	0.099	HIGH	128

HIGH = V_{50} (for 128-ply laminates impacted by aluminum spheres) + 50 f/s.

TABLE A-4. Penetration tests (L8 no. 3).

SHOT NO.	TEST NO.	DENSITY (lb/in^3)	VELOCITY (f/s)	THICKNESS (plies)
1	7R	0.284	2380	32
2	8	0.284	2380	128
3	5	0.284	LOW	32
4	6	0.284	LOW	128
5	6R	0.284	LOW	128
6	2	0.099	LOW	128
7	1R	0.099	LOW	32
8	1	0.099	LOW	32
9	4R	0.099	2380	128
10	7	0.284	2380	32
11	4	0.099	2380	128
12	3	0.099	2380	32

LOW = HIGH (from the previous L8) + 100 f/s.

The second L8 (spanning V_{50} velocities) is defined to be 25 f/s less than the lowest V_{50} and 50 f/s greater than the highest V_{50} obtained. The upper bound of the first L8 (involving nonpenetration velocities) is defined to be 100 f/s less than the lower bound of the second L8. The lower bound of the third L8 (involving penetration velocities) is defined to be 100 f/s greater than the upper bound of the second L8.

A.3 Projectiles

Projectiles will be aluminum (ρ=0.099 lb/in^3 (2.7 g/cm^3), E=10.7 msi) and steel (ρ=0.284 lb/in^3 (7.9 g/cm^3), E=30 msi) spheres. The projectile density is varied to evaluate the effect of the projectile's release wave on the damage generated. Each projectile's diameter, however, will remain constant at 0.50 inch to maintain a consistent contact area during impact.

A.4 Test Specimens

The composite material used throughout this study will be graphite/epoxy (AS4/3501-6). Two quasi-isotropic laminate thicknesses (32-ply and 128-ply) will be used in the study to assist in determining flexure effects on delamination. By varying the panel thickness and maintaining a constant impact energy, the reflecting tensile wave may have a chance to perform work on different numbers of ply interfaces before being attenuated. The relatively stiff 128-ply laminates are

expected to simplify stress wave resolution (more time transpires before the wave is reflected) and post-mortem fracture mode observations.

A.4.1 Specimen Configuration and Instrumentation

All sensors will be positioned along the shotline in the geometric center of the panel. (See Figure A.1) Sensors located on the midplane will be sandwiched between a pair of -45° plies (a nonfavorable delamination interface), whereas all other sensors will be mounted on "favorable" 0/-45 interfaces.

Carbon stress gages (relatively insensitive to in-plane stresses) and constantan strain gages (relatively insensitive to normal stresses) will be used throughout the study. All gages will be dispersed throughout each panel in an alternating fashion (as described earlier in Figure 20) and used to track the stress wave's progress and pin-point the transition plane's location. To eliminate the effect of flexure and provide a direct observation of stress wave's dilatation and Poisson's effects, strain gages will commonly be placed on the laminate's centerline. In some 128-ply laminates, stress and strain gages will be mounted back to back and placed within single interfaces. When back to back gages are used, gages will be installed in one of two different alternating sequences shown in Figure A.2.

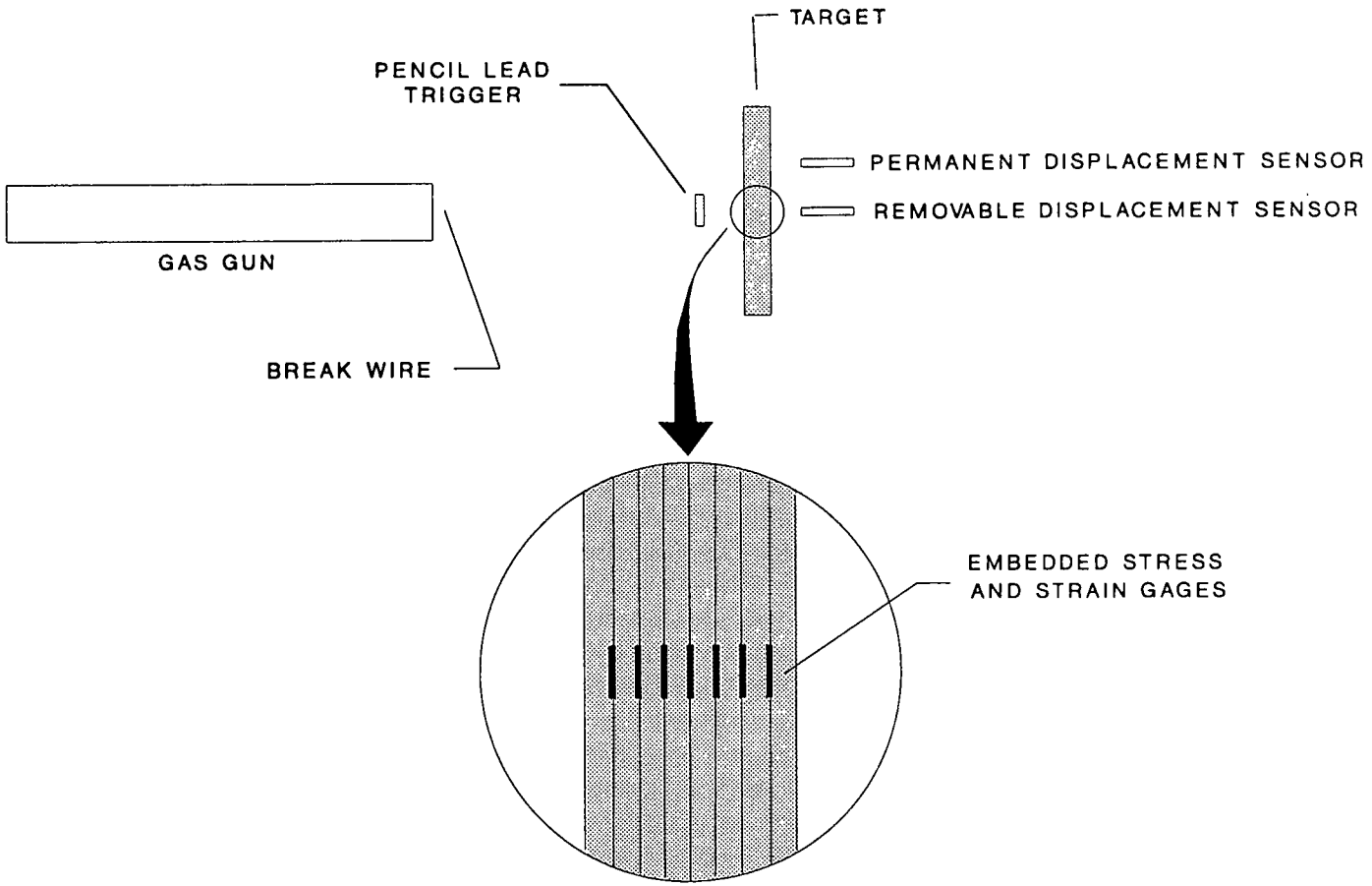

Figure A.1. Shotline through the imbedded instrumentation.

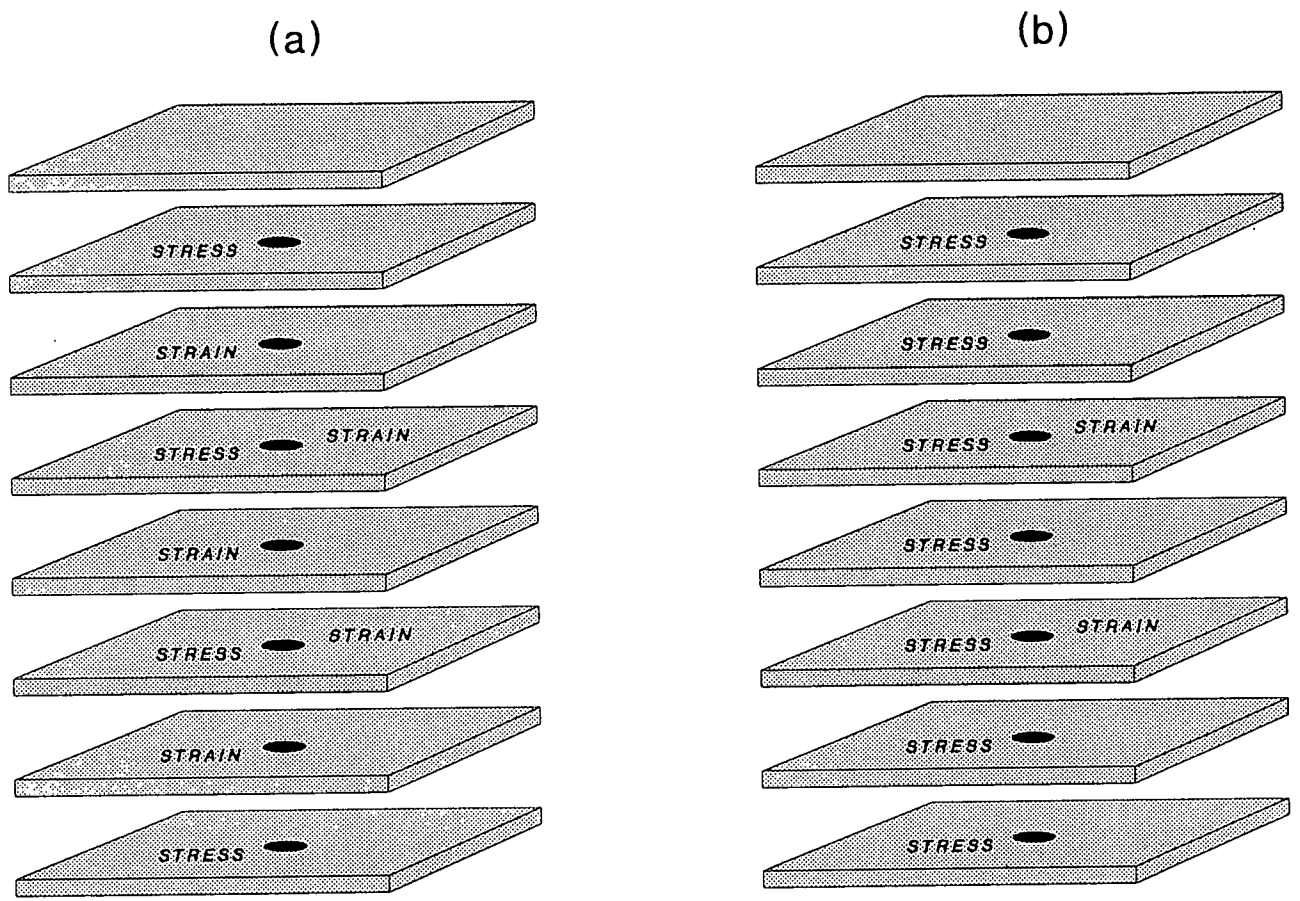

Figure A.2. Alternative gage stacking sequences for 128-ply laminates.

Significant reductions in measured stress wave amplitude will be correlated with damage generated.

In addition to the imbedded sensors, an external time-of-contact sensor will be installed on the specimen's surface. For low velocity impacts, this sensor will also expected to indicate the total contact time.

A.4.2 Specimen Bondlines

To ensure fracture modes are not affected by bondlines containing instrumentation, several tests will be repeated using monolithic laminates. An adjustment factor will be used to correlate post-bonded laminate damage with damage sustained by monolithic specimens. A lack of direct correlation between post-bonded and monolithic configurations is not expected to influence the validity of this study. Location of the fracture mode transition plane is expected to be a function of the stress wave and projectile velocities, rather than the extent of damage generated, or excess energy available. In any event, post-mortem studies (to include laminate deplying) will be performed to assist in evaluating the bondline's influence.

A.5 Displacement Measurements

For nonpenetrating projectiles, two fiber optic displacement sensors will be used to observe the target's rear

face; one on-center and one off-center. The on-center sensor will provide a direct measurement of maximum deflection, whereas the off-center sensor will obtain the flexure wave's velocity and be calibrated as a predictor of maximum deflection. During penetration tests, only the off-center sensor will be used.

If deflection is the primary cause of delamination, stiffer/thicker panels should deflect less and therefore sustain less delamination as illustrated in Figure A.3. Without adequate flexure, little or no Mode II initiated delamination is expected.

A.6 Post-Mortem Investigations

Post-mortem investigations will include C-scans (to evaluate the area of delamination and approximate volume of damage), cross section fractographs (to directly observe through-the-thickness fracture along the shotline), and laminate deplying (for a complete and detailed evaluation of through-the-thickness damage). Total through-the-thickness damage (delamination plus shear plugging) is determined precisely by injecting a dye (commonly gold chloride) into the region and disbonding the laminate ply by ply. Integration of the damage volume (or in the case of disbonding, summation of all areas) can then be correlated with the projectile's change in kinetic energy.

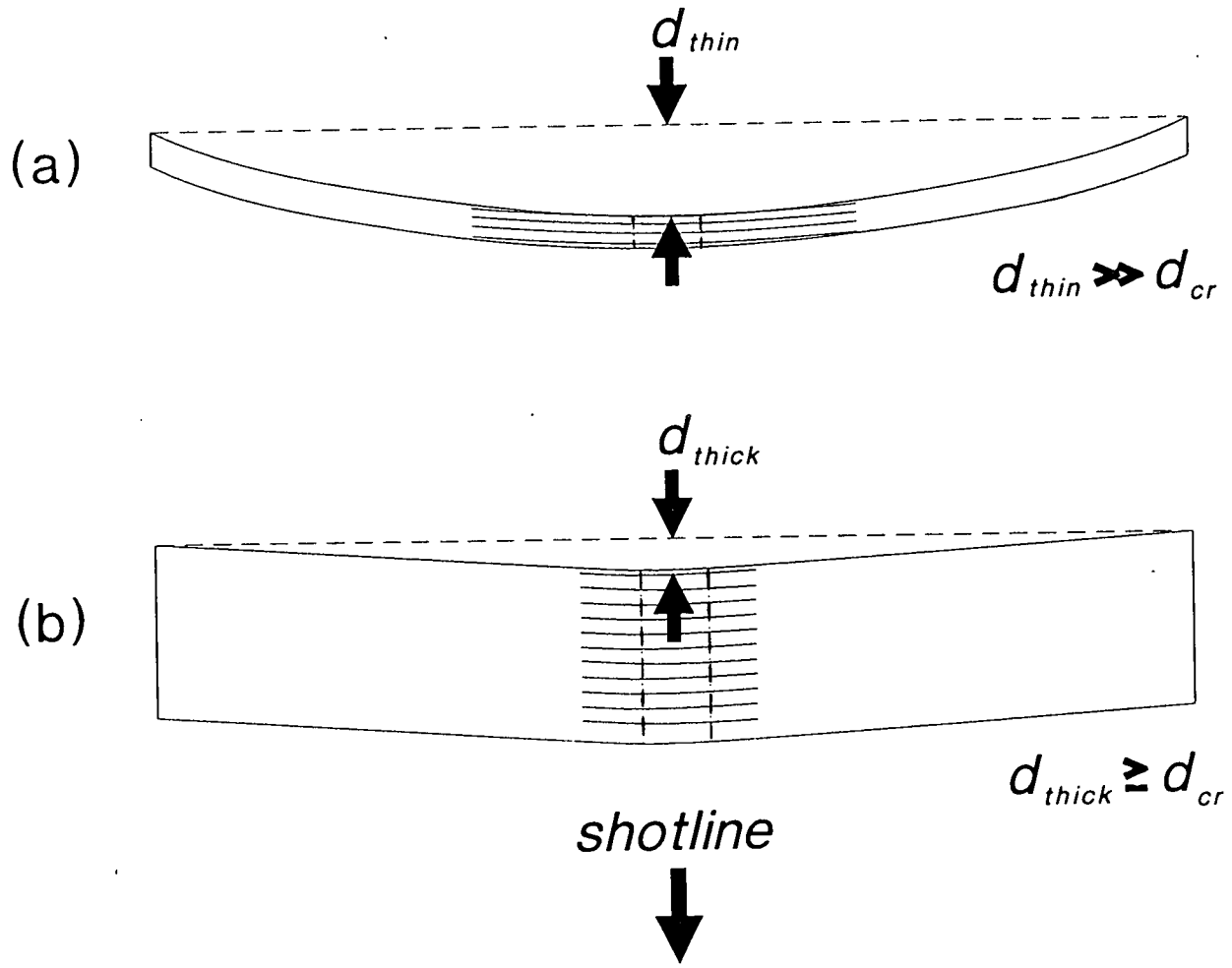

Figure A.3. Mode II generated delamination as a function of laminate thickness.

One must keep in mind however that several forms of damage occur during penetration (matrix cracking, delamination, fiber fracture, and fiber-resin interface disbonds) via several mechanisms (tensile, shear, and flexural waves, mechanical contact, etc.). Other factors contributing to the projectile's change in kinetic energy include material heating, transformation, and ejecta (spall). Although the change in kinetic energy may be predominated by one or two of these events, all are believed to have an influence.

The extent of damage will be correlated with stress and flexure wave amplitudes. Significant reductions in the measured stress wave amplitude (from interface to interface) will be correlated with damage generated, as observed during post-mortem studies. Integration of the damage volume (or in the case of disbonding, summation of all areas) will also be correlated with the projectile's change in kinetic energy. Cross sectional photomicrographs of the damaged zone will be obtained to directly observe the transition from shear plugging to delamination.

Energy absorbed (which can be attributed to damage generation) will be approximated by subtracting residual kinetic energies (of the projectile and spall) from the projectile's initial energy. The spall's mass will be assumed

equal to the panel's change in weight, with the average velocity equal to the projectile's residual velocity.

A.7 Pretest

Noninstrumented 128-ply laminates (fabricated from eight 16-ply sublaminates) will be subjected to V_{50} testing (using aluminum spheres) to define the upper bound velocity of the second L8 and lower bound of the third L8.

Observing the uniformity of aluminum spheres to be used in these tests, 16 were weighed, producing the following results:

Average projectile weight = $\bar{X}$ = 0.00644 lb

Standard deviation = σ = 0.00002 lb

Coefficient of variation = $\sigma/\bar{X}$ = 0.0031

A.8 Data Reduction Schemes

The area of delamination generated on each interface is considered a function of the instantaneous tensile stress wave amplitude and bending stiffness mismatch. In the case of tensile generated delamination, the G_{Ic} is also expected to affect in-plane delamination. In this study, the bending stiffness mismatches and G_{Ic} (approximately 1.0 lb/in) remain constant from specimen to specimen. Only the tensile wave amplitude varies, and does so according to the impact velocity. Direct correlations of delamination to the tensile

wave amplitude will therefore be considered further proof that delamination is the result of a tensile stress wave.

If the extent of delamination along a selected interface can be related to the tensile wave amplitude, wave duration, and the material's G_{Ic}, total damage within a laminate can be predicted. Determining the wave's energy loss over time will be critical since the energy lost is believed proportional to the area of delamination generated.

APPENDIX B

Calibration Procedures for Test Instrumentation

B.1 Stress Gage Calibration

After balancing bridges (in the pulsed power supply) associated with each gage, the power supply is manually triggered to generate a 120 μ-sec square wave pulse. Data acquired during the event is then surveyed to ensure that output from all gages register zero volts.

The calibration process continues by replacing each gage with a series of dummy resistors (with different resistance values) having resistance less than the gage. The change in resistance (%ΔR) is noted with respect to the original gage resistance. With each change in resistance, the pulsed power supply is triggered and an output voltage (V) recorded. (The %ΔR vs V curve generated for panel B1.3 is shown in Figure B.1.)

When the calibration procedure is completed, imbedded stress and strain gages are reattached to the pulsed power supply. Test output is in the form of volts (negative volts indicating a decrease in resistance and therefore compression). (Note: Although positive voltage output indicates tension, stress gages are not capable of registering an accurate tensile amplitude.) Voltage is then associated with a change in resistance from the calibration procedure. Once the change in resistance is known, a corresponding stress

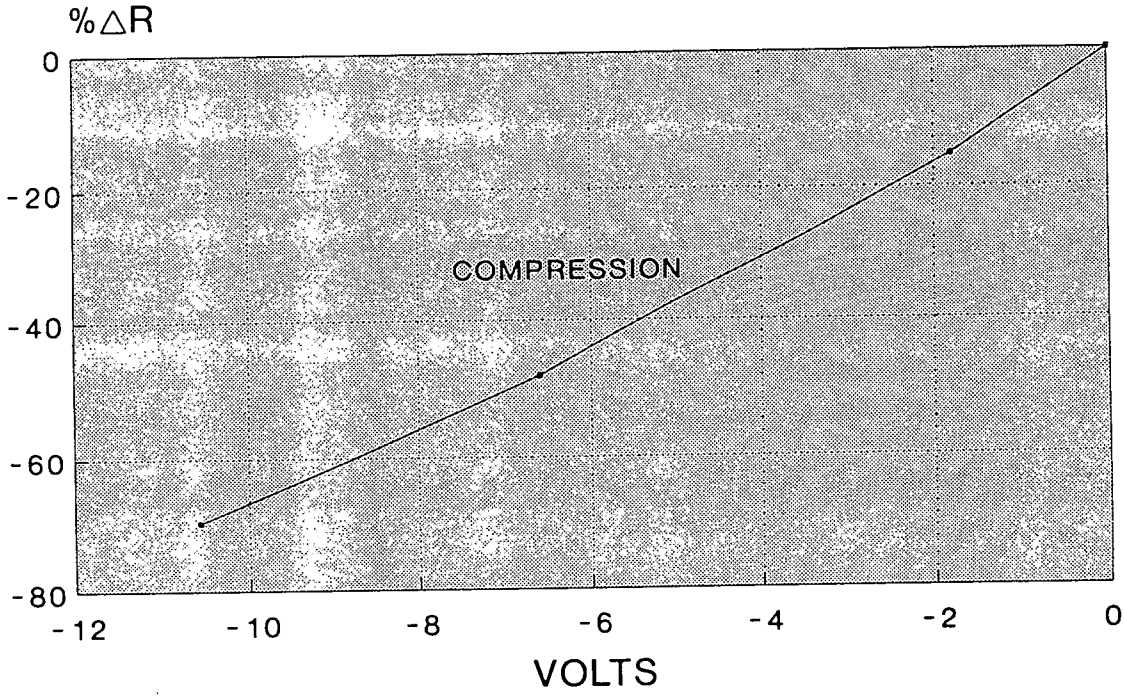

Figure B.1. Change in resistance vs voltage output from the stress gage (position 3) in specimen B1.3.

can be obtained from the data curve in Figure B.2 (supplied by the sensor manufacturer).

B.2 Strain Gage Calibration

The strain gage calibration procedure is nearly identical to that of the stress gages. Because the gages are capable of registering accurate tensile and compressive strains, dummy resistors having values both higher and lower than the strain gage resistance are included in the calibration procedure. (The %ΔR vs V curve generated for panel B1.3 is shown in Figure B.3.) Voltages recorded during the impact test are associated with a percent change in resistance (%ΔR). The

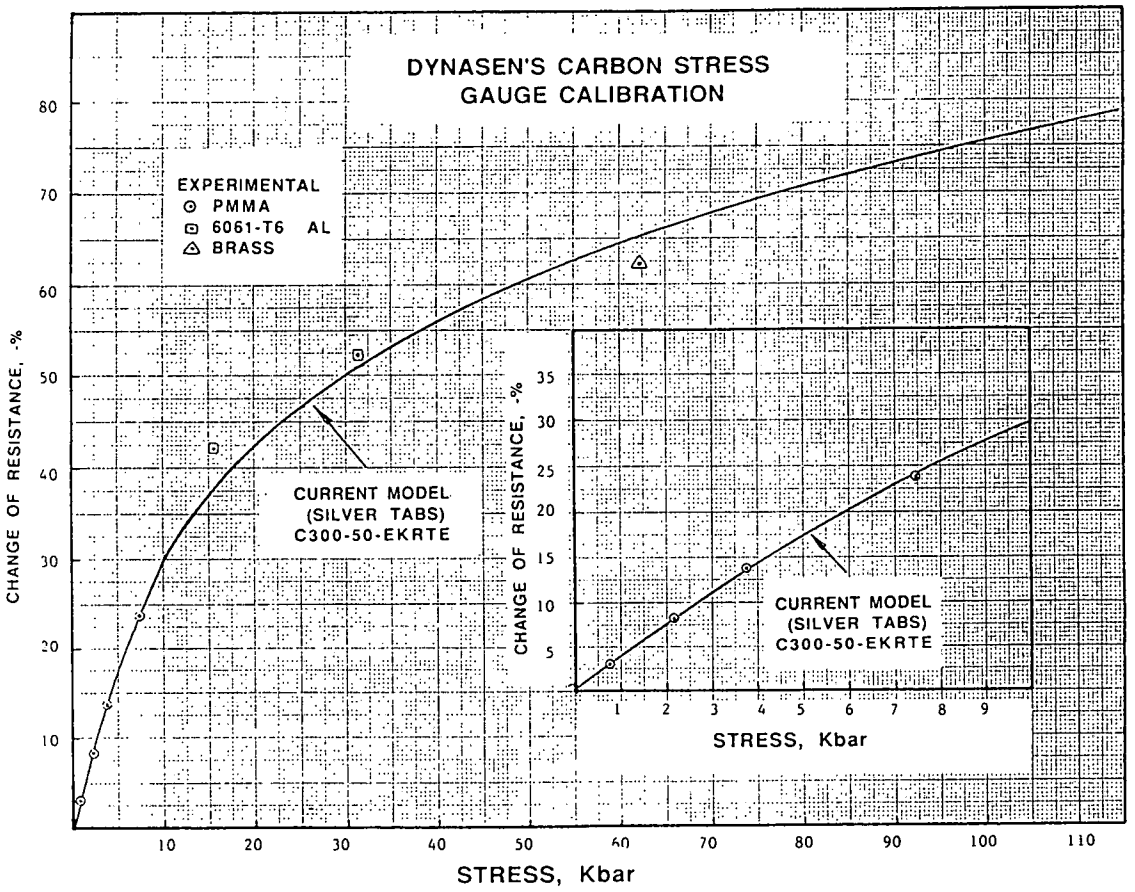

Figure B.2. Calibration curve for carbon stress gages.

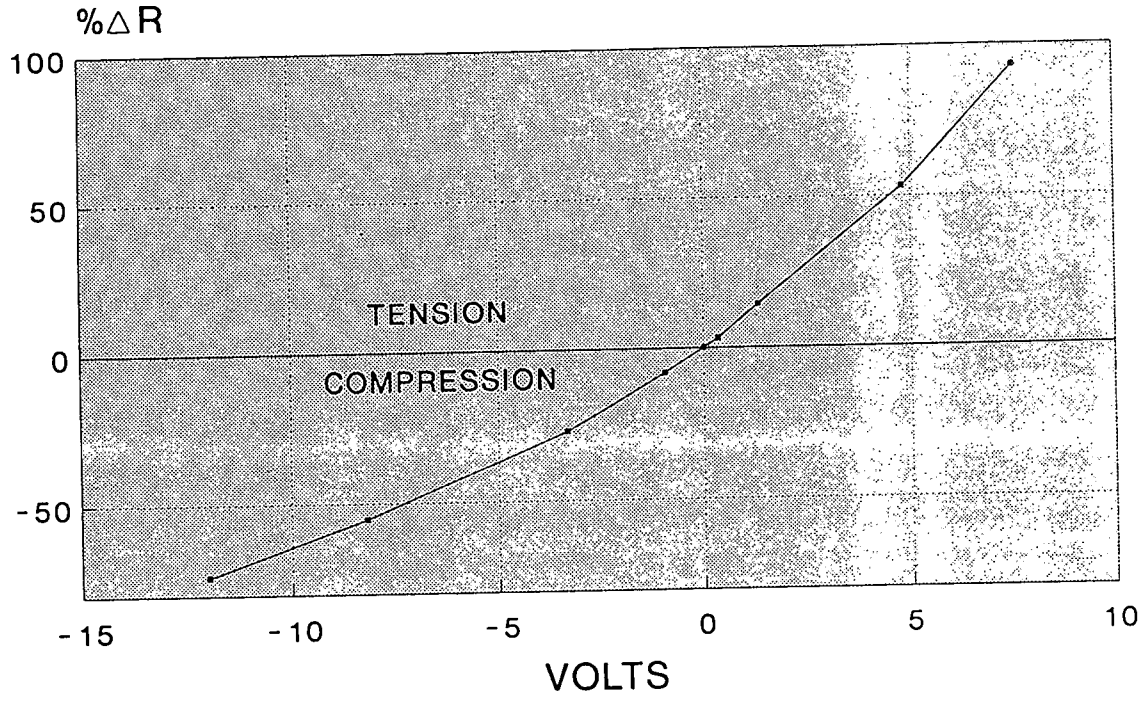

Figure B.3. Change in resistance vs voltage output from the strain gage (position 2) in specimen B1.3.

strain is then calculated using equation B.1, where G is the gage factor and ε is strain. (Note: All strain gages have a gage factor of 1.5 for biaxial strain conditions.)

$$\%\Delta R = G\ (\varepsilon) \qquad (B.1)$$

$$\%\Delta R = 1.5\ (\varepsilon)$$

$$\varepsilon = \frac{\%\Delta R}{1.5}$$

B.3 Fiber Optic Displacement Sensor Calibration

Prior to the calibration procedure, a spot of silver paint is applied to the rear surface of the test specimen to

enhance light reflection. With the fiber optic wand oriented perpendicular to the spot on the specimen's surface, it is moved to a distance from the surface which produces maximum voltage output (approximately 0.03-inch). The voltage gain is then adjusted to provide a voltage output of exactly 5 volts. With 5 volts now being the maximum output, further displacement of the sensor relative to the specimen's surface corresponds to the data curve in Figure B.4. Taking full advantage of the linear portion of the data curve, the sensor is then moved away from the specimen and locked into a position which provides a 3.75 volt output. (This corresponds to a distance from the specimen's surface of 0.15-inch.) In this linear range, a 1 mV change in voltage equates to an 87

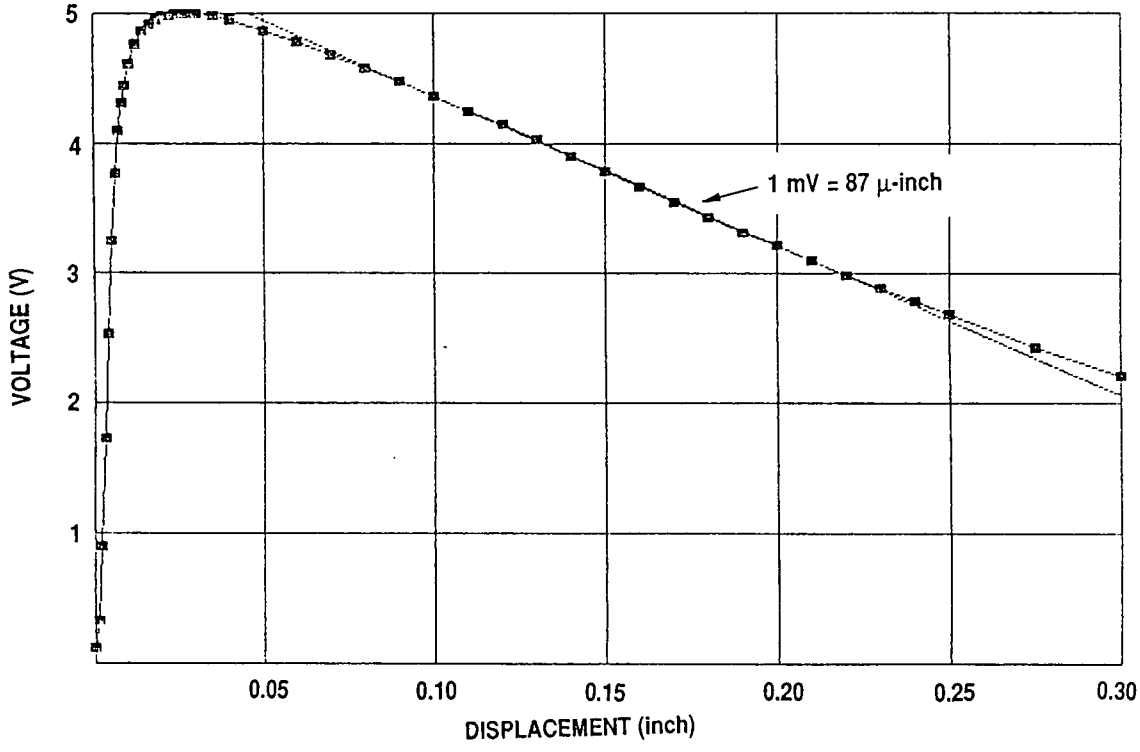

Figure B.4. Calibration curve for the displacement sensor.

μ-inch displacement. (Note that positive changes in voltage correspond to a decreased distance between the sensor and the panel surface.)

APPENDIX C

Estimations of Stress Wave Amplitudes as a Function of Depth

A lower bound estimate of the stress wave amplitude was calculated based on extrapolations obtained from Greszczuk[46]. Flat composite laminates (having differing modulus ratios) were impacted by 1.5-inch diameter spheres at 125 f/s. The resulting stresses are illustrated in Figure C.1. To estimate the stress wave magnitude if an AS4/3501-6 laminate were employed, one must first determine the associated E_R/E_Z ratio.

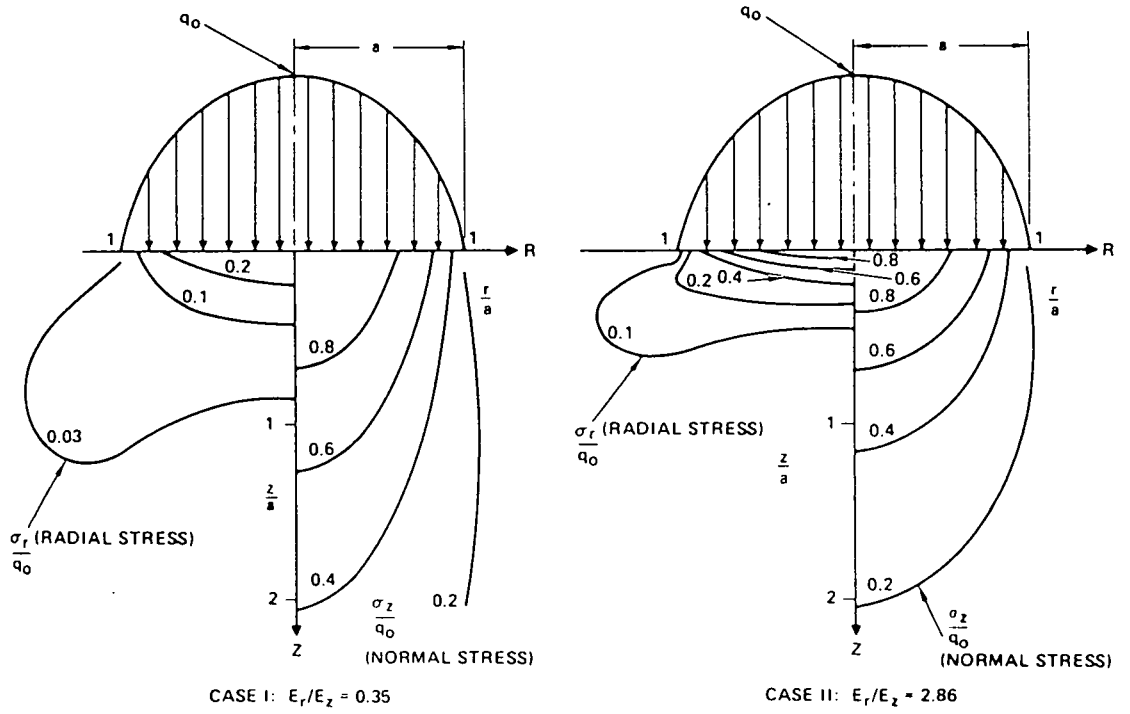

Figure C.1. Case I and case II stresses generated within a composite laminate (q_o = 400 ksi, a = 0.242-in, and v = 125 f/s)[46].

Material properties for AS4/3501-6 (graphite-epoxy) are as follows:

E_L = 20 msi

E_T = 1.982 msi (based on NDI results)

G_{12} = 0.91 msi

assume $\mu_{12} = \mu_{21} = \mu_{LT} = 0.25$

These properties are similar to that of a T300/epoxy plate, for which, internal stresses are known (Ref. 45). Solving for the effective in-plane modulus (E_{eff}):

For a balanced symmetric lay-up, $E_{eff} = \dfrac{Q_{11}\ Q_{12} - Q_{12}}{Q_{22}}$

For 0° plies, $Q_{11}^0 = \dfrac{E_L}{1 - \mu_{LT}^2} = \dfrac{20}{1 - (0.25^2)} = 21.33$

$$Q_{12}^0 = \frac{\mu_{LT}\ E_L}{1 - \mu_{LT}^2} = \frac{(0.25)\ 20}{1 - (0.25^2)} = 5.33$$

$$Q_{22}^0 = \frac{E_T}{1 - \mu_{LT}^2} = \frac{1.982}{1 - (0.25^2)} = 2.114$$

For $\pm$45° plies, the Q's are transformed as follows:

$$Q_{11}^{45} = Q_{11} \cos^4\theta + 2(Q_{12} + 2\ Q_{66}) \sin^2\theta \cos^2\theta + Q_{22} \sin^4\theta$$

$$= 21.33\ (0.25) + 2\ (5.33 + 1.82)\ (0.25) + 2.114\ (0.25)$$

$$= 9.436$$

Material properties for AS4/3501-6 (graphite-epoxy) are as follows:

E_L = 20 msi

E_T = 1.982 msi (based on NDI results)

G_{12} = 0.91 msi

assume $\mu_{12} = \mu_{21} = \mu_{LT} = 0.25$

These properties are similar to that of a T300/epoxy plate, for which, internal stresses are known (Ref. 45). Solving for the effective in-plane modulus (E_{eff}):

For a balanced symmetric lay-up, $E_{eff} = \dfrac{Q_{11}\ Q_{12} - Q_{12}}{Q_{22}}$

For 0° plies, $Q_{11}^0 = \dfrac{E_L}{1 - \mu_{LT}^2} = \dfrac{20}{1 - (0.25^2)} = 21.33$

$$Q_{12}^0 = \frac{\mu_{LT}\ E_L}{1 - \mu_{LT}^2} = \frac{(0.25)\ 20}{1 - (0.25^2)} = 5.33$$

$$Q_{22}^0 = \frac{E_T}{1 - \mu_{LT}^2} = \frac{1.982}{1 - (0.25^2)} = 2.114$$

For $\pm$45° plies, the Q's are transformed as follows:

$$Q_{11}^{45} = Q_{11} \cos^4\theta + 2(Q_{12} + 2\ Q_{66}) \sin^2\theta \cos^2\theta + Q_{22} \sin^4\theta$$

$$= 21.33\ (0.25) + 2\ (5.33 + 1.82)\ (0.25) + 2.114\ (0.25)$$

$$= 9.436$$

$$Q_{12}^{45} = (Q_{11} + Q_{22} - 4\,Q_{66})\,\sin^2\theta\,\cos^2\theta + Q_{12}\,(\sin^4\theta + \cos^4\theta)$$

$$= (21.33 + 2.114 - 3.64)\,(0.25) + 5.33\,(0.5)$$

$$= 7.616$$

$$Q_{22}^{45} = Q_{11}\,\sin^4\theta + 2\,(Q_{12} + 2\,Q_{66})\,\sin^2\theta\,\cos^2\theta + Q_{22}\,\cos^4\theta$$

$$= 21.33\,(0.25) = 2\,(5.33 + 1.82)\,(0.25) + 2.114\,(0.25)$$

$$= 9.436$$

For 90° plies, the Q's are transformed as follows:

$$Q_{11}^{90} = Q_{22}\,\sin^4\theta = 2.114\,(0.25) = 0.529$$

$$Q_{12}^{90} = Q_{12}\,\sin^4\theta = 5.33\,(0.25) = 1.33$$

$$Q_{22}^{90} = Q_{11}\,\sin^4\theta = 21.33\,(0.25) = 5.33$$

With 1/4 of the plies in the 0° direction, 1/2 in the $\pm$45° directions, and 1/4 in the 90° direction, the effective Q's are as follows:

$$Q_{11} = \frac{Q_{11}^{0} + 2\,(Q_{11}^{45}) + Q_{11}^{90}}{4} = \frac{21.33 + 2\,(9.436) + 0.529}{4}$$

$$= 10.18$$

Similarly,

$$Q_{12} = \frac{5.33 + 2\,(7.616) + 1.33}{4} = 5.47$$

$$Q_{22} = \frac{2.114 + 2\,(9.436) + 5.33}{4} = 6.58$$

E_{eff} in the 0° direction is:

$$E_{eff} = \frac{10.18\ (5.47)\ -\ 5.47}{6.58} = 7.63\ \text{msi} = E_R$$

$$E_T = E_Z$$

$$\frac{E_R}{E_Z} = \frac{7.63}{1.982} = 3.85$$

For cases I and II (Figure C.1), the E_R/E_Z ratios are 0.35 and 2.86, respectively. Figure C.2 illustrates an extrapolation from cases I and II to account for the new E_R/E_Z ratio of 3.85.

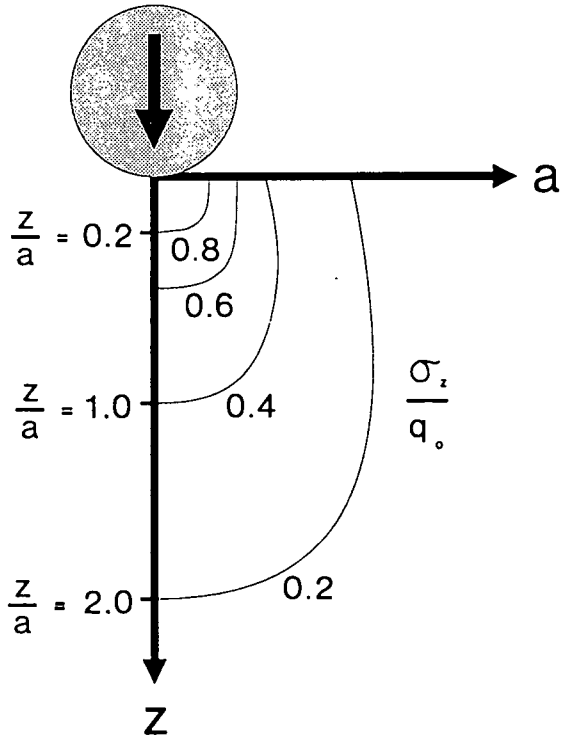

Figure C.2. Depth vs Pressure.

Assume an impact pressure q_o = 400 ksi (based on a 125 f/s impact with a sphere of radius 0.75-inch). (Ref. 45, p. 81.) The contact radius (a_o) is 0.242-inch. Based on self-similarity between the 0.75-inch radius sphere and the 0.25-inch radius sphere used in work associated with this thesis, the contact radius for the 0.25-inch sphere is:

$$a = \frac{0.242}{3} = 0.081$$

For 32-ply laminates, the sensor depths (z) are estimated to be 0.042, 0.084, and 0.126-inch based on a total thickness of 0.168-inch. (Note: The laminates later proved to be 0.191-inch thick). The magnitude of the compressive stress wave, as a function of depth within 32-ply laminates, is summarized in Table C-1. Figure C.3 illustrates the results. Times are based on an estimated stress wave velocity of 118,000 in/s.

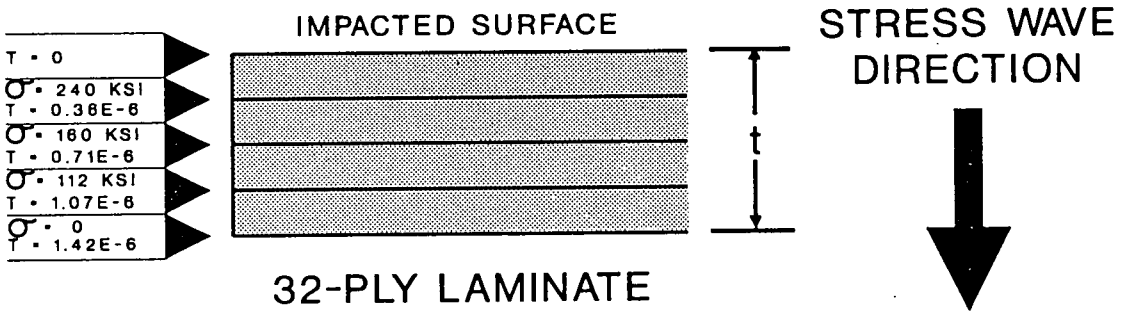

Figure C.3. Estimates of compression stress wave amplitude vs time and depth in 32-ply laminates (v = 125 f/s).

TABLE C-1. Estimates of the compressive stress wave magnitude, as a function of depth within a 32-ply AS4/3501-6 laminate, impacted by a 1/2-inch diameter sphere at 125 f/s.

DEPTH (z) (in)	DEPTH (z) / THICKNESS (t)	DEPTH (z) / CONTACT RADIUS (a)	STRESS (σ_{zz}) / PRESSURE (q_o)	STRESS (σ_{zz}) (ksi)	TIME FOR WAVE TO REACH DEPTH z (sec)
0	0	0	1	400	0
0.042	0.25	0.52	0.6	240	0.36×10^{-6}
0.084	0.50	1.04	0.4	160	0.71×10^{-6}
0.126	0.75	1.56	0.28	112	1.07×10^{-6}
0.168	1.00	2.08	NA	NA	1.42×10^{-6}

a = 0.081 in

q_o = 400 ksi

t = 0.168 in

c_L = 118,000 in/s

BIBLIOGRAPHY

1. Cantwell, W.J., P.T. Curtis, and J. Morton, "Impact and Subsequent Fatigue Damage Growth in Carbon Fibre Laminates", International Journal of Fatigue, Vol. 6, No. 2, April 1984, pp 113-118.

2. Avery, W.B., and D.H. Grande, "Influence of Materials and Layup Parameters on Impact Damage Mechanisms", 22nd International SAMPE Technical Conference, November 1990, pp 470-483.

3. Husman, G.E., J.M. Whitney, and J.C. Halpin, "Residual Strength Characterization of Laminated Composites Subjected to Impact Loading", Foreign Object Impact Damage to Composites, ASTM STP 568, American Society for Testing and Materials, 1975, pp 92-113.

4. Liu, D., "Impact-Induced Delamination - A View of Bending Stiffness Mismatching", Journal of Composite Materials, Vol. 22, July 1988, pp 674-692.

5. Foos, B.C., "Damage Progression in Composite Plates Due to Low Velocity Impact", Thesis, Dept. of Civil Engineering, Ohio State University, 1990.

6. Vasudev, A., K. Okajima, and S.J. Bless, "Effects of the Transverse Strength and the Density on the Penetration Mechanism of Thick Glass-Fiber-Reinforced-Plastics", March 1987.

7. Cristescu, N., L.E. Malvern, and R.L. Sierakowski, "Failure Mechanisms in Composite Plates Impacted by Blunt-Ended Penetrators", Foreign Object Damage to Composites, ASTM STP 568, 1975, pp 159-172.

8. Caprino, G., "Residual Strength Prediction of Impacted CFRP Laminates", Journal of Composite Materials, Vol. 18, November 1984, pp 508-518.

9. Crivelli, V.I., G. Caprino, A. Di Ilio, and L. Carrino, "Impact Tests on CFRP: A Static-Dynamic Analogy", 4th International SAMPE Conference, Bordeaux, October 1983.

10. Hsieh, C.Y., A. Mount, B.Z. Jang, and R.H. Zee, "Response of Polymer Composites to High and Low Velocity Impact", 22nd International SAMPE Technical Conference, November 1990, pp 14-27.

11. Wardle, M.W. and E.W. Tokarsky, "Drop Weight Impact Testing of Laminates Reinforced with Kevlar Aramid Fibers, E-Glass, and Graphite", Composites Technology Review, Vol. 5, No. 1, 1983, pp 4-10.

12. Elber, W., "The Effect of Matrix and Fiber Properties on Impact Resistance", Tough Composite Materials, NAS-LRC, Noyes Publication, 1985, pp 89-110.

13. Sjoblom, P.O., J.T. Hartness, and T.M. Cordell, "On Low-Velocity Impact Testing of Composite Materials", Journal of Composite Materials, Vol. 22, January 1988, pp 30-52.

14. Liu, D. and L.E. Malvern, "Matrix Cracking in Impacted Glass/Epoxy Plates", Journal of Composite Materials, Vol. 21, July 1987, pp 594-609.

15. Pinnell, M.F. and P.O. Sjoblom, "Low-Velocity Impact Testing of Thermoplastic and Thermoset Matrix Composite Materials", WRDC-TR-90-4087, Wright-Patterson AFB, November 1990.

16. Sierakowski, R.L. and S.K. Chaturvedi, "Impact Loading in Filamentary Structural Composites", The Shock and Vibration Digest, Vol. 15, No. 10, 1983, pp 13-31.

17. Sun, C.T. and S.H. Yang, "Contact Law and Impact Responses of Laminated Composites", NASA CR 159884, February 1980.

18. Kandalaft, I.F., "Visible Damage in Impacted Composite Plates", Masters Thesis, Ohio State University, 1990.

19. Gosse, J.H. and P.B.Y. Mori, "Impact Damage Characterization of Graphite/Epoxy Laminates", Proceedings of the American Society for Composites, 3rd Technical Conference on Composite Materials, September 1988, pp 344-353.

20. Hui, D., "Theoretical modeling of the Perforation of Laminated Plates By Rigid Projectiles", Final Report, 1990 AFOSR Summer Faculty Research Program, September 1990.

21. Cordell, T.M. and P.O. Sjoblom, "Low Velocity Impact Testing of Composites", Proceedings of the American Society of Composites, First Technical Conference, October 1986, pp 297-312.

22. Takeda, N., R.L. Sierakowski, and L.E. Malvern, "Microscopic Observations of Cross Sections of Impacted Composite Laminates", Composites Technology Review, Vol. 4, No. 2, 1982, pp 40-44.

23. Takeda, N., R.L. Sierakowski, and L.E. Malvern, "Wave Propagation Experiments on Ballistically Impacted Composite Laminates", Journal of Composite Materials, Vol. 15, March 1981, pp 157-174.

24. Foos, B.C., "Damage in Graphite/Epoxy Plates Subjected to Low Velocity Impact", Air Force Office of Scientific Research, September 1988.

25. Sun, C.T., "Impact Response and Damage in Composite Laminates", Fracture Analysis of Composite Laminates, 1985.

26. Ramkumar, R.L. and P.C. Chen, "Low-Velocity Impact Response of Laminated Plates", AIAA Journal, Vol. 21, No. 10, October 1983, pp 1448-1452.

27. Joshi, S.P. and C.T. Sun, "Impact-Induced Fracture Initiation and Detailed Dynamic Stress Field in the Vicinity of the Impact", Proceedings of the American Society for Composites, Second Technical Conference, September 1987, pp 117-185.

28. Boll, D.J., W.D. Bascom, J.C. Weidner, and W.J. Murri, "A Microscopy Study of Impact Damage of Epoxy-Matrix Carbon-Fibre Composites", Journal of Materials, Vol. 21, August 1986, pp 2667-2677.

29. Wu, H.T. and G.S. Springer, "Impact Induced Stresses, Strains, and Delaminations in Composite Plates", Journal of Composite Materials, Vol. 22, June 1988, pp 533-560.

30. Bless, S.J., R. Rondeau, and D.R. Askins, "Evaluation of Lightweight Armors for FSP Protection", WRDC-TR-89-4066, Wright-Patterson AFB, April 1989.

31. Evans, K.E. and N.J. Herne, "The Prediction of Damage Due to High Velocity Impact in Composite Laminates", Computer Aided Design in Composite Material Technology, Proceedings of the International Conference, Southhampton, England, April 1988, pp 383-393.

32. Wu, H.T. and G.S. Springer, "Measurements of Matrix Cracking and Delamination Caused by Impact on Composite Plates", Journal of Composite Materials, Vol. 22, June 1988, pp 518-532.

33. Guynn, E.G. and O'Brien, "The Influence of Lay-Up and Thickness on Composite Impact Damage and Compression Strength", AIAA/ASME/SAE 26th Structural Dynamics and Materials Conference, Orlando, 1985.

34. Romashchenko, V.A., Z.G. Alpaidze, and I.S. Dyachenko, "Stress Waves in the Coupling Zones of Composite Shells of Revolution", Translated from Problemy Prochnosti, No. 10, October 1989, pp 1360-1364.

35. Yarve, E.V., "Dynamic Response of Composite Plates to Impact Load", Contract F33615-88-C-5420, Task 20, Wright-Patterson AFB, May 1991.

36. Sierakowski, R.L., C.A. Ross, and L.E. Malvern, "Studies on the Fracture Mechanisms in Partially Penetrated Filament Reinforced Laminated Plates", US Army Research Office, DAAG29-79-G-0007, December 1981.

37. Woodward, R.L. and I.G. Crouch, "Ballistic Perforation of Laminated, Metallic Composites - An Approach to Modelling", Proceedings of the 11th International Symposium on Ballistics, Vol. II, Warhead Mechanisms and Terminal Ballistics, Brussels, May 1989, pp 301-310.

38. Joshi, S.P. and C.T. Sun, "Impact Induced Fracture in a Laminated Composite", Journal of Composite Materials, Vol. 19, January 1985, pp 51-66.

39. Dost, E.F., L.B. Ilcewicz, and J.H. Gosse, "Sublaminate Stability Based Modeling of Impact-Damaged Composite Laminates", Proceedings of the 3rd Technical Conference on Composite Materials, American Society for Composites, September 1988, pp 354-363.

40. Pettit, P.A., "Characteristics of Foreign 12.7mm API Projectiles Impacting Graphite/Epoxy Targets" WL-TR-91-3123, Wright-Patterson AFB, OH, February 1992.

41. Zukas, J.A., T. Nicholas, H.F. Swift, L.B. Ggreszczuk, D.R. Curran, "Impact Dynamics", John Wiley and Sons, New York, 1982.

42. Dutta, P.K., D. Hui, A. Mayer, and G. Czarnecki, "Stress Wave Propagation Through the Thickness of Laminated Plates Using PVDF Sensors", Technical Note, US Army Cold Regions Research and Engineering Laboratory, July 1991.

43. Kim, B.S. and F. Moon, "Impact Induced Stress Waves in an Anisotropic Plate", AIAA Journal, Vol. 17, No. 10, October 1979, pp 1126-1133.

44. Czarnecki, G.J., "Dual Mode Fracture of Composite Laminates Penetrated by Spherical Projectiles", proposed paper for the 18th ICAS Congress, Beijing, China, September 1992.

45. Ross, P.J., "Taguchi Techniques for Quality Engineering: Loss Function, Orthogonal Experiments, Parameter and Tolerance Design", McGraw-Hill Book Company, New York, 1988.

46. Greszczuk, L.B., "Damage in Composite Materials due to Low Velocity Impact", Impact Dynamics, John Wiley and Sons, New York, 1982, pp 55-94.

R0088 43369